Brushes of self-assembled nanotubes for temperature-responsive biocatalysis

Diana Guadalupe Ramirez Wong

Université Pierre et Marie Curie
Physique et chimie des matériaux (ED 397)
Laboratoire de Chimie de la Matière Condensée de Paris
&
Université catholique de Louvain
Institut de la Matière Condensée et des Nanosciences
Pôle Bio & Soft Matter

Brushes of Self-Assembled Nanotubes for Temperature-Responsive Biocatalysis

Thèse présentée par

Diana G. RAMIREZ WONG

Pour obtenir le grade de Docteur

Soutenue le 09 Septembre 2014, devant le jury composé de:

Philippe LAVALLE	Dir. de Recherche INSERM	Rapporteur
Pierre LABBE	Professeur à l'UJF (Grenoble)	Rapporteur
Jacques DEVAUX	Professeur à l'UCL	Président
Christine DUPONT	Professeur à l'UCL	Examinatrice
Yvette TRAN	Maître de Conférences ESPCI	Examinatrice
Christian BONHOMME	Professeur au College de France	Directeur de thèse
Sophie DEMOUSTIER	Professeur à l'UCL	Co-Directrice de thèse
Alain M. JONAS	Professeur à l'UCL	Co-Directeur de thèse

This thesis work was carried out in the International Doctoral School in Functional Materials (IDS-FunMat) framework, and is the result of a collaboration between:

Université catholique de Louvain
Institute of Condensed Matter and Nanosciences
Bio- and Soft Matter Division
(IMCN/BSMA)
Louvain la Neuve, Belgium
Under the supervision of
Prof. Alain M. Jonas &
Prof. Sophie Demoustier-Champagne

and

Université Pierre et Marie Curie
Chimie de la Matière Condensée de Paris
(CMCP)
Paris, France
Under the supervision of
Prof. Christian Bonhomme

and

ion track technology for innovative products
(it4ip s.a.) as industry partner

I dedicate this work to my parents,
for their love and encouragement.

Acknowledgements

I arrived almost four years ago to the BSMA group in Louvain-la-Neuve, and a little bit later to the CMCP group in Paris. Throughout these years I have learned valuable lessons and I have met great individuals who are an important part of the research work in your hands.

First and foremost I would like to express my gratitude to my supervisors: Prof. Alain Jonas, Prof. Sophie Demoustier-Champagne and Prof. Christian Bonhomme. They kept me on track and gave me advice, not simply with the scientific part, if not also with the mobility plan between universities. Always taking the time to answer my 5 minutes questions, which turned out into a 20 minutes session from time to time. Thanks for their patience and for sharing a part of their knowledge with me.

Sincerely thanks to the Professors that accepted to be members of the jury: Christine Dupont, Pierre Labbé, Philippe Lavalle, Jacques Deavux and Yvette Tran. I appreciate the time you took to read, correct, critique and enrich this work with your point of view. Special mention to Dr. Tran, who invited me to her lab for a short collaboration. She allowed me to use the facilities of her group, the hydrogel materials prepared by Mengxing Li, and to get the help from Mr. Bruno Bresson to perform AFM.

I must also acknowledge Etienne Ferain for the provision of the polycarbonate templates employed in this study, for his accessibility, and for letting me explore the production process and the research that is done at it4ip. Thanks as well to Prof. Karine Glinel, who was part of my PhD following committee. She kept her door opened for scientific

discussion and was always willing to help me and other students to deal with IDS-FunMat formalities.

I thank all the people who taught me how to use different lab equipments and gave some useful tips for synthesis & analysis: Delphine Magnin (Ellipsometry/SEM), Pascale Lipnik (TEM), Colette Douchamps (SEM), Sabine Bebelman (FTIR), Cécile D'Haese (AFM), Cristina Coehlo (NMR), Guillaume Laurent (NMR) and Carole Aime (CD). Big thanks to Aurore Becquevort and Hélène Gervais, who assisted me going trough administrative documents and even helped when I got sick.

For the friendly scientific discussion, the honest critique and the worthy advice, I want to thank my unofficial (sort-of) mentors Olivier Deschaume, Deepak Kalaskar, Antony Fernandes and Ali Dirani. Thanks to all BSMA members for the nice working atmosphere and specially to: Quentin who consistently payed attention to keep my level of glucose in the upper limit; Tilia, Tjasa and Remi that made sure I smiled in good and not-so-good days; Maxim, Amir, Edwin, Hailu and Ronggang for the long talks about science, culture, job opportunities, politics, religion and the improbable; to Nassima, Saghi, Camille, Catherine, Sabrina and Imen for their kindness and help in diary-life issues.

I wish to thank to the IDS-FunMat organizing committee, Laurent Servant, Marianne Delmas, Thierry Tassaing, Audrey Sidobre and many others that are following the status and progress of all the students enrolled in the program. Also to the different teams that planned the annual training school. Thanks to the IDS-FunMates for their cheerful spirit, specially to the ones that spent some time in UCL: Annie, Naresh, Ara, Maryna, Walter, Peng, Alina, Vusala and Victor. I enjoyed the cooking meetings and our early Christmas celebration.

Merci à ma famille belge: Olimpia Trefois, Alexandru Vaireanu et Liliane Hebeler, merci d'être toujours là, pour les conseils et l'occasion

de partager des moments privilégiés avec vous.

Merci aussi à la famille Bonhomme: Christian, Laure et Delphine, qui m'ont accueillie dans leur maison à plusieurs reprises.

Thanks specially to the people I forgot to mention but were there for me.

Abstract

Inspired by the elegant solutions that Nature has provided to control and promote specific site-reactions, here I present an attempt to mimic filamentous biocatalytic interfaces. Brushes of self-assembled nanotubes with an enzymatic component (β-lactamase) were prepared taking advantage of preexisting nanofabrication techniques, such as layer-by-layer and hard-templating.

First, the effects of geometrical confinement and its consequences were investigated by comparison of (chitosan/β-lactamase)$_n$ film assembly on flat surfaces and in nanoporous membranes.

In a second stage, polyelectrolyte nanotubes with controlled dimensions were prepared in nanoporous membranes and further anchored on a surface by chemical crosslinking to obtain brushes of nanotubes. The kinetic studies revealed the presence of active enzyme in the brushes and enhanced activity preservation when β-lactamase was deposited as the inner layers of the nanotubes.

As a final step, a variety of thermo-responsive coatings with different architectures were tested to control substrate diffusion on top of β-lactamase-based multilayer films. The integration of stable thermo-responsive elements was proven, although further experiments are required to control biocatalysis with additional layers and using more complex mechanisms, such as coupled thermal and mechanical responses.

Knowing that there are more challenges to face before reaching optimum nanotube brushes and apply them for controlled biocatalysis, this study has presented some elements that may pave the way towards the integration of different techniques for the fabrication of complex biocatalytic nanostructures.

Résumé

Nous nous sommes inspirés des solutions élégantes que la Nature propose, concernant le contrôle et l'optimisation de réactions spécifiques, pour présenter ici une tentative d'imitation des interfaces biocatalytiques au niveau de nanotubes. Des brosses de nanotubes autoassemblés à l'aide d'un composé enzymatique (β-lactamase) ont été préparées grâce à des techniques de nanofabrication telles que le « layer-by-layer » et le « hard templating ».

Dans un premier temps, les effets de confinement géométriques et ses conséquences ont été étudiés et comparés dans le cas d'assemblages de films de (chitosan/β-lactamase)$_n$ sur des surfaces planes et au sein de membranes nanoporeuses.

Dans un second temps, des nanotubes de polyélectrolytes de dimensions contrôlées ont été préparés dans des membranes nanoporeuses afin d'être ensuite ancrés sur une surface par un couplage chimique (dans le but d'obtenir des brosses de nanotubes). Des études cinétiques révèlent la présence d'enzymes actives dans les brosses ainsi formées et une amélioration de la préservation de l'activité quand la β-lactamase a été déposée dans les couches intérieures des nanotubes.

Enfin, une variété de couches thermo-sensibles présentant différentes architectures a été testée pour contrôler la diffusion du substrat sur les films multicouches de β-lactamase. L'intégration d'éléments thermo-sensibles stables a été prouvée. Cependant, des expériences complémentaires sont nécessaires pour contrôler la biocatalyse impliquant des couches supplémentaires et ce, en utilisant des mécanismes plus complexes tels que le couplage de réponses à la fois thermiques et mécaniques.

Tout en sachant qu'il reste un bon nombre de challenges auxquels il faut faire face avant d'obtenir des brosses de nanotubes optimales et avant de les utiliser pour la biocatalyse contrôlée, cette étude présente quelques éléments qui ouvrent la voie vers l'intégration de différentes techniques pour la fabrication de nanostructures complexes pour la biocatalyse.

Contents

List of acronyms and abbreviations

AAO Porous anodic aluminium oxide

AFM Atomic Force Microscopy

ATR Attenuated Total Reflection

BIBB 2-bromoisobutyryl bromide

CD Circular Dichroism

chit Chitosan chloride

CMP Carboxymethylpullulan

DDA Degree of deacetylation

EDC 1-Ethyl-3-(3-dimethylaminopropyl) carbodiimide

FTIR Fourier Transform Infrared Spectroscopy

LbL Layer-by-Layer

LCST Lower Critical Solution Temperature

MAS Magic Angle Spinning

MES 2-(4-Morpholino)ethanesulfonic acid buffer

NHS N-hydroxysuccinimide

NIPMAM *N*-isopropylmethacrylamide

NMR Nuclear Magnetic Resonance

NNPAM *N,N*-propylacrylamide

PAA Poly(acrylic acid, sodium salt)

PAH Poly(allylamine hydrochloride)

PC Polycarbonate

PCm Track-etched polycarbonate membrane

PDADMAC Poly(diallyldimethylammonium chloride)

PDI Polydispersity index

PE Polyelectrolyte

PEMA Polyelectrolyte multilayer assembly

PHEMA Poly(2-hydroxyethyl methacrylate)

$PMEO_2MA$ Poly(2-(2-methoxyethoxy)ethyl methacrylate)

PNIPAM Poly(*N*-isopropylacrylamide)

PNIPAM* Poly(*N*-isopropylacrylamide), 2% ene functionalized

PSS Poly(sodium 4-styrenesulfonate)

VPTT Volume Phase Transition Temperature

Chapter 1

Introduction

Design of new materials and devices has been inspired by nature since the beginning of the human civilization: from the wings of birds to the aircraft wing design, the polar bear fur to thermal energy collectors [1], the lotus leaf to superhydrophobic coatings [2], the gecko feet to reversible adhesives [3], etc. Natural shapes, patterns and structures go beyond beauty and constitute our best models for well engineered materials. Millions of years of evolution are responsible for the functional and hierarchical organization present in living organisms, which spans from the nano- to the macro-scale. It is therefore no surprise that the ultimate goal of device miniaturization is also to mimic cellular components and the way these tiny structures interact with their surroundings.

In the last three decades, nanotechnology has allowed us to formulate a variety of well defined nano-sized shapes *e.g.*, nanosphere, nanowire, nanocage, nanofiber, nanotube, etc. through several top-down or bottom-up strategies [4, 5, 6]. These achievements have opened up great possibilities to diverse yet unique materials with advanced functions, including high-performance nanosensors, nanoreactors, nanocatalysts, drug delivery, etc. For some of these applications, the organization and assembly of nanostructures into more complex and functional elements is extremely important, rather than the use of separate units. The use of arrays of nanoobjects and their immobilization onto surfaces can lead to new functions or the amplification of certain properties [6]. For example, nanoscopic and spatially distributed features can alter the cell spreading on planar surfaces, and even the ways in which cell differentiate [7], which has important consequences on bio-

materials design.

Towards the fabrication of new nanostructured and bioinspired materials, sophisticated natural components can be also added to target biological or chemical interactions, *e.g.* the incorporation of available biological molecules with specific functions. In fact, one of the new areas of great interest is nanobiocatalysis, which consists in the insertion of enzymes in nanostructured supports to catalyze chemical reactions. The large surface area available in nanostructured materials results in an improved enzyme loading, and consequently in an increased enzyme activity per unit mass or volume compared to conventional materials. Moreover, a uniform size distribution of nanomaterials and their similarity in size with enzymes leads to improved biocatalytic systems, specially regarding enzyme stability and activity [8]. Diverse thin film coatings and other strategies have been prepared and studied as enzyme carriers or enzyme supports for biomedical and industrial applications [9]. While the vast majority of enzyme supports are spherical compartments, enzyme immobilization in cylindrical features has also been proven effective [10]. The idea of spherical compartments was inspired by the organelles present in the cell, whereas the nanotube shape resembles living filamentous structures (*e.g.* bacteria).

In the presented frame, **the objective** of my thesis was *to prepare temperature responsive biocatalytic surfaces, based on brushes of self-assembled nanotubes that contain an enzyme* (Figure 1.1). Hence, the brush of nanotubes could catalyze the reaction with a specific substrate as a function of the temperature of the media. Besides the methods involved in the fabrication of this responsive nanotube surfaces, there were scientific questions related to the synthesis of the nanotube brush and its potential as a catalytic surface versus a planar coating. The most relevant issues addressed in this work are (i) the effects of confinement, (ii) the building of a nanotube brush of soft matter components, and (iii) the optimal insertion of responsive coatings to control biocatalysis.

As biocatalytic unit, β-lactamase from *Enterobacter cloacae* was selected because it is considered as a robust and rather small enzyme. β-lactamases are the main cause for resistance against penicillin-like antibiotics in Gram-negative bacteria; they were first isolated from *Escherichia coli* in 1965, spread worldwide a few years later and have survived to date after a variety of specific developed

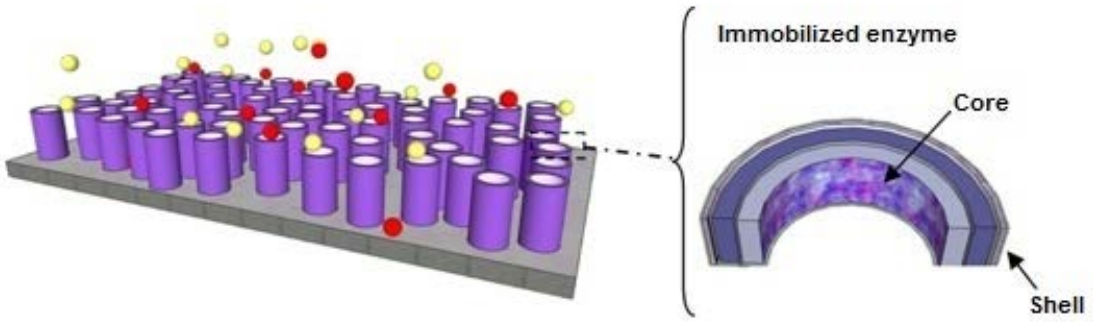

Figure 1.1: Schematic representation of a biocatalytic nanotube brush. The enzyme could be immobilized either in the core or the shell of the nanotubes and the external surface of the brush can be functionalized with a responsive polymer. The yellow dots represent the substrate upon which the enzyme is acting and the red dots represent the resulting product.

inhibitors [11]. Moreover, the detection of β-lactamase can be done by a simple colorimetric test [12] and its not-so-high molar mass makes it a good candidate to be studied by Nuclear Magnetic Resonance (NMR).

To prepare multilayer enzyme-based structures, chitosan was chosen as the soft interconnection between a rigid inert surface and the enzyme. Chitosan is in fact found as a structural material in some fungi but it is mainly obtained from the deacetylation of chitin, which is extracted from shells of crustacean and mollusks and the second most abundant biopolymer after cellulose [13]. Like other polysaccharides, chitosan is highly hydrophilic, biodegradable and biocompatible [14, 15].

The bio-active segment of the nanotubes was made of chitosan and β-lactamase and they were synthesized by layer-by-layer (LbL) and hard templating, using a polycarbonate membrane as a template. The brush construction was achieved by grafting the nanotubes prepared within a membrane template onto previously functionalized silicon wafers, similarly to a previously reported method [16]. Finally, the inclusion of thermo-response was attempted by several methods onto planar films, and in the case of the brushes a hydrogel coating was anchored to control the substrate diffusion.

In the following chapters the content of this study is organized as follows:

- Chapter 2 provides a basic description of the three central pillars of this work and its highest level applications. LbL assembly, membrane-templating and stimuli-responsive materials are described as well as their interconnection for the fabrication of high-tech devices and applications.

- Chapter 3 discusses the influence of substrate geometry and confinement on the LbL growth of biomacromolecular films and their resulting biocatalytic activity. A detailed analysis of enzyme immobilization within cylindrical submicron pores and on planar surfaces reveals some interesting stoichiometric differences and these results are linked to the observed catalytic activities.

- Chapter 4 focuses on the fabrication of brushes of self-assembled nanotubes containing an active enzyme (β-lactamase). The successful strategy for nanotube brush synthesis also allows the selective adsorption of the biocatalytic component either in the core or in the shell part of the nanotubes. Kinetic studies reveal that the activity is significantly better preserved when β-lactamase is incorporated in the core of the nanotubes.

- Chapter 5 presents several strategies to prepare thermoresponsive thin films with different architectures atop β-lactamase multilayer assemblies, to obtain thermoresponsive biocatalytic surfaces. The ability of these films to control substrate diffusion (*i.e.* nitrocefin) is evaluated by nitrocefin hydrolysis below and above the LCST/VPTT.

Finally, Chapter 6 summarizes the results obtained in the present study and draws some perspectives of further research to apply brushes of nanotubes for biocatalytic responsive surfaces.

References

[1] Thomas Stegmaier, Michael Linke, and Heinrich Planck. Bionics in textiles: flexible and translucent thermal insulations for solar thermal applications. *Philosophical Transactions of the Royal Society A: Mathematical, Physical and Engineering Sciences*, 367(1894):1749–1758, 2009.

[2] Lei Zhai, Fevzi C Cebeci, Robert E Cohen, and Michael F Rubner. Stable superhydrophobic coatings from polyelectrolyte multilayers. *Nano Letters*, 4 (7):1349–1353, 2004.

[3] Haeshin Lee, Bruce P Lee, and Phillip B Messersmith. A reversible wet/dry adhesive inspired by mussels and geckos. *Nature*, 448(7151):338–341, 2007.

[4] Charles R Martin. Membrane-based synthesis of nanomaterials. *Chemistry of Materials*, 8(8):1739–1746, 1996.

[5] Katsuhiko Ariga, Jonathan P Hill, and Qingmin Ji. Layer-by-layer assembly as a versatile bottom-up nanofabrication technique for exploratory research and realistic application. *Physical Chemistry Chemical Physics*, 9(19):2319–2340, 2007.

[6] Chunli Bai and Minghua Liu. Implantation of nanomaterials and nanostructures on surface and their applications. *Nano Today*, 7(4):258–281, 2012.

[7] Samir Mitragotri and Joerg Lahann. Physical approaches to biomaterial design. *Nature materials*, 8(1):15–23, 2009.

[8] Jungbae Kim, Jay W Grate, and Ping Wang. Nanobiocatalysis and its potential applications. *Trends in biotechnology*, 26(11):639–646, 2008.

[9] Omar S Sakr and Gerrit Borchard. Encapsulation of enzymes in layer-by-layer (LbL) structures: Latest advances and applications. *Biomacromolecules*, 14(7):2117–2135, 2013.

[10] Teruyuki Komatsu. Protein-based nanotubes for biomedical applications. *Nanoscale*, 4(6):1910–1918, 2012.

[11] Sarah M Drawz and Robert A Bonomo. Three decades of β-lactamase inhibitors. *Clinical microbiology reviews*, 23(1):160–201, 2010.

[12] Cynthia H O'Callaghan, A Morris, Susan M Kirby, and AH Shingler. Novel method for detection of β-lactamases by using a chromogenic cephalosporin substrate. *Antimicrobial Agents and Chemotherapy*, 1(4):283–288, 1972.

[13] Felippe J Pavinatto, Luciano Caseli, and Osvaldo N Oliveira Jr. Chitosan in nanostructured thin films. *Biomacromolecules*, 11(8):1897–1908, 2010.

[14] Marguerite Rinaudo. Main properties and current applications of some polysaccharides as biomaterials. *Polymer International*, 57(3):397–430, 2008.

[15] Barbara Krajewska. Application of chitin-and chitosan-based materials for enzyme immobilizations: a review. *Enzyme and microbial technology*, 35(2): 126–139, 2004.

[16] Khek-Khiang Chia, Michael F. Rubner, and Robert E. Cohen. pH-responsive reversibly swellable nanotube arrays. *Langmuir*, 25(24):14044–14052, 2009.

Chapter 2

State of the Art

This chapter has for objective to describe the fundamentals and the highest level applications achieved by the central techniques employed in this work: layer-by-layer assembly, membrane templating and stimuli-responsive materials.

2.1 Layer-by-layer assembly

Layer-by-layer assembly (LbL) was introduced by Decher and co-workers in 1992 [1, 2] and is nowadays a well established technique to prepare multilayer thin films. The method is quite simple and it allows to tailor the surface of materials using the self-assembly of polyions. Typically, a solid support with a preferably charged surface is alternatively exposed to solutions of positive and negative molecules, respectively [3] (Figure 2.1). Since each adsorption step leads to a charge reversal of the surface, the subsequent deposition results in a complex layer. One or more rinsing steps after the adsorption of each layer are used to avoid contamination of the next polyion solution and they also help to stabilize weakly adsorbed layers. Further cycles of alternate adsorption and rinsing result in the stepwise growth of polymer films.

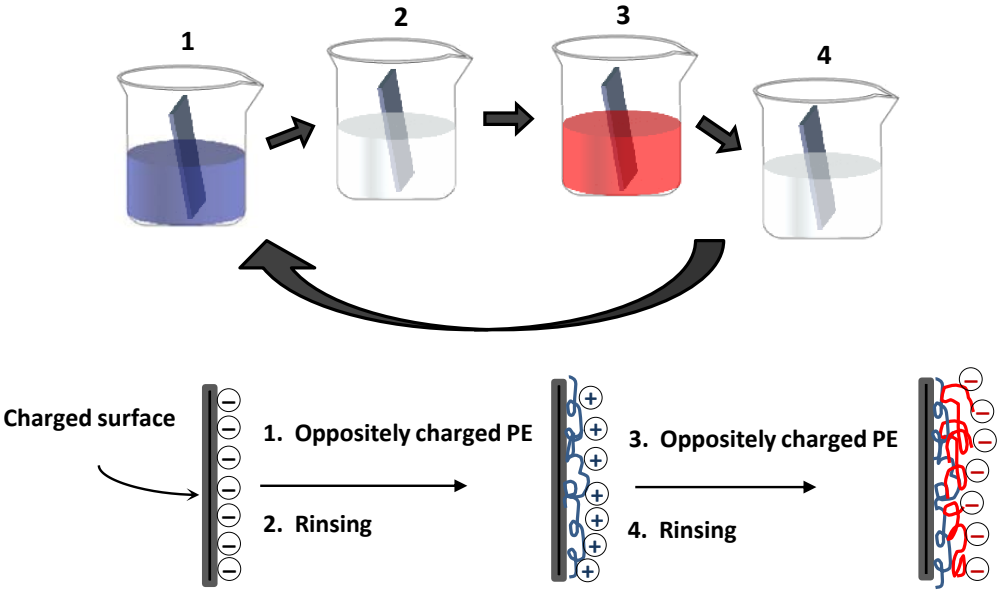

Figure 2.1: Schematic representation of the layer-by-layer process of adsorption for a couple of polyelectrolytes bearing different charge. The solid substrate is dipped in the polyelectrolyte and the rinsing solutions step by step to prepare a multilayered thin film.

Besides the simplicity of the LbL method, there is a series of advantages

that make it attractive for numerous applications [4]. The step-by-step procedure permits a fine structuring along the growth axis and precise control over the total thickness of the films, in the range of a few angstroms up to several hundreds of nanometers. Since LbL only involves adsorption from solution, any support bearing a charged surface can be used in principle, with no restrictions of size or topology. While the choice of supports has been largely dominated by their convenience for analytical methods (*e.g.* glass, quartz, silicon wafers, gold), flat templates are probably the most common topology to prepare LbL multilayer films. However, the use of spherical and porous templates permits the synthesis of different shapes, such as capsules and tubular structures (Figure 2.2, Templates). Moreover, a variety of charged nanoobjects can be used for LbL, for example: molecular clusters, organic dyes, dendrimers, polypeptides, nucleic acids and DNA, viruses, etc. (Figure 2.2, Building blocks).

While the initial conception of the multilayer assembly pointed out the electrostatic interactions as the main driving forces, it is now acknowledged that the gain in entropy due to the release of counterions plays an important role in the adsorption [12]. Also, it has been reported that the multilayer assembly can be achieved by: hydrogen-bonding, coordination-bonding, charge transfer, molecular recognition, hydrophobic interactions or a combination of these [13]. Thanks to the different interactions, a variety of building blocks can be used "as-is", and do not require prior activation.

Among the list of advantages of LbL, it is important to underline the compatibility with physiological conditions. The fact that the assembly is performed in aqueous solutions is favorable to preserve fragile bioactive elements in contrast to other encapsulation systems that require solvents. In addition, it has been reported that trapped water is present in LbL films, despite drying processes applied, which is extremely important for the inclusion and further application of bioactive molecules [13].

Figure 2.2: Schematic representation of the kinds of building blocks and the shape of the templates that can be employed for LbL assembly. References: (i) Multilayered [5], (ii) Free-standing [6, 7], (iii-vi) 3D structures [7, 8, 9, 10, 11].

2.2 Proteins and Enzymes in LbL

2.2.1 Protein: Basics

Proteins are biological macromolecules, essential part of living organisms that participate virtually in every process between cells. They cover a variety of functions and act for example: as structural elements, as transport elements, catalyzing chemical reactions, participating in cell signaling, etc. Proteins differ from one to another in their chemical structure (illustrated in Figure 2.3), which is basically a sequence of amino acids (primary structure). Some sequences of amino acids result in highly regular sub-structures (secondary structure, *e.g.* α-helix, β-sheet) and the whole sequence presents a particular folding in a three-dimensional structure, so called tertiary structure. Moreover, some proteins form clusters of two or more polypeptide chains into a particular geometry via non covalent interactions. Each polypeptide chain could function independently of each other or may work cooperatively (*e.g.* hemoglobin tetramer), and this level of organization is called quaternary structure. [14]. By formation of such ternary and quaternary structures, amino acids far apart in the sequence are brought close together in three dimensions to form a functional region, an active site. Hence, the spatial arrangement of the amino acid residues determines the function of the protein in the cell and the way a protein interacts with other molecules and folds in different environments.

The interaction between proteins and interfaces have significant consequences, desired or undesired, always relevant for medical and technological applications. Since protein adsorption might facilitate the accumulation of biological components from biological fluids at interfaces, it could be undesirable, for example in food processing equipment or cardiovascular implants. Conversely, thin protein coatings can be designed to obtain biocompatible devices or to functionalize surfaces for bioseparations, immunoassays, diagnostics and catalysis.

2.2.2 Protein adsorption at solid surfaces

The adsorption of proteins from an aqueous solution onto solid surfaces occurs widespread in natural and man-made systems by different mechanisms. Yet spon-

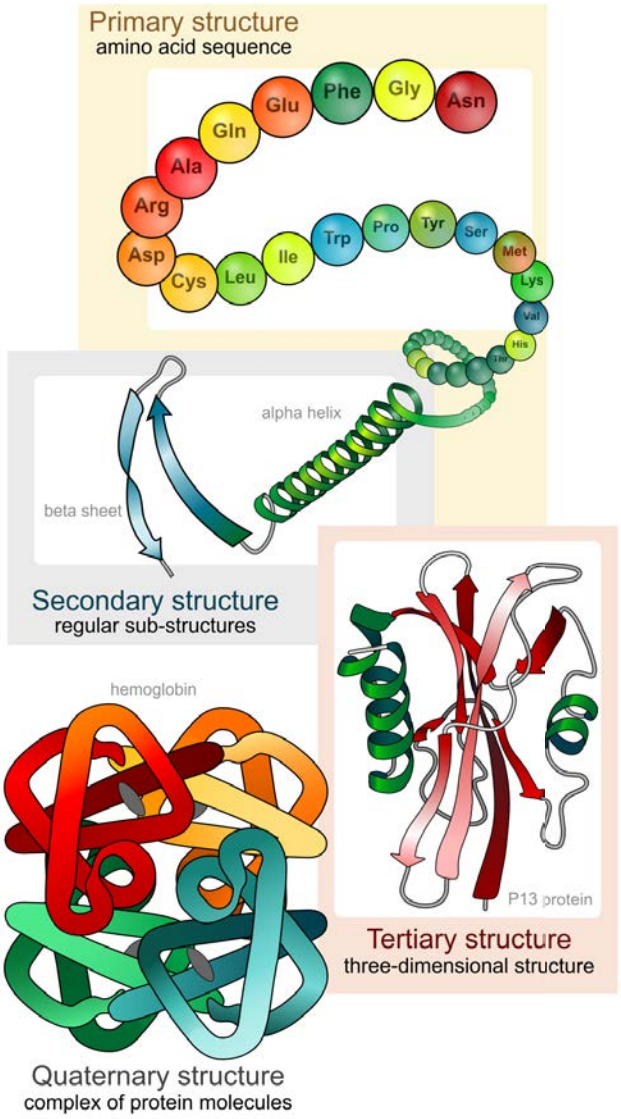

Figure 2.3: Schematic representation of the protein structure: from primary to quaternary structure. Extracted from [15].

taneous protein adsorption is always linked to a negative change in Gibbs energy for a given system under constant conditions of pressure and temperature [16, 17]. In this scenario, the major interactions that determine the overall adsorption process are (1) hydration changes (of the sorbent surface and the protein molecule itself), (2) electrostatic interactions and (3) changes in the conformational entropy of the protein [17].

Influence of protein properties. The convoluted composition and structure of proteins could be decomposed into individual domains exhibiting specific properties like hydrophilic/hydrophobic, polar/non-polar or charged/uncharged. Therefore, no simple model could accurately describe protein adsorption. However, a classification with respect to their interfacial behavior can be achieved by considering size, structural stability and composition [18]. Small and rigid proteins (*e.g.* Lysozyme) are referred as 'hard proteins' suggesting a little tendency for structural alterations upon adsorption. Intermediate size proteins (plasma proteins) can undergo conformational re-orientations upon surface contact and exist in two or more adsorbed states with different adhesion energy. High molecular weight proteins, such as lipoproteins and glycoproteins are dominated by the content of lipids or glycans to determine their preference for hydrophobic/hydrophilic surfaces.

Influence of surface properties. In general, proteins tend to adhere more strongly to non-polar than to polar, to high surface tension than to low surface tension and to charged than to uncharged surfaces [17, 18]. It has been hypothesized that non-polar surfaces destabilize proteins which leads to strong inter-protein and protein-surface interactions. While unmodified surfaces can be utilized to study protein adsorption, diverse techniques of surface modification such as silanization and the use of sel-assembled monolayers are employed to tune the surface energy an polarity.

Influence of external parameters [18]. Temperature, pH, ionic strength and buffer composition have a decisive influence on protein adsorption. The temperature affects the equilibrium state and the kinetics of protein adsorption, causing an increase on the amount of surface adsorbed proteins at higher temperatures. On the other hand, the pH determines the electrostatic state of the proteins and the adsorption rates are high when the protein and substrate bear opposite charges. However, the total mass load is generally maximized at the isoelectric point. The concentration of dissolved ions, called ionic strength, also affects the range of persistence of electrostatic interactions: shorter electrostatic interactions are present at higher ionic strength. Thus, the adsorption of charged proteins to oppositely charged supports is hampered whereas the adsorption to like-charged substrates is enhanced.

After a protein has been adsorbed onto a surface, protein-protein interactions modulate the amount of protein adsorbed by changing surface affinities, positive cooperative effects, size exclusion effects, overshooting adsorption kinetics, or surface aggregation [18].

2.2.3 Protein coatings for biotechnological applications

While the adsorption of proteins onto oppositely charged surfaces (*e.g.*, mica, silicon, glass) occurs spontaneously, the nanofabrication of protein thin films has largely grown after LbL assembly was introduced by Decher and collaborators. The encapsulation and immobilization of proteins by LbL is superior to previously reported techniques, such as physical adsorption, solvent casting, covalent binding, electropolymerization and Langmuir-Blodgett deposition [19]. These methods either produce irregular protein films at low density, either are very specific and of limited application (Langmuir-Blodgett). On the other hand, LbL films allow to concentrate and protect bioactive molecules in a defined volume. Proteins can either be adsorbed on surfaces as multilayers, surrounded by polyelectrolyte multilayers (PEM) boundaries (*e.g.* capsules) or entrapped in previously assembled multilayeres that act as reservoirs (Figure 2.4).

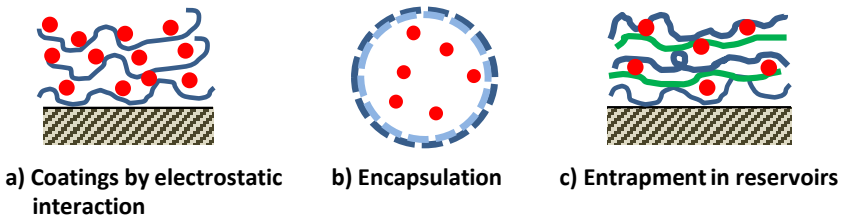

Figure 2.4: Schematic representation of different protein loading in LbL films

Hong *et al.* reported the first sandwiched protein multilayers (*i.e.* streptavidin) using a polyelectrolyte precursor (*i.e.* biotinylated poly-L-lysine) onto photostructured surfaces to trigger biospecific recognition [20]. And a few years later, the group of Kunitake was the first to investigate the applicability of LbL to prepare multilayered protein films [21] by treating the proteins as amphoteric polyelectrolytes. The pH of the protein solution was set apart from the isoelectric point (pI) so that proteins were sufficiently charged (positively charged at a pH

$\leq$ pI, and negatively charged if pH $\geq$ pI). While the assembly of polyelectrolyte-protein film was reported successful, the direct assembly of oppositely charged proteins was not achieved. To explain this result, the authors suggested that the electrostatic attraction cannot be maximized with globular proteins due to the patched nature of the charge on the surface of proteins. However, flexible linear polyions might produce optimized electrostatic attraction since they can penetrate in between proteins molecules and act as electrostatic glue. As a consequence, the assembly of protein multilayers was achieved by using linear polyion interlayers. This approach was employed to prepare the first multienzyme reactor [22], and also to enhance cell spreading on material surfaces [23].

The preparation of LbL capsules was introduced by Caruso and Mhwald *et al.* in 1998 [8] and rapidly attracted great attention because of the ability to tailor properties, such as size, composition, porosity, stability, surface functionality and colloidal stability. The method consist basically in the combination of LbL on a spherical template with *a posteriori* core dissolution. Besides the fabrication of capsules with protein multilayered walls [24], protein aggregates and crystals were also encapsulated in LbL films [25, 26] or alternatively, the proteins were loaded in previously assembled hollow LbL capsules [27, 28, 29].

The exponential growth mode for LbL films was discovered at the beginning of the 2000s and this mode was reported suitable to prepare multilayered reservoirs which could encapsulate drugs and bioactive elements [19, 30]. For example, the polyelectrolyte couple poly(L-lysine)/hyaluronate was used by the group of Schaaf and Lavalle to prepare fibronectin reservoirs [31]. And in a more recent study, the lateral mobility of human serum albumin was studied in the same LbL assembly as a function of protein concentration [32]. Similarly, the group of Li *et al.* reported the stimuli-free load and release of proteins in poly(ethylenimine)/alginate films as a potential delivery system [33]. In fact, the reservoirs are commonly capped with a couple of linearly growing polyelectrolyte films to ensure the retention of the macromolecules. Although, the term 'reservoir' in LbL refers to exponential growth films, protein load has also been achieved in polysaccharide linearly growing films [34].

2.2.4 Enzyme immobilization

Enzymes are a special category of proteins: they accelerate the chemical reactions that comprise the metabolism of all living cells in order to proceed at the pace required to sustain life. They work under mild reaction conditions (physiological pH and temperature), in environmentally acceptable solvents (usually water), are also biodegradable, they have high activities and are chemo-, regio- and stereoselective. In every enzyme tertiary structure there is a pocket called active site, which takes a particular shape at specific pH and temperature conditions, in order to host a smaller molecule called substrate (Figure 2.5). The substrate binds to the active site, forming an enzyme/substrate complex, where the substrate is chemically modified. The substrate becomes a product and is released to facilitate a chemical reaction. An active site can activate one kind of substrate, or a few of them, so biocatalysis is highly specific. Moreover, the use of enzymes as catalysts affords synthetic routes which generate less waste, are even shorter and, hence, are both environmentally and economically more attractive than traditional organic syntheses [35].

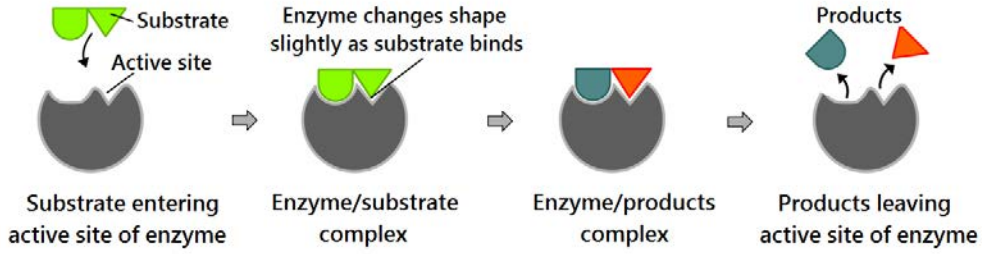

Figure 2.5: Schematic representation of an enzyme active site and how it works. Extracted from [15].

Trying to incorporate biocatalysis in industrial applications, came the need for enzyme immobilization to facilitate handling and recycling. Nowadays, similar approaches can be exploited for medical applications in the diagnosis and treatment of diseases. The use of polyelectrolyte layers for enzyme immobilization was no different than for proteins: LbL assembly represented a breakthrough for thin film nanofabrication. Nonetheless, any process of immobilization may have

a detrimental impact on the catalytic activity even when it is performed in water (instead of using organic solvents). Figure 2.6 shows the effects of enzyme immobilization that could affect the catalytic performance. First of all, the tertiary or quaternary structure of the enzyme could change (so called enzyme distortion), mainly due to the multi-interactions between the enzyme and the support, or the interaction with polyion layers [36]. Distortion can lead to less efficient catalysis although some enzymes display higher activity after immobilization (*e.g.* lipases) [37]. Second of all, the active center may be physically blocked after immobilization. The blockage of the active center may have special relevance when the substrate of the enzyme is moderately large and/or the spatial orientation of the enzyme is not favorable. Finally, immobilization may provoke diffusion problems. Porous supports are a particular case, because large substrates might be unable to reach an enzyme confined in small pores of rigid supports.

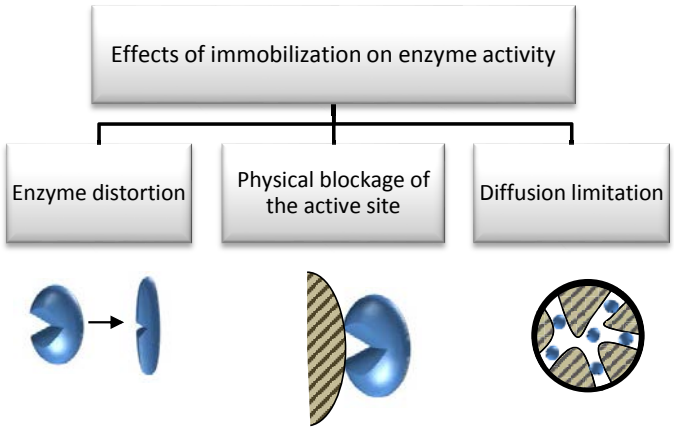

Figure 2.6: Schematic representation of the effects of enzyme immobilization that might alter catalytic efficiency.

2.2.5 Chitosan for enzyme immobilization

Preserving bioactivity is crucial for the construction of microreactors and sensors for medical applications. For the synthesis of films containing enzymes, there is a trend to use biocompatible, biodegradable and nontoxic materials in order to avoid detrimental enzyme-polyion interactions. A variety of modified polysaccha-

rides, especially chitosan, have been the subject of numerous studies to design biocompatible surfaces [38, 39]. Chitosan is a polysacharide obtained by the partial deacetylation of chitin. Its polyglucosamine chains hold reactive amino and hydroxyl groups (Figure 2.7), and the amino groups make it a cationic polyelectrolyte (pKa $\approx$ 6.5). The multilayer assemblies chitosan/enzyme have been synthesized below neutral pH to prepare sensors and vehicles for drug delivery and/or improve physical and biological properties of materials [40].

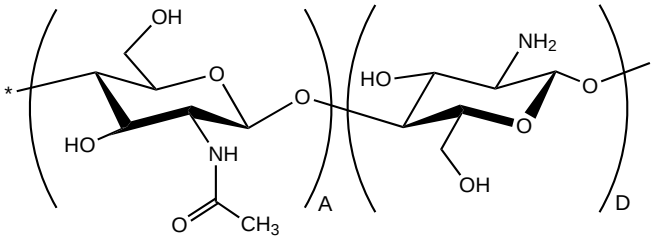

Figure 2.7: Chitosan molecular structure. The polymer is a partially deacetylated chitin structure. A represents the monomer units that remained acetylated and D, the amino-functionalized units.

Although there is no universal support for all enzymes and their applications, a number of desirable characteristics should be common to any material considered for immobilizing enzymes. Chitosan preserves well the activity of enzymes in a solid film, probably because chitosan retains a considerable amount of bound water molecules (hydrophilic). Moreover, it has available reactive functional groups that allow chemical reactions and modifications. It is moldable to different geometrical configurations that provide the system with permeability and surface area suitable for a chosen biotransformation [38]. As a consequence, chitosan and its derivatives are used in the form of powders, flakes and gels of different geometrical configurations. This last property is specially important in LbL biomaterial design; in fact, a frequent target is to emulate cellular compartments. To this end, many authors have used spherical particles as templates to produce polyelectrolyte multilayer capsules, micelles and microspheres with enzyme interior [13]. In this manner, the confinement of chemical reactions proceeds similarly to natural cell organelles. Another, less common strategy consists of the surface modification of porous membranes and nanotube fabrication through a combination of LbL and hard-templating [41].

2.3 Membrane templating and LbL

The use of membranes as templates for nanofabrication was introduced by Martin in the 1990s [42, 43]. This method was called hard-templating or simply "template method". Filling the pores of a nanoporous membrane, or "template" generates nanorods and the conformal deposition on the pore walls creates nanotubes (Figure 2.8). The obtained nanostructures can be released after membrane removal or remain embedded inside the template.

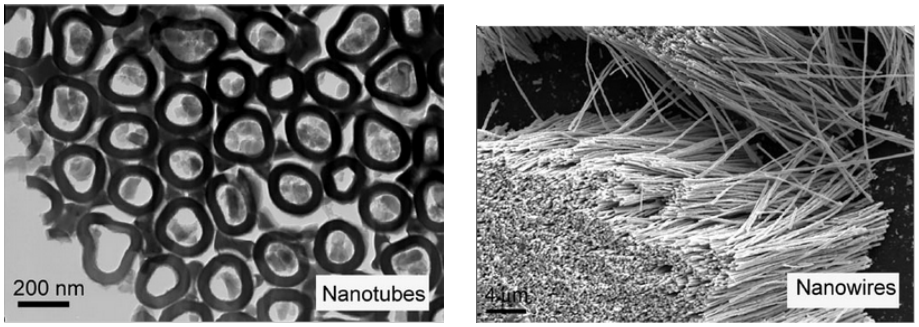

(a) (b)

Figure 2.8: Images of the nanotubes and nanowires that can be prepared by hard templating, observed by (a) TEM and (b) SEM. Excerpted from [44].

Porous anodic aluminium oxide (AAO, Figure 2.9a) was the first adopted robust nanotemplate, since it has uniform cylindrical nanopores, organized in a close-packed hexagonal arrangement. A large range of pore diameters (5-400 nm) and pore lengths (nanometers to tens of microns) can be obtained by controlling the parameters of electrolytic oxidation and etching of pure Al [45]. The highly regular characteristics of the AAO lead to monodisperse 1D nanomaterials, whose dimensions replicate those of the template. The second most used template is the track-etched polycarbonate membrane (PCm, Figure 2.9b), that also has straight and cylindrical nanopores. Track-etched membranes are prepared by the bombardment of a polycarbonate film with heavy energetic ions and subsequent etching with a strong base. Due to the nature of this process, the pores in PCm are randomly distributed but they can have high aspect ratios and the pore size can be tuned between 10 nm to several μm [46]. While the pore density in a PCm

can be spans from 10^5 to $10^{10}\cdot$ cm^{-2}, the AAO pore density is usually higher and up to $10^{11}\cdot$ cm^{-2} [47]. The choice of template depends again on the application of the modified membrane or the resulting nanotubes/nanorods. While AAO can be etched in pH $\leq$ 4.5 and pH $\geq$ 8.5, PCm can be dissolved in common organic solvents such as dichloromethane.

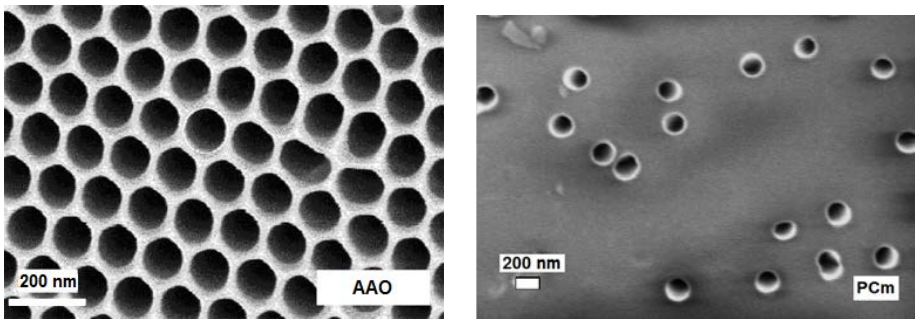

(a) (b)

Figure 2.9: TEM images of the porous surface of the membrane templates (a) AAO and (b) PCm. The AAO image excerpted from [44].

The first efforts to combine hard-templating and LbL assembly were reported in 2003 [48, 49]. The assembly proceeds essentially in the same way as on flat surfaces, except that the times given for polyelectrolyte adsorption are larger to ensure the polyelectrolyte diffusion through the pores. Both reports showed that via the combination of these methods it is possible to prepare flexible multilayer heterostructured nanotubes made of polyelectrolytes. The combined strategy enables to get control over the morphology of the resulting nanotubes with the membrane design, but also to control the wall thickness, wall components and resulting properties by playing with the building blocks, ionic strength and pH of the working solutions.

2.3.1 Polyelectrolyte adsorption in pores

LbL deposition within nanopores is likely to be more sensitive to the nature of the polyelectrolyte species and the ionic parameters, than deposition on planar surfaces. A common observation for polyelectrolyte adsorption in pores is, for

example, a thicker film layer compared to the equivalent corresponding layer prepared on a flat surface [50].

Jonas et al. have also found a new kind of multilayer growth in nanopores with poly(vinylbenzylammoniumchloride)/ poly(styrene sulfonate) (PVBAC/PSS) [51], and poly(allylamine hydrochloride)/PSS [50]. In this new growth model, the thickness of the adsorbed layers depends strongly on the pore diameter for smaller pores, but the adsorption is comparable to flat surfaces in larger pores. They discussed the existence of two regimes of growth and the formation of entangled structures inside the pore as a controlling factor to go from regime I (similar to flat surfaces) to regime II (slower kinetics). In the second regime, a dense gel is formed in the pores and it dominates the degree of polymer interpenetration and the local structure of the multilayer (Figure 2.10). Moreover, their results suggest that the topological confinement within nanopores causes film reorganization and that the charge overcompensation eventually vanishes during the assembly. In this sense, Rubner et al. have suggested that the surface charge on nanopore walls provides a level of electrostatic repulsion over the width of the pore sufficient to deplete the transport of the building blocks required for LbL assembly. Thus, a decreased level of charge overcompensation would occur after the deposition of each layer [52]. This effect is smaller in larger pores, but becomes stronger as the number of layers increases or even with a few layers, if the building blocks are large [45].

2.3.2 Protein decorated membranes and based nanotubes

The load of bioactive species, as proteins and enzymes, in micro or nano-membranes is of great interest for separation applications. Moreover, the production of nanotubes using porous membranes as templates has been explored to prepare a variety of smart materials with potential applications for drug and gene delivery vehicles and sensing.

The contributions of Caruso [53] and Martin [54] set the basis for the fabrication of membrane-supported catalyst and bioactive nanotubes, respectively. In their work was demonstrated that nanoporous membranes offer the possibility to increase considerably the total surface area and bioactivity, which is governed by

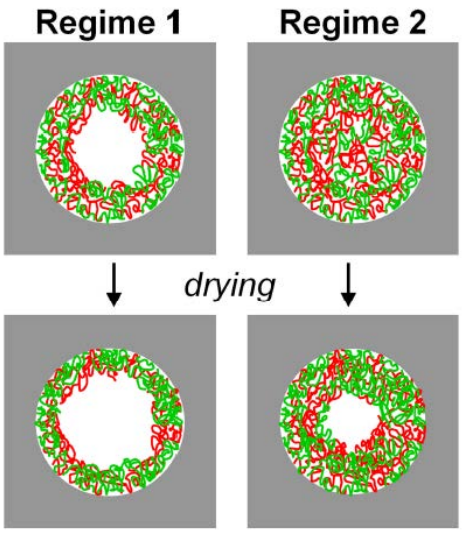

Figure 2.10: Schematic representation of the two regimes of growth in nanopores, suggested by Jonas and collaborators [50].

the pore size, the porosity, and the number of enzyme containing layers.

A few research groups have confirmed the applicability of the method to prepare nanotubes based on protein multilayers, such as collagen [55], glucose oxidase [56], hemoglobin [57], bovine serum albumin [57], avidin [56], ferritin [58, 59, 60] and human serum albumin [41, 58, 61, 62, 63, 64, 65]. Particularly the group of Komatsu has developed some level of expertise in the nanotube synthesis with poly-L-arginine (PLA) and human serum albumin (HSA) (Figure 2.11 i). Using (PLA/HSA) nanotubes, they investigated the adsorption of a single interior enzyme layer for biocatalysis [61], and alternatively, the addition of an interior antigen layer for virus entrapment [63]. In both cases, the inner compartment of the nanotubes was exploited for biological interactions, and acting as a size selective platform (Figure 2.11 ii, iii). In more recent publications, the group reported the synthesis of solid nanotubes comprising α-Fe_2O_3 [58, 59, 60] and gold nanoparticles [66]. These last results showed more robust LbL nanotubes and improved catalytic properties due to the inclusion of inorganic matterials.

Besides the potential applications of LbL modified membranes for enzyme immobilization, few reports have addressed the advantages of submicron coated membranes for biocatalysis [41, 53, 67, 68]. The following Chapter presents a

detailed study of the consequences of enzyme adsorption on flat surfaces and within nanopores. The reorganization of the film is observed as variations in stoichiometry along the assembly, and these results are linked to the biocatalytic performance.

While the use of freed protein nanotubes has not received the same attention as the spherical features in the same order of dimension, the use of nanotube arrays anchored to surfaces offers potential for surface/interface functionalization. Rubner and Cohen *et al.* prepared a poly(allylamine hydrochloride)/poly(acrylic acid) (PAH/PAA) nanotube arrays on a solid support [69], illustrating one more application of the combination LbL-membrane templating. This concept was then extended to protein assemblies by Komatsu *et al.* to synthesize biocatalytic nanotube arrays (Figure 2.12) [64]. The large surface area available in a dense array of nanotubes makes this strategy attractive for highly sensitive sensors and the fabrication of mini devices for sensing and delivery integrated in one system. Two different methods of synthesis for nanotube array fabrication are presented in Chapter 4, and the consequences of enzyme immobilization and selective deposition are discussed.

2.4 Stimuli-responsive polymers

2.4.1 Response and phenomena behind

Stimuli-responsive polymers display dramatic property changes responding to small changes in the environment. These polymers are able to recognize a stimulus as a signal, feel the magnitude of this signal, and then change their chain conformation in direct response [70]. There are different stimuli which can be classified as either physical or chemical. Chemical stimuli, such as pH, ionic factors and chemical agents, will change the interactions between polymer chains or between polymer chains and solvents at the molecular level. The physical stimuli, such as temperature, electric or magnetic fields, and mechanical stress, will affect the relative level of various energy sources and alter molecular interactions at critical onset points.

Among a variety of stimuli-responsive polymers, probably the most studied

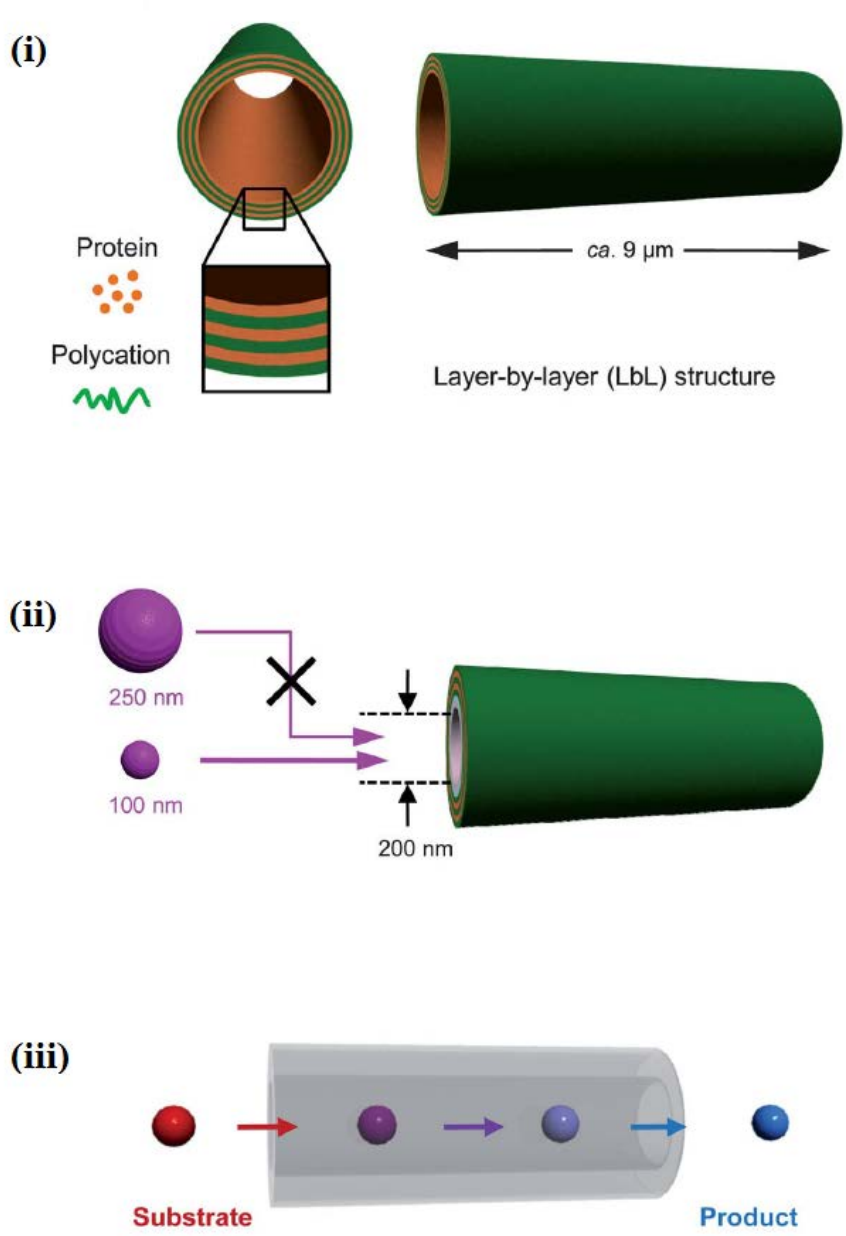

Figure 2.11: Schematic representation of (i) a protein nanotube prepared by LbL, (ii) Selective molecular capture in a nanotube, (iii) How a biocatalytic nanotube works. Images excerpted from [62].

ones are those sensible to pH and temperature changes in the physiological range, so they can be employed for life science applications [71]. The temperature re-

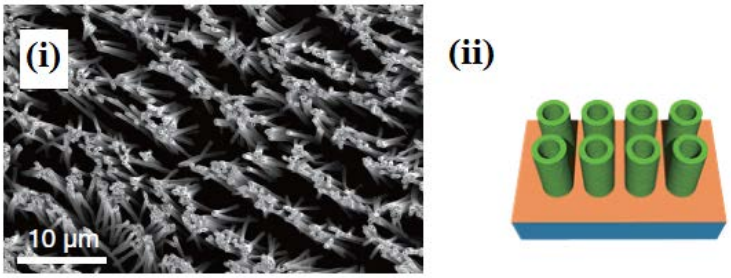

Figure 2.12: SEM image (i) and schematic representation (ii) of an array of nanotubes made of poly-L-arginine (PLA), human serum albumin (HSA), poly-L-glutamic acid (PLG) and avidin (Avi): $(PLA/HSA)_2PLA/PLG/Avi$. Image adapted from [64].

sponse is associated to a Lower Critical Solution Temperature (LCST) transition in a given solvent, *e.g.* water. Below the LCST, the responsive polymer is soluble in aqueous solution and it aggregates above the LCST. This transition is reversible, thus by playing with changes of temperature around the LCST value, the polymer aggregates and redissolves [72].

At a molecular level, the LCST transition is accompanied by conformational changes of the polymer, from a random coil to a collapsed globule (Figure 2.13). If the responsive polymer is crosslinked or anchored on a surface (*i.e.* , in a film), then it is capable of exuding water in response to the phase transition, which results in a contraction and stiffening of the hydrogel or the film, a phenomena named Volume Phase Transition Temperature (VPTT). For the sake of clarity, this text uses indistinctly the acronym LCST referring to free chains in solution or to crosslinked films, which is most widely extended.

The modification of synthetic surfaces with stimuli-responsive coatings is useful to perform processes like bioseparation, antifouling, actuators or valves, and vehicles for controlled and targeted release of therapeutic agents [73]. For this purpose, poly(N-isopropylacrylamide) (PNIPAM) is one of the most popular temperature-responsive polymers, with a LCST of *ca.* 32 °C [74]. Besides a low LCST, the success of PNIPAM is due to its biocompatibility and low toxicity, which is extremely important for the synthetic materials in contact with bioactive units and organisms.

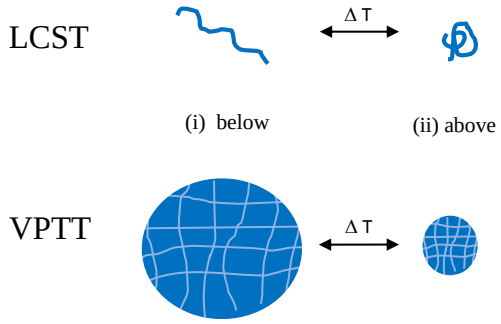

Figure 2.13: Schematic representation of LCST and VPTT transition in a stimuli-responsive polymer.

2.4.2 LCST in LbL assemblies

Due to the fine control obtained by LbL at the nanoscale level, its versatile and green characteristics, the synthesis of stimuli-responsive films by LbL has been explored for some time. The most simple strategies for stimuli-response inclusion consist of the direct adsorption of block copolymers containing PNIPAM segments or microgel particles loaded between polyelectrolyte layers [75, 76, 77]. The level of interpenetration between the responsive polymer and the polyion of opposite charge could, however, reduce the magnitude of the response in these assemblies [78]. A purely responsive film can also be anchored on previously synthesized LbL assemblies, as Armes and Advincula have demonstrated [79, 80]. The insertion of PNIPAM brushes on LbL films would be useful to protect sensible molecules or to keep apart active species from undesired interfacial reactions by changes of temperature.

Other stimuli have also been incorporated to LbL assemblies, like pH. A very sophisticated example of this responsive behavior and it integration in LbL nanotubes was presented and discussed by Rubner and Cohen et al. (Figure 2.14) [69]. The nanotubes were assembled layers of PAH/PAA, which exhibit swelling/deswelling variations under pH changes. In this case, the soft surface could work as an actuator due to the significant changes in the nanotubes dimensions.

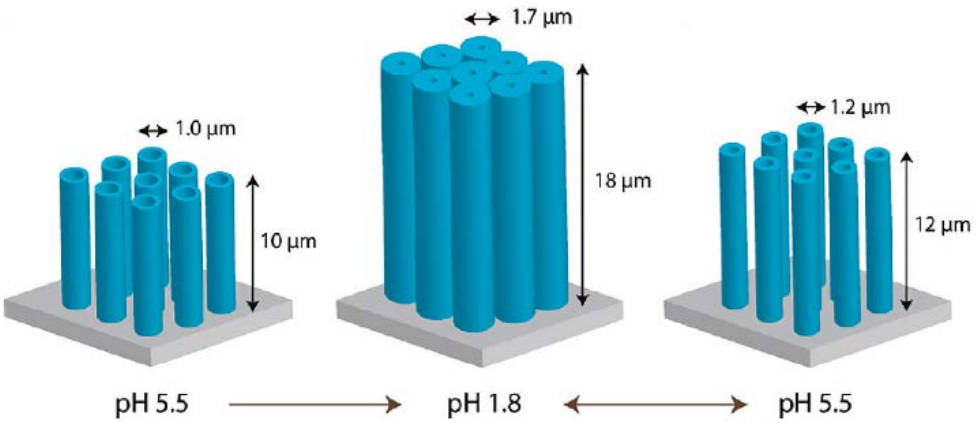

Figure 2.14: Schematic representation of a pH-responsive nanotube array. The nanotubes are a LbL assembly based on PAH/PAA [69].

2.4.3 Mechanically triggered response on LbL

A completely different approach that does not involve LCST, is the growth of LbL assemblies on a flexible support. The group of Schaaf and Lavalle has studied the design of multilayered LbL coatings to mimic mechanotransduction [31, 81, 82]. In their design, the alternation of "linear" and "exponential" growing multilayers lead to a coating with multiple strata with different mechanical properties (Figure 2.15). The linear-growth multilayers based on poly(diallyldimethylammonium)/ poly(sodium 4-styrenesulphonate (PDADMAC/PSS), possess tunable permeability under stretch. On the other hand, exponentially-growing poly-(L-lysine)/ hyaluronic acid (PLL/HA) act as microcontainers for active compounds, *e.g.* enzyme or substrate. The assembly of (PLL/HA) below (PDADMAC/PSS) layers results then in a (PLL/HA) bioactive reservoir capped with a (PDADMAC/PSS) barrier. Moreover, the assembly is synthesized on a silicone sheet, so that it could be stretched by a mechanical force.

In a first report, the "reservoir" was loaded with an enzyme [31] and exposed to a solution containing the substrate. Thereby, the capping barrier avoids the reaction when the film is in contact with the corresponding substrate solution. However, if the film is stretched, the capping barrier (PDADMAC/PSS) becomes more permeable and biocatalysis occurs. As a second part of the study, the substrate molecules were loaded in the reservoir and the enzyme adsorbed atop

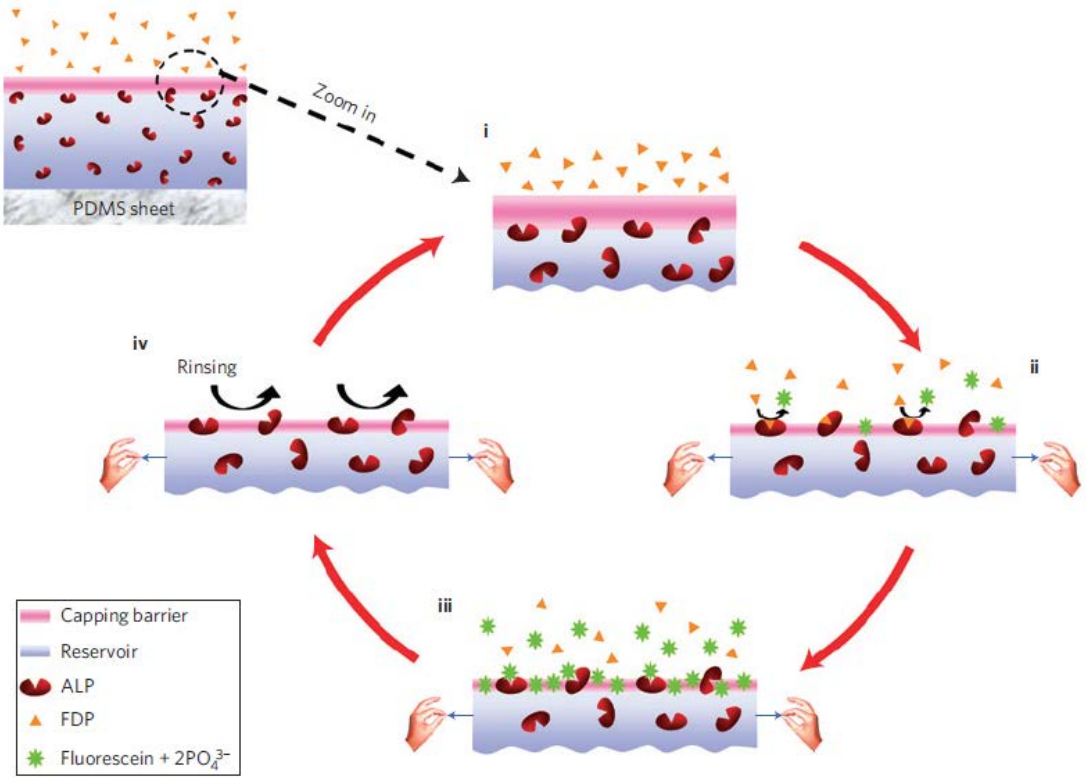

Figure 2.15: Schematic representation of the mechanism involved in mechanically sensitive bioactive coating. The film contains an enzyme (ALP) embedded in the reservoir multilayers (PLL/HA) and is covered by a capping barrier (PDAD-MAC/PSS). The yellow triangles (FDP) illustrate the substrate in solution and the green stars, the corresponding product after it interacts with the enzyme. The sequence of the graphics is: (i) Unstretched film blocks the interaction enzyme-substrate, (ii) partial stretching starts catalysis, (iii) full stretching accelerates the rate of reaction, (iv) Intermediate rinsing step is done with a stretched film to ensure the substrate removal. Image excerpted from [31].

the capping barrier, leading to an "all in one" biocatalytic platform [82]. In the later strategy, the simple stretching promotes and stops biocatalysis and all the elements are already comprised in the film. The methodology used in both reports proves that LbL can exhibit stimuli-responsive properties with a thoughtfully designed structure. The combination of stimuli-responsive polymers and structured multilayered films is the subject of discussion in Chapter 5.

References

[1] Gero Decher, Jong-Dal Hong, and Johannes Schmitt. Buildup of ultrathin multilayer films by a self-assembly process: III. Consecutively alternating adsorption of anionic and cationic polyelectrolytes on charged surfaces. *Thin solid films*, 210:831–835, 1992.

[2] Gero Decher and Johannes Schmitt. Fine-tuning of the film thickness of ultrathin multilayer films composed of consecutively alternating layers of anionic and cationic polyelectrolytes. In *Trends in Colloid and Interface Science VI*, volume 89, pages 160–164. Springer, 1992.

[3] Gero Decher. Fuzzy nanoassemblies: Toward layered polymeric multicomposites. *Science*, 277(5330):1232–1237, 1997.

[4] Patrick Bertrand, Alain M. Jonas, André Laschewsky, and Roger Legras. Ultrathin polymer coatings by complexation of polyelectrolytes at interfaces: suitable materials, structure and properties. *Macromolecular Rapid Communications*, 21(7):319–348, 2000.

[5] Gero Decher. Polyelectrolyte multilayers, an overview. *Multilayer thin films: Sequential assembly of nanocomposite materials*, pages 207–243, 2003.

[6] Chaoyang Jiang, Sergiy Markutsya, and Vladimir V Tsukruk. Compliant, robust, and truly nanoscale free-standing multilayer films fabricated using spin-assisted layer-by-layer assembly. *Advanced Materials*, 16(2):157–161, 2004.

[7] Chaoyang Jiang and Vladimir V Tsukruk. Freestanding nanostructures via layer-by-layer assembly. *Advanced Materials*, 18(7):829–840, 2006.

[8] Angus P.R. Johnston, Christina Cortez, Alexandra S. Angelatos, and Frank Caruso. Layer-by-layer engineered capsules and their applications. *Current Opinion in Colloid & Interface Science*, 11(4):203 – 209, 2006.

[9] Katsuhiko Ariga, Jonathan P Hill, and Qingmin Ji. Layer-by-layer assembly as a versatile bottom-up nanofabrication technique for exploratory research

and realistic application. *Physical Chemistry Chemical Physics*, 9(19):2319–2340, 2007.

[10] Yajun Wang, Alexandra S Angelatos, and Frank Caruso. Template synthesis of nanostructured materials via layer-by-layer assembly. *Chemistry of Materials*, 20(3):848–858, 2008.

[11] Rui R Costa and João F Mano. Polyelectrolyte multilayered assemblies in biomedical technologies. *Chemical Society Reviews*, pages –, 2014.

[12] Regine v Klitzing. Internal structure of polyelectrolyte multilayer assemblies. *Physical Chemistry Chemical Physics*, 8(43):5012–5033, 2006.

[13] Omar S Sakr and Gerrit Borchard. Encapsulation of enzymes in layer-by-layer (LbL) structures: Latest advances and applications. *Biomacromolecules*, 14(7):2117–2135, 2013.

[14] R.A. Harvey, R.A. Harvey, and D.R. Ferrier. *Structure of Proteins*, chapter 2, pages 13–24. Lippincott's illustrated reviews. Lippincott Williams & Wilkins, 2011. ISBN 9781608314126.

[15] HBIO1. Enzymes. `http://www.biologyguide.net/unit1/2_enzymes.htm`, 2004. Accessed on 23-04-2014.

[16] Willem Norde. Adsorption of proteins from solution at the solid-liquid interface. *Advances in Colloid and Interface Science*, 25:267 – 340, 1986.

[17] Willem Norde. Driving forces for protein adsorption at solid surfaces. *Macromolecular Symposia*, 103(1):5–18, 1996.

[18] Michael Rabe, Dorinel Verdes, and Stefan Seeger. Understanding protein adsorption phenomena at solid surfaces. *Advances in colloid and interface science*, 162(1):87–106, 2011.

[19] Thomas Boudou, Thomas Crouzier, Kefeng Ren, Guillaume Blin, and Catherine Picart. Multiple functionalities of polyelectrolyte multilayer films: new biomedical applications. *Advanced Materials*, 22(4):441–467, 2010.

[20] Jong-Dal Hong, Klaus Lowack, Johannes Schmitt, and Gero Decher. Layer-by-layer deposited multilayer assemblies of polyelectrolytes and proteins: from ultrathin films to protein arrays. In *Trends in Colloid and Interface Science VII*, pages 98–102. Springer, 1993.

[21] Yuri Lvov, Katsuhiko Ariga, Izumi Ichinose, and Toyoki Kunitake. Assembly of multicomponent protein films by means of electrostatic layer-by-layer adsorption. *Journal of the American Chemical Society*, 117(22):6117–6123, 1995.

[22] Mitsuhiko Onda, Yuri Lvov, Katsuhiko Ariga, and Toyoki Kunitake. Sequential reaction and product separation on molecular films of glucoamylase and glucose oxidase assembled on an ultrafilter. *Journal of Fermentation and Bioengineering*, 82(5):502 – 506, 1996. ISSN 0922-338X.

[23] Corinne R Wittmer, Jennifer A Phelps, W Mark Saltzman, and Paul R Van Tassel. Fibronectin terminated multilayer films: protein adsorption and cell attachment studies. *Biomaterials*, 28(5):851–860, 2007.

[24] Claire S Peyratout and Lars Dähne. Tailor-made polyelectrolyte microcapsules: from multilayers to smart containers. *Angewandte Chemie International Edition*, 43(29):3762–3783, 2004.

[25] Frank Caruso, Dieter Trau, Helmuth Möhwald, and Reinhard Renneberg. Enzyme encapsulation in layer-by-layer engineered polymer multilayer capsules. *Langmuir*, 16(4):1485–1488, 2000.

[26] Nadejda G Balabushevitch, Gleb B Sukhorukov, Natalia A Moroz, Dmitry V Volodkin, Natalia I Larionova, Edwin Donath, and Helmuth Mohwald. Encapsulation of proteins by layer-by-layer adsorption of polyelectrolytes onto protein aggregates: Factors regulating the protein release. *Biotechnology and bioengineering*, 76(3):207–213, 2001.

[27] Olga P. Tiourina, Alexei A. Antipov, Gleb B. Sukhorukov, Natalia I. Larionova, Yuri Lvov, and Helmuth Mhwald. Entrapment of -chymotrypsin into hollow polyelectrolyte microcapsules. *Macromolecular Bioscience*, 1(5): 209–214, 2001. ISSN 1616-5195.

[28] Radostina Georgieva, Sergio Moya, M Hin, Rita Mitlöhner, Edwin Donath, Holger Kiesewetter, Helmuth Möhwald, and Hans Bäumler. Permeation of macromolecules into polyelectrolyte microcapsules. *Biomacromolecules*, 3 (3):517–524, 2002.

[29] Dmitry V Volodkin, Alexander I Petrov, Michelle Prevot, and Gleb B Sukhorukov. Matrix polyelectrolyte microcapsules: new system for macromolecule encapsulation. *Langmuir*, 20(8):3398–3406, 2004.

[30] Constant Vodouhê, Erell Le Guen, Juan Mendez Garza, Gregory Francius, Christophe Déjugnat, Joëlle Ogier, Pierre Schaaf, Jean-Claude Voegel, and Philippe Lavalle. Control of drug accessibility on functional polyelectrolyte multilayer films. *Biomaterials*, 27(22):4149–4156, 2006.

[31] Damien Mertz, Cédric Vogt, Joseph Hemmerlé, Jérôme Mutterer, Vincent Ball, Jean-Claude Voegel, Pierre Schaaf, and Philippe Lavalle. Mechanotransductive surfaces for reversible biocatalysis activation. *Nature Materials*, 8(9):731–735, 2009.

[32] Cedric Vogt, Vincent Ball, Jerome Mutterer, Pierre Schaaf, Jean-Claude Voegel, Bernard Senger, and Philippe Lavalle. Mobility of proteins in highly hydrated polyelectrolyte multilayer films. *The Journal of Physical Chemistry B*, 116(17):5269–5278, 2012.

[33] Weiyong Yuan, Zhisong Lu, Huili Wang, and Chang Ming Li. Stimuli-free reversible and controllable loading and release of proteins under physiological conditions by exponentially growing nanoporous multilayered structure. *Advanced Functional Materials*, 22(9):1932–1939, 2012. ISSN 1616-3028.

[34] Gabriela V Martins, Esther G Merino, Joao F Mano, and Natália M Alves. Crosslink effect and albumin adsorption onto chitosan/alginate multilayered systems: An in situ qcm-d study. *Macromolecular bioscience*, 10(12):1444–1455, 2010.

[35] Roger A Sheldon. Enzyme immobilization: the quest for optimum performance. *Advanced Synthesis & Catalysis*, 349(8-9):1289–1307, 2007.

[36] Cristina Garcia-Galan, Ángel Berenguer-Murcia, Roberto Fernandez-Lafuente, and Rafael C Rodrigues. Potential of different enzyme immobilization strategies to improve enzyme performance. *Advanced Synthesis & Catalysis*, 353(16):2885–2904, 2011.

[37] Cesar Mateo, Jose M Palomo, Gloria Fernandez-Lorente, Jose M Guisan, and Roberto Fernandez-Lafuente. Improvement of enzyme activity, stability and selectivity via immobilization techniques. *Enzyme and Microbial Technology*, 40(6):1451–1463, 2007.

[38] Barbara Krajewska. Application of chitin-and chitosan-based materials for enzyme immobilizations: a review. *Enzyme and microbial technology*, 35(2): 126–139, 2004.

[39] Marguerite Rinaudo. Main properties and current applications of some polysaccharides as biomaterials. *Polymer International*, 57(3):397–430, 2008.

[40] Felippe J Pavinatto, Luciano Caseli, and Osvaldo N Oliveira Jr. Chitosan in nanostructured thin films. *Biomacromolecules*, 11(8):1897–1908, 2010.

[41] Teruyuki Komatsu. Protein-based nanotubes for biomedical applications. *Nanoscale*, 4(6):1910–1918, 2012.

[42] Charles R Martin. Nanomaterials- A membrane-based synthetic approach. *Science*, 266(5193):1961–1966, 1994.

[43] Charles R Martin. Membrane-based synthesis of nanomaterials. *Chemistry of Materials*, 8(8):1739–1746, 1996.

[44] Labtalk: Template tunes nanowire-nanotube hybrid arrays. `http://nanotechweb.org/cws/article/lab/38377`, 2009. Accessed on 24-04-2014.

[45] Omar Azzaroni and KH Aaron Lau. Layer-by-layer assemblies in nanoporous templates: nano-organized design and applications of soft nanotechnology. *Soft Matter*, 7(19):8709–8724, 2011.

[46] Etienne Ferain and Roger Legras. Track-etch templates designed for micro- and nanofabrication. *Nuclear Instruments and Methods in Physics Research Section B: Beam Interactions with Materials and Atoms*, 208:115–122, 2003.

[47] Diyaa AlMawlawi, Neil Coombs, and Martin Moskovits. Magnetic properties of Fe deposited into anodic aluminum oxide pores as a function of particle size. *Journal of applied physics*, 70(8):4421–4425, 1991.

[48] Sufen Ai, Gang Lu, Qiang He, and Junbai Li. Highly flexible polyelectrolyte nanotubes. *Journal of the American Chemical Society*, 125(37):11140–11141, 2003.

[49] Zhijian Liang, Andrei S Susha, Aimin Yu, and Frank Caruso. Nanotubes prepared by layer-by-layer coating of porous membrane templates. *Advanced Materials*, 15(21):1849–1853, 2003.

[50] Cécile J Roy, Christine Dupont-Gillain, Sophie Demoustier-Champagne, Alain M Jonas, and Jessem Landoulsi. Growth mechanism of confined polyelectrolyte multilayers in nanoporous templates. *Langmuir*, 26(5):3350–3355, 2010.

[51] Halima Alem, Françoise Blondeau, Karine Glinel, Sophie Demoustier-Champagne, and Alain M Jonas. Layer-by-layer assembly of polyelectrolytes in nanopores. *Macromolecules*, 40(9):3366–3372, 2007.

[52] Jun Young Kim, Jonathan P DeRocher, Pan Mao, Jongyoon Han, Robert E Cohen, and Michael F Rubner. Formation of nanoparticle-containing multilayers in nanochannels via layer-by-layer assembly. *Chemistry of Materials*, 22(23):6409–6415, 2010.

[53] Aimin Yu, Zhijian Liang, and Frank Caruso. Enzyme multilayer-modified porous membranes as biocatalysts. *Chemistry of materials*, 17(1):171–175, 2005.

[54] Shifeng Hou, Jiahai Wang, and Charles R Martin. Template-synthesized protein nanotubes. *Nano letters*, 5(2):231–234, 2005.

[55] Jessem Landoulsi, Cécile J Roy, Christine Dupont-Gillain, and Sophie Demoustier-Champagne. Synthesis of collagen nanotubes with highly regular dimensions through membrane-templated layer-by-layer assembly. *Biomacromolecules*, 10(5):1021–1024, 2009.

[56] Shelley A Dougherty, Dawei Zhang, and Jianyu Liang. Fabrication of protein nanotubes using template-assisted electrostatic layer-by-layer methods. *Langmuir*, 25(22):13232–13237, 2009.

[57] Caihong Tao, Shengrong Yang, and Junyan Zhang. Template-synthesized protein nanotubes with controlled size based on layer-by-layer method. *Chinese Journal of Chemistry*, 28(2):325–328, 2010.

[58] Xue Qu, Gang Lu, Eishun Tsuchida, and Teruyuki Komatsu. Protein nanotubes comprised of an alternate layer-by-layer assembly using a polycation as an electrostatic glue. *Chemistry-A European Journal*, 14(33):10303–10308, 2008.

[59] Xue Qu, Nao Kobayashi, and Teruyuki Komatsu. Solid nanotubes comprising α-fe2o3 nanoparticles prepared from ferritin protein. *ACS nano*, 4(3): 1732–1738, 2010.

[60] Ryunosuke Kato and Teruyuki Komatsu. Structure and photocatalytic activity of iron oxide nanotubes prepared from ferritin. *Journal of Inorganic and Organometallic Polymers and Materials*, 23(1):167–171, 2013.

[61] Teruyuki Komatsu, Hiromi Terada, and Nao Kobayashi. Protein nanotubes with an enzyme interior surface. *Chemistry-A European Journal*, 17(6):1849–1854, 2011.

[62] Teruyuki Komatsu, Takaaki Sato, and Christoph Boettcher. Human serum albumin nanotubes with esterase activity. *Chemistry-an Asian Journal*, 7 (1):201–206, 2012.

[63] Teruyuki Komatsu, Xue Qu, Hiromi Ihara, Mitsuhiro Fujihara, Hiroshi Azuma, and Hisami Ikeda. Virus trap in human serum albumin nanotube. *Journal of the American Chemical Society*, 133(10):3246–3248, 2011.

[64] Ryunosuke Kato and Teruyuki Komatsu. Protein nanotube arrays immobilized on solid substrates: Molecular trap in aqueous medium. *Chemistry Letters*, 40(12):1338–1339, 2011.

[65] Xue Qu and Teruyuki Komatsu. Molecular capture in protein nanotubes. *ACS nano*, 4(1):563–573, 2010.

[66] Shun Goto, Yusuke Amano, Motofusa Akiyama, Christoph Bottcher, and Teruyuki Komatsu. Gold nanoparticle inclusion into protein nanotube as a layered wall component. *Langmuir*, 29(46):14293–14300, 2013.

[67] V Smuleac, DA Butterfield, and D Bhattacharyya. Layer-by-layer-assembled microfiltration membranes for biomolecule immobilization and enzymatic catalysis. *Langmuir*, 22(24):10118–10124, 2006.

[68] Scott R Lewis, Saurav Datta, Minghui Gui, Eric L Coker, Frank E Huggins, Sylvia Daunert, Leonidas Bachas, and Dibakar Bhattacharyya. Reactive nanostructured membranes for water purification. *Proceedings of the National Academy of Sciences*, 108(21):8577–8582, 2011.

[69] Khek-Khiang Chia, Michael F. Rubner, and Robert E. Cohen. pH-responsive reversibly swellable nanotube arrays. *Langmuir*, 25(24):14044–14052, 2009.

[70] Eun Seok Gil and Samuel M Hudson. Stimuli-reponsive polymers and their bioconjugates. *Progress in polymer science*, 29(12):1173–1222, 2004.

[71] Hidenori Kuroki, Ihor Tokarev, and Sergiy Minko. Responsive surfaces for life science applications. *Annual Review of Materials Research*, 42:343–372, 2012.

[72] Maria R Aguilar, Carlos Elvira, Alberto Gallardo, Blanca Vázquez, and Julio S Román. Smart polymers and their applications as biomaterials. *Topics in tissue engineering*, 3:1–27, 2007.

[73] Martien A Cohen Stuart, Wilhelm TS Huck, Jan Genzer, Marcus Müller, Christopher Ober, Manfred Stamm, Gleb B Sukhorukov, Igal Szleifer, Vladimir V Tsukruk, Marek Urban, et al. Emerging applications of stimuli-responsive polymer materials. *Nature Materials*, 9(2):101–113, 2010.

[74] Howard G. Schild. Poly(n-isopropylacrylamide): experiment, theory and application. *Progress in Polymer Science*, 17(2):163–249, 1992.

[75] Roland Steitz, Vincent Leiner, Klaus Tauer, Victor Khrenov, and Regine v Klitzing. Temperature-induced changes in polyelectrolyte films at the solid–liquid interface. *Applied Physics A*, 74(1):s519–s521, 2002.

[76] Michael J Serpe, Clinton D Jones, and L Andrew Lyon. Layer-by-layer deposition of thermoresponsive microgel thin films. *Langmuir*, 19(21):8759–8764, 2003.

[77] John F Quinn and Frank Caruso. Facile tailoring of film morphology and release properties using layer-by-layer assembly of thermoresponsive materials. *Langmuir*, 20(1):20–22, 2004.

[78] Karine Glinel, Christophe Déjugnat, Michelle Prevot, Björn Schöler, Monika Schönhoff, and Regine v Klitzing. Responsive polyelectrolyte multilayers. *Colloids and Surfaces A: Physicochemical and Engineering Aspects*, 303(1): 3–13, 2007.

[79] Cong-Duan Vo, Andreas Schmid, Steven P. Armes, Kenichi Sakai, and Simon Biggs. Surface ATRP of hydrophilic monomers from ultrafine aqueous silica sols using anionic polyelectrolytic macroinitiators. *Langmuir*, 23(2):408–413, 2007. doi: 10.1021/la063003j.

[80] Timothy M Fulghum, Derek L Patton, and Rigoberto C Advincula. Fuzzy ternary particle systems by surface-initiated atom transfer radical polymerization from layer-by-layer colloidal core-shell macroinitiator particles. *Langmuir*, 22(20):8397–8402, 2006.

[81] Damien Mertz, Joseph Hemmerlé, Jérôme Mutterer, Sophie Ollivier, Jean-Claude Voegel, Pierre Schaaf, and Philippe Lavalle. Mechanically responding nanovalves based on polyelectrolyte multilayers. *Nano Letters*, 7(3):657–662, 2007.

[82] Cedric Vogt, Damien Mertz, Karim Benmlih, Joseph Hemmerle, Jean-Claude Voegel, Pierre Schaaf, and Philippe Lavalle. Layer-by-layer enzymatic plat-

form for stretched-induced reactive release. *ACS Macro Letters*, 1(7):797–801, 2012.

Chapter 3

Enzyme multilayer films and modified porous membranes for biocatalysis

In this chapter we investigate the influence of substrate geometry and confinement on the layer-by-layer growth of biomacromolecular films and their resulting biocatalytic activity. Detailed analysis of enzyme immobilization within cylindrical submicron pores and on planar surfaces reveals some interesting differences.

3.1 Introduction

Layer-by-layer assembly (LbL) of bioactive molecules offers a wide range of applications in the biomedical field, from improved biocompatibility of implants to drug delivery, diagnostics and bioseparations. LbL assembly is a simple and versatile method that allows the build-up of functional coatings under mild conditions and a very good control of the film properties at the nanoscale [1, 2, 3, 4]. As originally described [5], LbL assembly consists in the alternate adsorption of a polyanion and a polycation onto oppositely charged surfaces. In the last twenty years, a variety of biomolecules *e.g.*, proteins, virus, colloids and polysaccharides, have been incorporated in LbL films [3, 6, 7, 8]. As the library of available molecules for LbL assembly increases, researchers attempt to gain a better understanding of the involved phenomena involved and to develop industrial processes.

Investigation of protein and enzyme adsorption in LbL systems started almost two decades ago and still continues nowadays [4, 9]. One of the main reported advantages of LbL versus other techniques is the large amount of proteins loaded in specific microenvironments, compared to techniques as solvent casting, covalent binding, electropolymerization or monolayer physical adsorption. In addition, the polyion of opposite charge could help to preserve the secondary structure when facing denaturating agents [4, 10]. Since LbL process has no restrictions with respect to adsorbing substrate size and topology [11], protein multilayer films have been deposited on planar substrates, colloidal particles and membranes [4, 12]. Therefore, different architectures from protein planar films and coated microparticles, to hollow capsules, coated membranes and nanotubes have been prepared. While most of the LbL research has been done on planar or spherical surfaces, some groups also investigated deposition in membranes with cylindrical pores [12, 13, 14].

The preparation of complex architectures by LbL paves the way to manufacture microreactors and sensing devices in a bottom-up approach. Nevertheless, the synthesis is not straightforward due to the confinement of macromolecules in convoluted surfaces. Previous studies showed differences on the mechanism of polyelectrolyte layer adsorption between flat surfaces and nanopores [13, 15, 16]. On the bright side, the available high surface area on micro or nanos-

tructured surfaces makes them attractive supports for biocatalysis. Caruso and collaborators reported the assembly of enzymes by LbL in planar surfaces and porous membranes [17], using peroxidase/poly(styrenesulfonate) complexes with poly(allylamine hydrochloride) layers. They investigated whether or not it was possible to counterbalance substrate diffusion restrictions on LbL films with larger surface area. Their results showed enhanced activity in the membranes after a few layers were adsorbed, and up to an order of magnitude larger activities than identical films deposited on nonporous supports.

In the present study, we prepared chitosan/β-lactamase multilayer films on flat surfaces and within porous templates by LbL. Chitosan was used as polycation due to its well known protein-friendly behavior [18, 19, 20] and β-lactamase as polyanion, as it acts as a resistant and rather small enzyme [21]. A detailed comparison of growth, chemical composition and activity was performed to gain better understanding about the influence of support geometry on biocatalytic thin films.

3.2 Experimental section

3.2.1 Polyelectrolytes

Chitosan chloride (chit, DDA > 90%, Mw∼ 270k, Novamatrix) was used as polycation and β-lactamase (TEM-1 from *Enterobacter cloacae*, Sigma-Aldrich) was used as polyanion (isoelectric point, pI ≈ 4.9). Both polyelectrolytes were dissolved in MES (2-(4-morpholino)ethanesulfonic acid) buffer solution (100 mM, pH 6.5) to keep a concentration of 1 $mg.mL^{-1}$. Single-side polished silicon wafers (Si, <100> orientation, ACM) were cleaned in piranha solution prior to LbL deposition to prepare flat films. Conversely, track etched polycarbonate membranes (PCm) with a nominal 200 nm pore diameter, 21 μm thickness and a pore density of $6 \times 10^{8} \cdot cm^{-2}$, were provided by It4ip, Seneffe, Belgium (http://www.it4ip.be) and used as received to prepare nanotubes.

3.2.2 Layer-by-layer build-up

Polyelectrolyte multilayers were deposited by alternately dipping the support (Si wafers or PCm, Figure3.1) in polycation-polyanion solutions. The build-up started with polycation adsorption (5 min for Si wafers, 30 min for PCm), followed by two rinsing steps in MES buffer (2 min each) to remove loosely attached polyelectrolyte chains. Then, the surface with an excess of positive charge was dipped in the polyanion solution (also 5 or 30 min for Si wafer or PCm, respectively) and rinsed twice to complete one LbL cycle. This process was repeated until the desired number of cycles (n) was achieved. In the case of PCm, each 2 cycles a cotton swab with basic solution (NaOH pH∼ 12) of high ionic strength (3M NaCl) was used to scrub out the films that grew out of the pores [16].

3.2.3 Ellipsometry

Dry thickness of flat films deposited on Si wafers was measured by ellipsometry. We used a spectroscopic ellipsometer Uvisel from Horiba-Jobin-Yvon at an incidence angle of 70° in a wavelength range from 400 to 800 nm. Ellipsometric data were fitted using the DeltaPsi 2 software with a three layered model: silicon

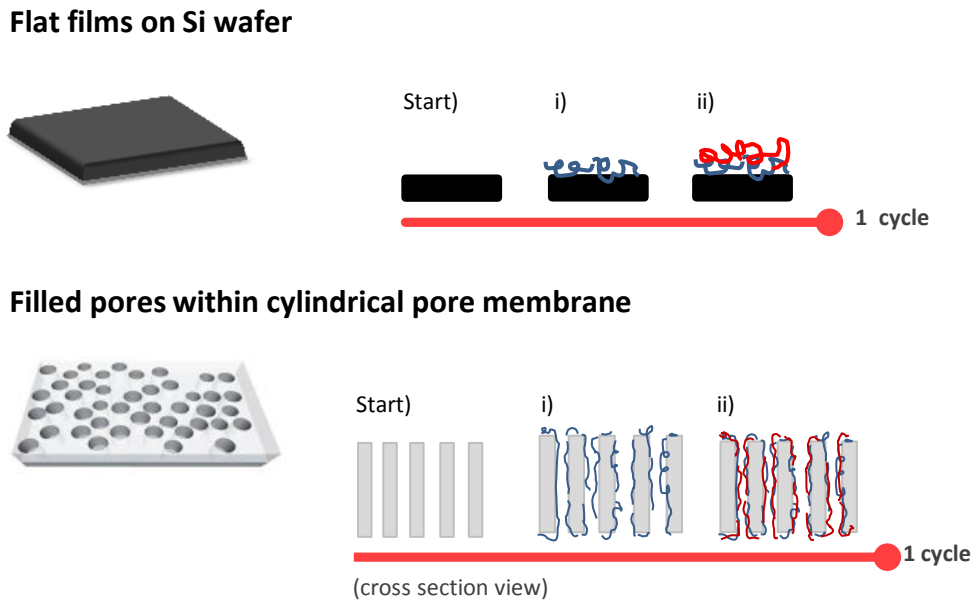

Figure 3.1: Different supports for LbL deposition and schematic adsorption to complete one LbL cycle. Polycation (i) and polyanion (ii) were adsorbed on silicon wafers (top) and within the pores of a PC membrane (bottom).

(bulk), native silicon oxide (1.5 nm thickness), and a polymer film. The refractive index of the multilayer films was modeled by a transparent Cauchy layer and the measurement was carried out three times at different points on the substrate to obtain an average thickness for a sample.

To ensure the validity of the data, the goodness of the fit was verified (minimizing the squared difference, χ^2) and the refractive index was kept between 1.40 and 1.57 for all the thin films prepared in this section.

3.2.4 Gas-Flow Porometry Measurements

Polyelectrolyte multilayer growth in membrane nanopores was monitored by measuring the evolution of the mean diameter of the pores as a function of the number of LbL cycles. This was performed using gas-flow porometry on air-dried samples at room temperature, following a protocol previously reported by our group [16]. Briefly, a PCm was hold perpendicularly to a nitrogen flux with a known pressure ranging between 10^4 -10^5 Pa, then the flux downstream from the sample was

measured (mL.min^{-1}) using a flowmeter (Agilent). After at least 10 flow measurements, an average flow was taken (with a maximum ± 5% margin of error) and the pore size calculated using a relationship based on Knudsen diffusion and the Hagen-Poiseuille flow. The Knudsen diffusion flux and the viscous flux (J_{diff} and J_{visc}, mol.m^{-2}.s^{-1}) model a steady laminar flow of an incompressible fluid through a rigid-walled tube of constant radius, and are expressed respectively by:

$$J_{diff} = \frac{4}{3}\frac{d}{l}\frac{(P_{up} - P_{down})}{\sqrt{2\pi MRT}} \tag{3.1}$$

$$J_{visc} = \frac{d^2}{l}\frac{(P_{up}^2 - P_{down}^2)}{64\mu RT} \tag{3.2}$$

where d is the pore diameter (m), l is the thickness of the membrane (m), P_{up} and P_{ddown} are the pressures (Pa) upstream and downstream from the membrane, respectively, M is the gas molar weight (kg.mol^{-1}), μ is the dynamic viscosity of the gas (kg.m^{-1}s^{-1}), R is the ideal gas constant (J.K^{-1}mol^{-1}) and T is the gas temperature (K). The total volume flow rate ϕ (m^3.s^{-1}) from Eqs. 1.1 and 1.2 can be expressed by

$$\phi = (SP)\frac{RT}{P_{atm}}(J_{diff} + J_{visc}) \tag{3.3}$$

where S is the effective section area of the membrane (m^2), P_{atm} is the atmospheric pressure (Pa), and P is the transparency of the membrane, defined as

$$P = N\frac{\pi d^2}{4} \tag{3.4}$$

where N is the pore density (m^{-2}). Finally, the film thickness of a given sample was calculated as half of the difference between the pore diameter of the virgin membrane and the pore diameter after LbL deposition.

3.2.5 Electron Microscopy

Once LbL deposition in the PCm was performed, the samples were air-dried and then the PC was dissolved in dichloromethane. The released nanotubes were then collected by passing the solution through a TEM copper grid several times and imaged with a LEO 922 TEM microscope operating at 200 kV.

3.2.6 Infrared Spectroscopy

Multilayer flat films were removed from the silicon wafers with the help of a razor blade and analyzed as powder by Attenuated Total Reflectance Fourier Transform Infrared (ATR-FTIR) spectroscopy with a Perkin Elmer Spectrum 400 FTIR spectrometer on a single reflection diamond top-plate. The crystal area was cleaned before each acquisition and the background corrected. Spectra were recorded at a resolution of 4 cm^{-1} with 32 averaged interferograms from 650 to 4000 cm^{-1}.

Alternatively, the infrared spectra of the samples was recorded by a Nicolet Nexus 870 spectrometer in transmittance mode. In this case, the multilayered films were supported on the silicon wafer and the signal of the support was subtracted. The chamber was purged with nitrogen for 10 minutes before acquisition, and 64 scans were collected and averaged for each spectrum with a resolution of 4 cm^{-1}.

3.2.7 Nuclear Magnetic Resonance

The resulting films (chitosan/β-lactamase)$_n$ and their pure components were analyzed by solid-state ^{1}H Magic Angle Spinning (MAS) NMR at high magnetic field (16.4 T, 700 MHz Bruker spectrometer) using an ultra-fast MAS probe (diameter 1.3 mm) and a Bruker temperature control unit BCU Xtreme. The flat films were removed from the silicon wafers with a razor blade and the nanotubes were collected over polytetrafluoroethylene (teflon, PTFE) after membrane removal to avoid the signals raising from polycarbonate (indeed, PTFE molecules are free of hydrogen). Pure samples of chitosan and β-lactamase were analyzed without any further purification. All ^{1}H NMR spectra were referenced towards TMS (0 ppm)

by using adamantane as a secondary reference (1.87 ppm), and the analysis of the resulting spectra was done with DMFit software developed at CEMHTI [22]. Temperature and spinning rate dependence were studied and their influence is reported as Supporting Information at the end of this chapter.

To estimate the enzyme content in multilayer films (chitosan/β-lactamase) it was assumed that the ^{1}H NMR signal of the films is solely the sum of chitosan and β-lactamase pure spectra in variable ratios (Eq. 3.5, where A stands for the area of a given resonance peak). Furthermore, the area below the ^{1}H NMR signal was defined as a function of the number of protons *per* molecule (NH), the number of molecules (n) and a constant (k) (Eq. 3.6).

$$A_{TOT} = A_{chit} + A_{\beta-lac} \tag{3.5}$$

$$A_i = kNH_i n_i \tag{3.6}$$

Thus, the ratio of areas chitosan/β-lactamase was calculated and used to determine the molar ratio according to the Eq. 3.7, as follows:

$$\frac{n_{chit}}{n_{\beta-lac}} = \frac{A_{chit}}{A_{\beta-lac}} \frac{NH_{\beta-lac}}{NH_{chit}} \tag{3.7}$$

As the film is just made of the two polyelectrolytes, the molar ratio can be converted in molar fraction (y, Eq. 3.8-3.9), weight fraction (x, Eq 3.10) and finally the amount of enzyme can be calculated if the volume of the sample is known and a density of 1 g·cm^{-3} is considered (chitosan and β-lactamase have a density of 0.8 and 1.4 g·cm^{-3}, respectively).

$$y_{\beta-lac} + y_{chit} = 1 \tag{3.8}$$

$$y_{\beta-lac} = (1 + \frac{n_{chit}}{n_{\beta-lac}})^{-1} \tag{3.9}$$

$$x_{\beta-lac} = \frac{y_{\beta-lac} \times Mw_{\beta-lac}}{y_{\beta-lac} \times Mw_{\beta-lac} + (1 - y_{\beta-lac}) \times Mw_{chit}} \tag{3.10}$$

Where Mw stands for molecular weight, Mw_{chit} is 269000 g.mol^{-1} and $Mw_{\beta\text{-lac}}$ is

31515 g.mol^{-1} (considering the amino acid sequence Q6W9J1 reported by UniProt database [23]).

3.2.8 Activity assay

For all the films containing β-lactamase, the kinetics of nitrocefin hydrolysis (Figure 3.2) were followed by UV/Vis spectrophotometry (Agilent Cary 50) to determine the initial rate of hydrolysis V_0. The absorption spectrum was collected from 350 to 800 nm in standard cuvettes with 1.0 cm pathlength. Absorbance at 390 nm and at 485 nm were used to calculate the concentration of nitrocefin and the hydrolyzed substrate after reaction, using Lambert-Beer law. Extinction coefficients (ϵ) were determined after a calibration curve under the following working conditions: buffer MES 100mM, pH 6.5 and room temperature (ϵ_{390}=20000 M^{-1}cm^{-1}, ϵ_{485}=16700 M^{-1}cm^{-1}).

The immobilized enzyme was added to nitrocefin solution (2mL, 50μM in 100 mM MES buffer pH 6.5) as 1cm^2 of multilayer (chitosan/β-lactamase)$_n$ flat film on Si wafer or the LbL coating in PCm. All samples were stirred at 150 rpm (unless stated otherwise) on a shaker platform and samples were taken at different times until the amount of hydrolyzed nitrocefin reached a plateau (after around 90 min). A single value of activity reported for a (chitosan/β-lactamase)$_n$ film represents the average of duplicates in a series, and all the samples were prepared and analyzed in parallel.

3.2.9 Circular Dichroism

To characterize the structural changes of β-lactamase after immobilization, circular dichroism (CD) spectra of flat films were acquired from 320 to 190 nm on a Jasco J-810 spectropolarimeter. Instead of silicon wafers, 1 mm fused silica slides (Hellma Quartz Suprasil) were used to prepare the flat films. Each spectrum is an average of 3 scans and the signal was corrected for background using the quartz clean slide. The analysis was performed at room temperature.

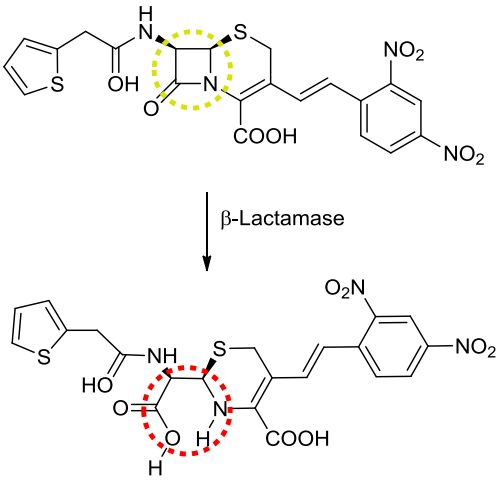

(a)

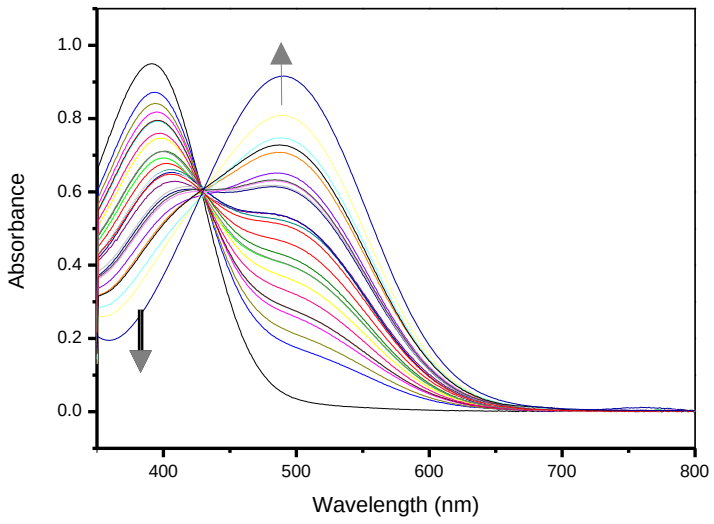

(b)

Figure 3.2: Hydrolysis of nitrocefin by β-lactamase (a) Nitrocefin absorbs at a wavelength of 390 nm, whereas hydrolyzed nitrocefin absorbs at 485 nm. (b) The evolution of the reaction can be followed by UV/Vis spectra as a function of time.

3.3 Results and Discussion

3.3.1 LbL growth on flat surfaces and nanopores

Multilayer films (chitosan/β-lactamase)$_n$ were prepared either on top of silicon wafers, called "flat films" thereafter, or within the pores of a polycarbonate membrane (PCm), called "filled pores" thereafter. Dried film thickness was determined by ellipsometry for flat films, and calculated from gas flow porometry measurements for filled pores (Figure 3.3). A linear-like growth was observed for flat films. However, the line describing flat films growth can be divided in two segments (Figure 3.3): the first one ($0 \leq n \leq 4$) exhibits a less steep slope than the second one ($4 \leq n \leq 12$). Slightly slower growth in early stages of LbL is not uncommon, and can be interpreted as an induction period. Schaaf *et al.* [24] attributed this phenomena to the influence and proximity to the support. On the contrary, the thickness of the multilayers within a PCm evolved as an inverted exponential decay. The thickness increased rapidly until 4 cycles, then the gain on thickness *per cycle* decreased from 4 to 12 cycles and became negligible afterwards. The larger adsorption of polyelectrolytes at the very beginning of LbL deposition in the pores *vs* flat surfaces is interpreted as an increase in surface contacts of the diffusing macromolecule, as discussed by Janshoff *et al.* in more details [25]. The transition from a first "fast growing" to a second (and slower) regime of growth was previously reported by our group [16], for poly(allylamine hydrochloride)/poly(styrene sulfonate) assembly in cylindrical nanopores. This transition is associated to a decreased diffusion of the polyelectrolyte chains into the pores, which occurs when adsorbed polyelectrolytes start to interconnect with each other across the pore. It is also important to note that the films (chitosan/β-lactamase)$_n$ never fully closed the pores to gas flow after the LbL. Instead, a minimum pore size $\sim$ 60 nm was reached for a starting pore size of 180 nm. To understand the last finding, we recall that LbL buildup occurs in aqueous media and a pore that might be closed under water would remain open after drying as the thickness of the film decreases when the polymer chains shrink [16]. Furthermore, the thickness of filled pores (chitosan/β-lactamase)$_4$ was close to the value reported for (poly-L-arginine/myoglobin)$_3$ by Qu *et al.* [26] in a 400 nm pore.

Therefore, the later result suggests that the film thickness in the pores depends on the globular size of the chosen protein (β-lactamase: 3 nm $\times$ 4nm $\times$ 5nm [27]) for n $\leq$ 4. However, as the pore becomes smaller the confinement is stronger, leading to very different growth curves between flat surfaces and pores [16, 28].

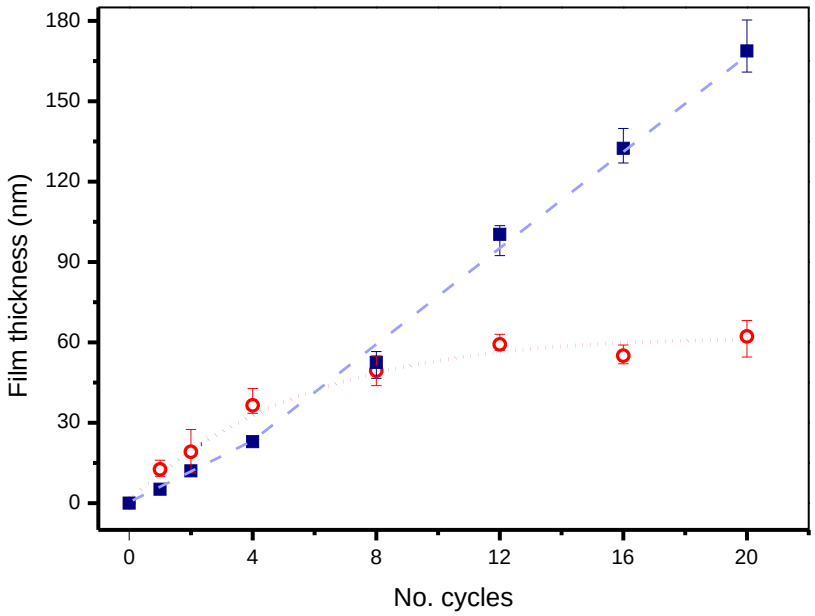

Figure 3.3: Evolution of film thickness as a function of the number of cycles (chitosan/β-lactamase)$_n$ on flat films (■) and filled pores in PCm (○). Error bars correspond to the range of thickness values measured for at least two independent experiments. Dashed and dotted lines are guides to the eye.

(chitosan/β-lactamase)$_n$ nanotubes can be obtained after template dissolution and characterized by TEM. As can be seen on Figure 3.4, the outside diameter (180 $\pm$ 5 nm) and the length (19 $\pm$ 1μm) are in good agreement with the characteristic of the PCm that were used as templates. Both nanotube images show very flexible nanotubes regardless the number of LbL cycles. It seems that the large aspect ratio together with the intrinsic lack of rigidity from chitosan or β-lactamase favors the presence of twists and waves in the observed nanotubes.

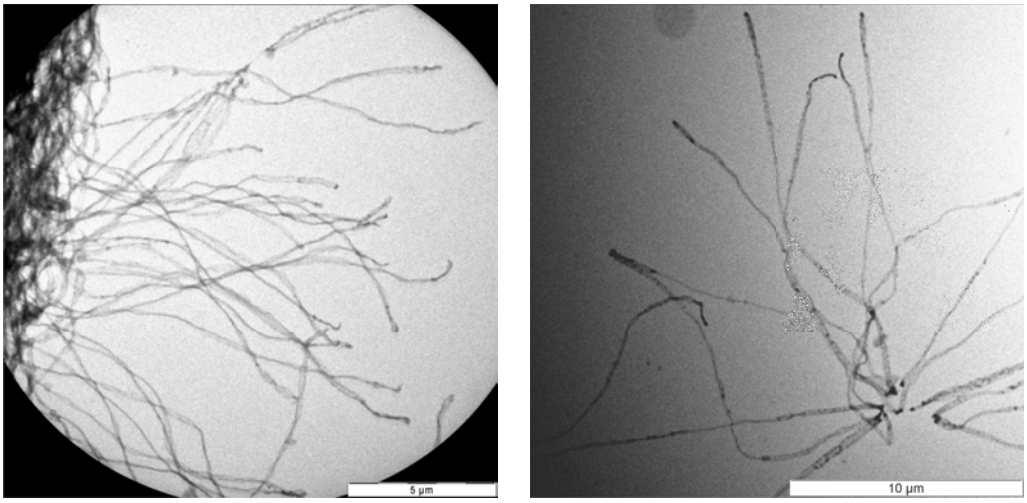

(a) 3 cycles (b) 20 cycles

Figure 3.4: Flexible nanotubes (chitosan/β-lactamase)$_n$ obtained from the PCm and observed by TEM after membrane removal, (a) n = 3 and (b) n = 20.

3.3.2 Enzyme content

A first attempt to determine the chemical composition of the multilayer flat films (chitosan/β-lactamase)$_n$ was done by infrared spectroscopy using either transmittance mode or ATR-FTIR. The film was analyzed on top of the silicon wafer for transmittance mode, or collected as powder for ATR-FTIR. Figure 3.5 shows the ATR spectrum of the pure components (chitosan, β-lactamase) and the resulting film. Infrared signals were assigned (Table 3.1) according to Almodovar *et al.* and Cerchiara *et al.* [29, 30] for chitosan, and following Barth [31] and Jena Library [32] for β-lactamase.

The ATR-FTIR spectra of the flat film (chitosan/β-lactamase) is in fact a mixture of the pure components and a similar result was observed using transmittance mode (Supporting Information 3.5). However, it is difficult to elucidate the chemical composition of the films, as the IR spectra of the pure polyelectrolyte precursors are very similar due to the dominant presence of amide, carbonyl and hydroxyl groups and therefore, similar absorption bands. To overcome those similarities, we moved on to a more sensitive technique in terms of chemical environment: solid-state ^{1}H MAS NMR.

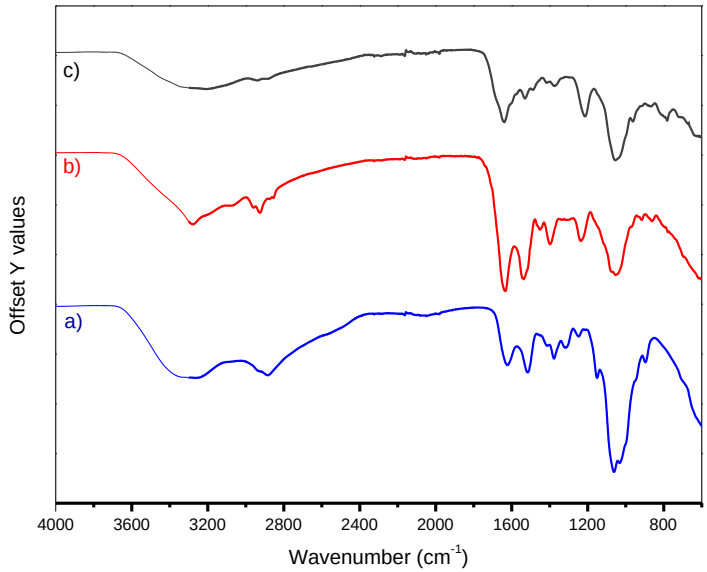

Figure 3.5: ATR-FTIR spectra of the polyelectrolytes involved on LbL buildup a) chitosan, b) β-lactamase, and c) (chitosan/β-lactamase)$_{18}$ film.

Table 3.1: Assignment of chitosan(top) and β-lactamase(bottom) infrared bands.

Absorption (cm^{-1})	Peak assignment
3500-3200	-OH Stretching from aliphatic chains
2916, 2850	C-H Stretching from aliphatic chains
1625, 1515	NH_2 Scissoring
1379	-OH Bending
1152	C-O-C Asymmetric stretch
1100-1000	Saccharide ring vibrations and C-N stretch
3300, 3100	N-H stretching vibration (amide A, amide B)
3000-2850	CH stretch alkanes
1636	C=O backbone stretching vibration (amide I)
1541	N-H bending and C-N stretching vibration (amide II)
1400-1240	COO^- and C-O stretching from Asp[i] and Glu[ii]
1150, 1075	C-O stretching from Thr[iii]
1030	C-O stretching from Ser[iv]

[i] Aspartic acid, [ii] Glutamic acid, [iii] Threonine, [iv] Serine.

The ^{1}H NMR spectra of chitosan and β-lactamase were collected as a single pulse at 30 °C under strong magnetic field (700 MHz), Figure 3.6. While it was possible to assign chemical shifts for chitosan according to Lavertu's reference

[33], the full chemical shift description for the protein signals would require multinuclear NMR or perdeuterated molecules and was out of the scope of this study. In general, it is known that the backbone peaks are present from 12 to 6.5 ppm and all this range has been reported in detail by Savard *et al.* [34]. Nonetheless, the region of interest here is associated to some of the lateral chains where chemical shifts of chitosan do not overlap. More precisely, in the region from 2 to 0 ppm (darker area on Fig. 3.6), the alkyl groups from β-lactamase display an intense signal and chitosan spectra appears almost "clean". This fact made possible to calculate the stoichiometry chitosan: β-lactamase, because the individual contribution of each molecular specie to the spectrum of a mixture (chitosan: β-lactamase) can be identified. Herein, we assumed that the ratio between the total area of β-lactamase (15 to 0 ppm) and the area between 2 to 0 ppm is a *constant*. Thus, this *constant* was easily extracted from the pure β-lactamase spectrum (collected under the same conditions than the films/nanotubes). Then, the area associated to β-lactamase ($A_{\beta-lac}$) in the spectrum of a mixture (chitosan + β-lactamase) was calculated multiplying the area 2 to 0 ppm by the *constant*. And finally, the total area of β-lactamase ($A_{\beta-lac}$) was subtracted from the total area of the mixture (A_{TOT}) to determine the area associated to chitosan (A_{chit}). The ratio of areas was further converted into molar ratio and β-lactamase weight fraction as described above (Section 3.2.7).

A set of multilayer films and nanotubes (chitosan/β-lactamase)$_n$ were collected as powder or supported on teflon membranes and analyzed by ^{1}H fast MAS NMR using the same protocol than for the pure polyelectrolytes. In the Figure 3.7, it is possible to observe at a glance that 1) β-lactamase was present in every kind of film (see the 2 to 0 ppm region), 2) the flat films show significant broadening of the signal around -0.5 ppm. The nature of this negative signal is unknown. At first, we thought this broadening was related to the rotor (solid-state NMR sample holder); since the broad signal faded away as the number of cycles (n) increased, meaning that the amount of sample increased as well. Nonetheless, the shoulder below 0 ppm remained in flat films after subtracting the rotor signal contribution from all the samples.

More important to observe in the Figure 3.7, the signal of the nanotubes remained almost constant along the build-up, whereas the flat films clearly changed

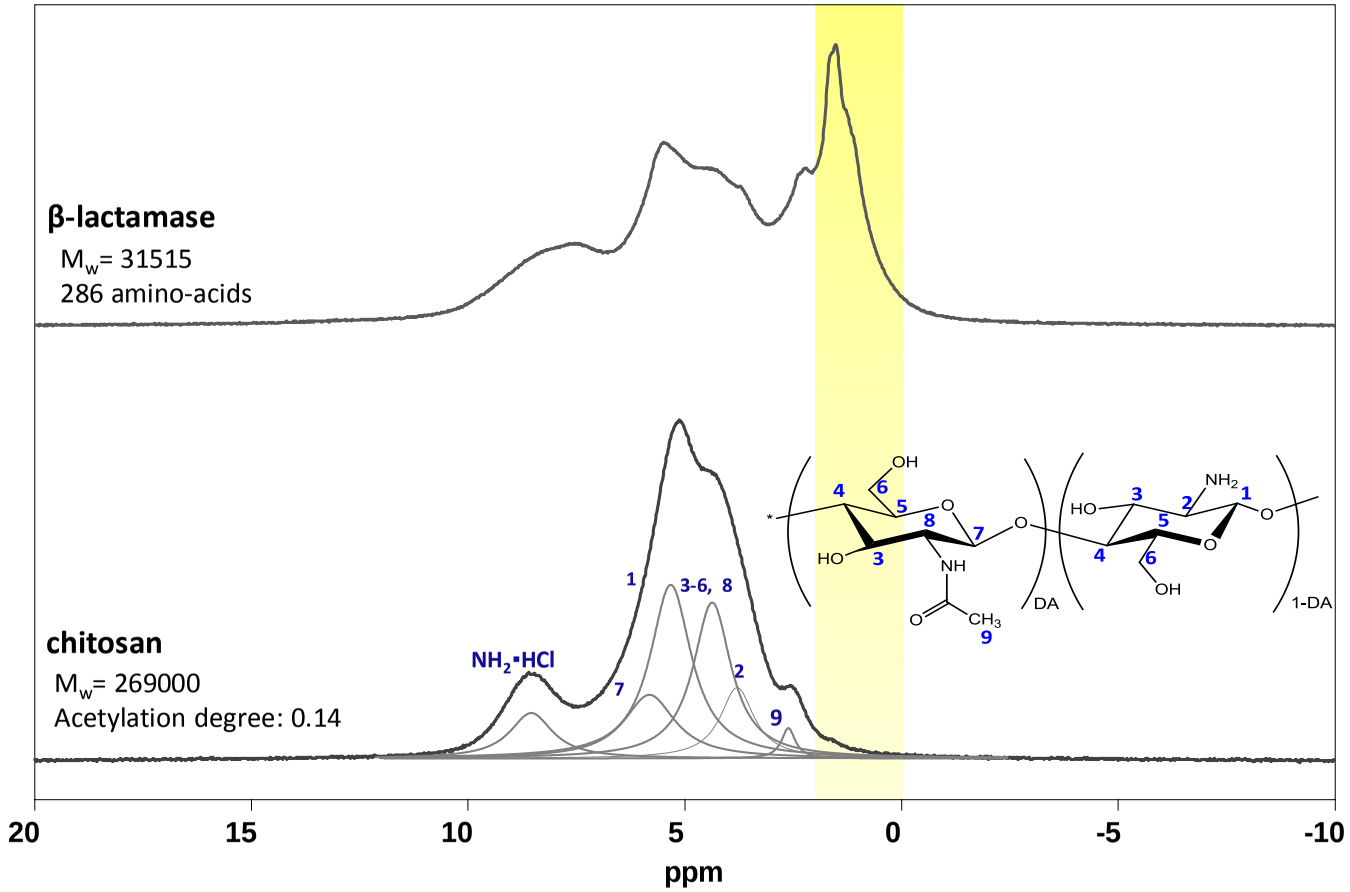

Figure 3.6: ^{1}H fast MAS NMR spectra of the pure polyelectrolytes chitosan(bottom), β-lactamase(top). Darker area (2 - 0 ppm) where the spectra do not overlap was used to determine chemical composition in multilayer films. *Note: In the chemical structure of chitosan, DA stands for degree of acetylation, and (1-DA) for degree of deacetylation.

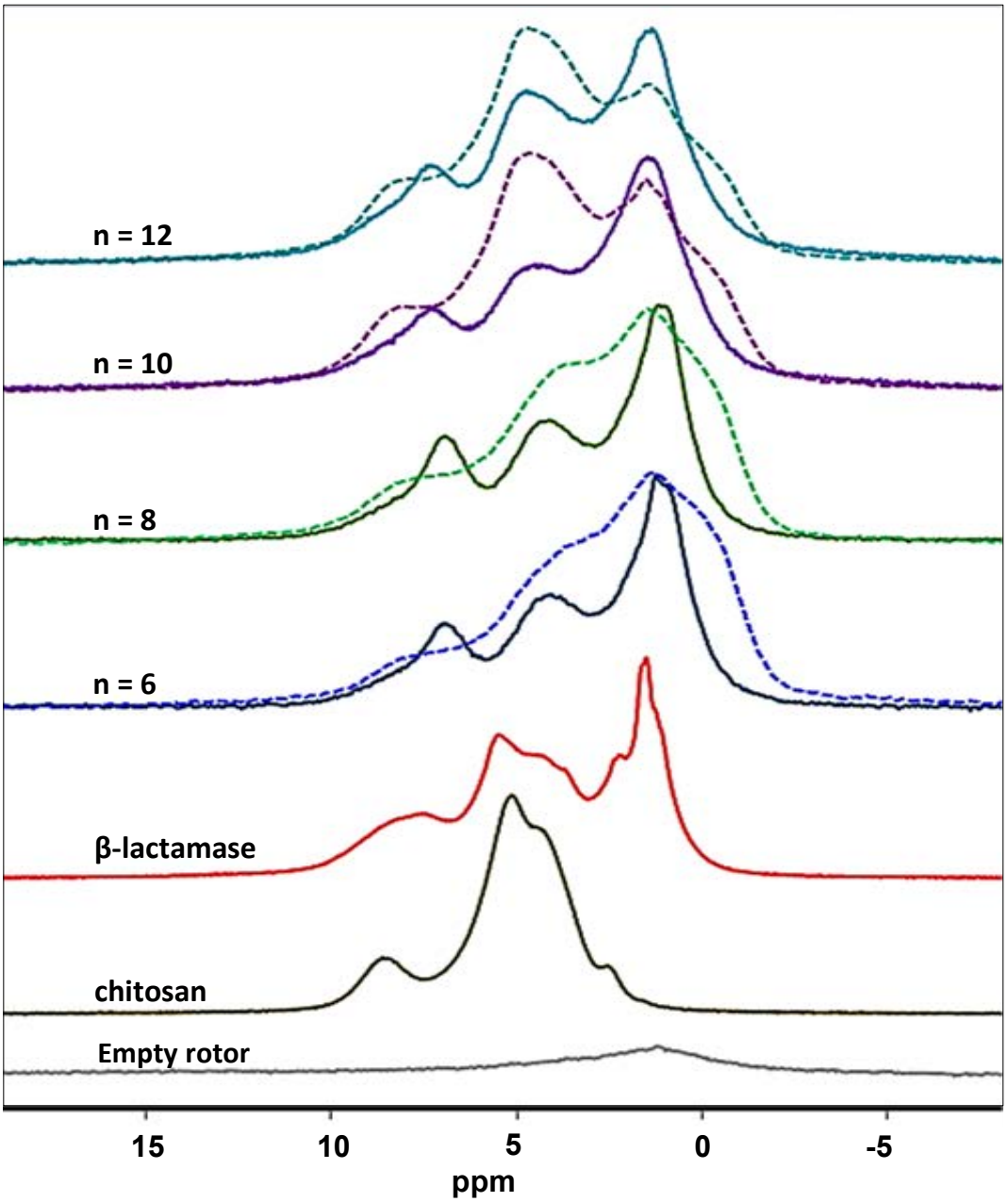

Figure 3.7: ^{1}H MAS NMR spectra of the empty rotor, chitosan, β-lactamase, the resulting films (chitosan/β-lactamase)$_{n}$ as flat films (dashed lines) or nanotubes (solid lines). All the samples were analyzed as powders.

from n = 6 to 12 cycles. Since the components of the various films are identical, it was assumed that variations in the spectra are related to different ratios of the chemical species involved. To investigate these phenomena, the chemical composition was calculated for all the films considering that the area between 0 and 2 ppm corresponds only to β-lactamase. If the number of protons in alkyl chains and the total number of protons is constant for the enzyme at any given time, then the total area contribution of the enzyme in a mixture can be calculated. Therefore, the molar ratio chitosan: β-lactamase was calculated using the ratio of areas, and converted to weight fraction, Table 3.2. It was found that in the nanotubes, the weight fraction is very high and it fluctuates around 0.90, or expressed as molar ratio ≈ 20 repeating units of chitosan per β-lactamase molecule. This value is close to the results obtained for the binding of β-lactoglobulin to sodium poly(styrenesulfonate), observed by Dubin *et al.* [35], where in average 17 units repeating units are bound to a protein molecule. Different titration techniques, such as calorimetry and turbidimetry, led also to 10 to 100 repeating units binding to a protein molecule to achieve charge compensation [35, 36].

Table 3.2: β-lactamase weight fraction (x) in (chitosan/β-lactamase)$_n$ LbL

n	Flat Films	Nanotubes
6	0.92	0.93
8	0.91	0.92
10	0.79	0.86
12	0.67	0.89

* Mass fraction can vary up to 5%, depending on the baseline correction of the spectra and the precise integrated area.

Conversely, the relative amount of enzyme in flat films shows a much stronger decrease along the build-up. Roughly speaking, the enzyme weight fraction drops from 0.90 to 0.70 from n= 6 to 12 cycles. In this situation, the number of repeating units of chitosan *per* enzyme rises from 20 to 80. To explain this result, we could think about a restructuring film that presents (1) changes in topography of the absorbing surface *i.e.* increasing roughness of the film and formation of aggregates, and/or (2) local changes in the zeta potential of the surface that

were overcompensated. As Dubin *et al.* [35] explained, the more repeating units surround a single protein, the more loose is the interaction polymer-protein. On the other hand, structural changes are insignificant in the nanotubes because an enzyme that is released from one site can be easily reabsorbed due to the large surface area. Again, there is a maximum value of thickness in the pores (around 60 nm), above which negligible changes in stoichiometry were detected.

3.3.3 Enzyme conformation

To assess potential conformational changes of the enzyme due to its immobilization in the multilayered films, circular dichroism spectrum of a (chitosan/β-lactamase)$_6$ dry film was compared to the reported CD spectrum [37, 38] of the enzyme in solution (Figure 3.8). The three characteristic bands (one positive at 190 nm, two negative at 208 and 220 nm) previously reported [38] for β-lactamase were observed for the dry film. In the far UV region, the CD spectrum of the LbL film looks quite similar to the native structure of the enzyme under optimum conditions [39], which is a combination between the characteristic antiparallel β-sheet and a random coil configuration.

The investigation of enzymes by CD on solid surfaces is scarce in the literature [40]. Up to now, monitoring of structural changes after the adsorption onto solid surfaces is done by comparison of the spectra of free and immobilized peptides and proteins [41, 42]. The similarity of both spectra is relevant, yet the best way to evaluate the correlation between a native and an immobilized protein structure is to calculate the secondary structure fractions (of α-helix and β-sheet) using standard algorithms [40]. Herein, the spectra of the solution that was employed to prepare the film was also collected, but is not presented due to the strong absorbance of the MES buffer below 220 nm. Moreover, the enzyme employed for this study was acquired commercially and is not 100 % pure. Therefore, we can only limit our conclusion to the fact that no major conformational changes were detected versus the reported structure, and β-lactamase bioactivity is not dramatically affected when surrounded by chitosan; although the packing of the enzymes can limit the access of substrate molecules to the active site.

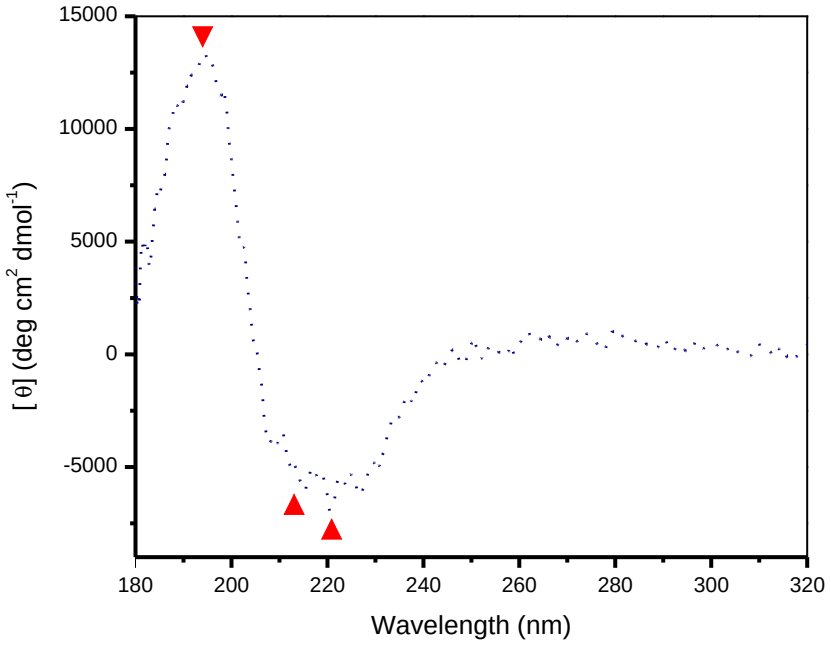

Figure 3.8: CD spectra of the film (chitosan/β-lactamase)$_6$ on a quartz slide. ▲ ▼ point out the characteristic adsorption bands.

3.3.4 Enzyme Activity in the Multilayer Assembly

To test the bioactivity in flat films and filled pores (chitosan/β-lactamase), both kind of films were brought in contact with a nitrocefin solution and stirred (see section 3.2.8). The initial rate of hydrolysis was calculated using a colorimetric test and plotted versus the number of LbL cycles (Figure 3.9) and the thickness of the films (Figure 3.10), since diffusion of nitrocefin might be crucial to understand the activity within the films. In Figure 3.9, we can observe that the rate of hydrolysis varies with the number of layers and the kind of support (Si wafer or PCm). In flat films, the rate of hydrolysis increases almost linearly with the number of cycles. However, the average activity *per* layer slightly decreases after 8 cycles. A similar trend is observed in Figure 3.10 after 50 nm film thickness. As previously shown, the weight fraction of enzyme decreases slowly after 6 cycles (Fig.3.7, Table 3.2), suggesting that we deposited layers with less enzyme and

more chitosan (comparatively) after six cycles. Albeit the total amount of enzyme was larger in thicker films, the trajectory that nitrocefin has to follow to reach β-lactamase molecules in the bottom layers and come back to the continuous phase of the solution is longer. In other words, substrate diffusion becomes more important in thicker films [43, 44] and that might explain the fact that the rate of hydrolysis looks as a a logaritmic function of the thickness. It seems like, the adsorption of more layers (n $\geq$ 16 LbL cycles) might result in slight or negligible gain of activity. In the case of the films that filled the pores, a sharp increase on hydrolysis rate is observed for the first 4 LbL cycles; then, a plateau was reached. Similarly, the adsorption in the pores is minor after n $\geq$ 4 (Figure 3.3). Hence, a maximum value of activity is reached when the film growth starts saturating (Fig. 3.10). Martin *et al.* [45] reported a similar trend for (glutaraldehyde/glucose oxidase)$_n$ nanotubes embedded in the template. In this scenario, the substrate molecule (*i.e.* nitrocefin) is exposed to a large amount of enzyme distributed in individual pores, thus the limiting factor might be the flow through-out the pores.

On one hand, the advantage of using PCm as a support to assemble (chitosan/β-lactamase)$_n$ is that with n = 4 cycles, we get a initial rate of hydrolysis comparable to the activity of n = 12 cycles adsorbed on Si wafers (both samples with same geometrical area 1 cm^2). On the other hand, the films (chitosan/β-lactamase)$_n$ on Si wafers show the largest rates of hydrolysis with n$\geq$ 12 cycles. Moreover, the total surface area in 1 cm^2 of the membrane is *ca.* 70 cm^2, while the activity in the pores at n = 4 does not even triplicate the value of a flat film (Figure 3.9).

Besides the limitations due to substrate diffusion in the pores, we explored in more details what occurs in terms of amount of enzyme. Thus, a series of nanotubes (chitosan/β-lactamase) with 1 $\leq$ n $\leq$ 8 was prepared using similar polycarbonate templates ($\approx$ 21 μm thick, 200 nm pore size) in order to evaluate the bioactivity *vs* total amount of enzyme. The number of LbL cycles was chosen in such a way that we could observe the region where the growth reaches saturation. The total amount of enzyme was estimated using the weight fraction determined by ^{1}H fast MAS NMR and the volume calculated with the final pore size measured by gas porometry after LbL. A density of 1 g·cm^{-3} was used as a rough approximation for all nanotubes (chitosan/β-lactamase)$_n$.

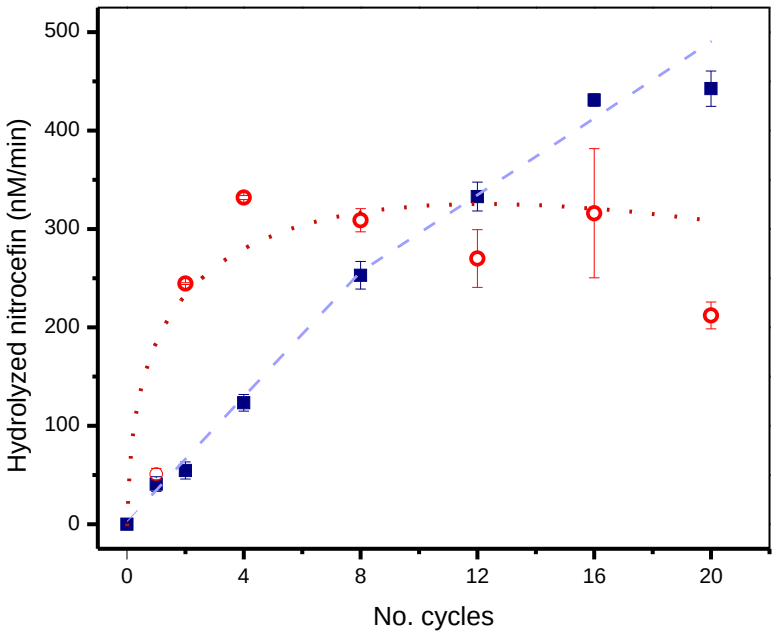

Figure 3.9: Rate of nitrocefin hydrolysis as a function of the number of LbL cycles (chitosan/β-lactamase)$_n$ in films (■) and in filled pores (○). Dashed and dotted lines are guides to the eye. Error bars correspond to the range of values measured on a sample series prepared and tested in parallel.

In the Figure 3.11, we can observe that the amount of enzyme reaches a plateau after 4 LbL cycles and the rate of nitrocefin hydrolysis is larger at the same point ($\sim 150\mu$ g/cm^2). In agreement with previous reported results, protein loading can increase or decrease the apparent activity [46, 47, 48]. Besides the restricted diffusion of nitrocefin in the pores, there is a decreased mobility of the enzyme within the film as it becomes more dense. As a consequence, local changes on surface charge and pH might take place, resulting in loss of specific bioactivity (activity *per* unit of mass).

The specific activity of the enzyme in the nanotubes can also be obtained after the amount of enzyme in the pores has been calculated. To compare flat films and filled pores, the activity of the flat films analyzed by NMR (Table 3.2) was estimated using previous data (Figures 3.3, 3.9). In the Figure 3.12, the specific

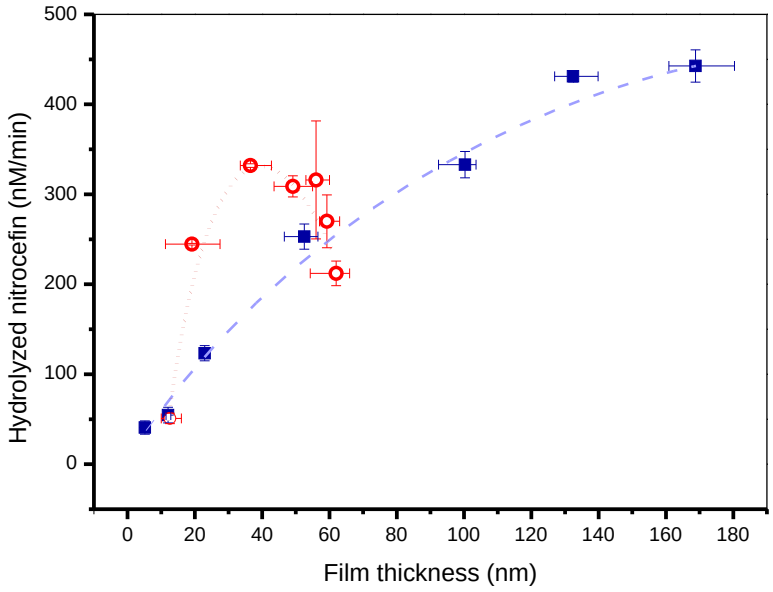

Figure 3.10: Rate of nitrocefin hydrolysis vs thickness for (chitosan/β-lactamase)$_n$ flat films (■) and filled pores (○). Dashed and dotted lines are guides to the eye.

activity of filled pores and flat films is presented in units of mol of hydrolyzed nitrocefin per mol of enzyme, per minute. The error bars for the flat films are unusually large due to the rough activity estimation. Nonetheless, a molecule of enzyme loaded in a flat film hydrolyzes nitrocefin at least 20 fold faster than an enzyme molecule in the pores. Therefore, the diffusion of the substrate into the films is the critical parameter for the initial rate of hydrolysis.

Finally, it is important to compare the activity of the enzyme in a flat thin film *vs.* the enzyme in solution. For this purpose, 1 cm^2 of (chitosan/β-lactamase)$_3$ flat film was compared against an aliquot of β-lactamase solution (taken as 100 μL of a 1-10 μg.L^{-1} solution). The amount of enzyme in the film was estimated to be *ca.* 1.0 μg considering the NMR calculations. Figure 3.13 shows the activities of the film and the solution added as a droplet. It is important to mention that the activities in this particular graph are not directly comparable to previous Figures due to a different stirring speed. Nevertheless, the enzymatic activity

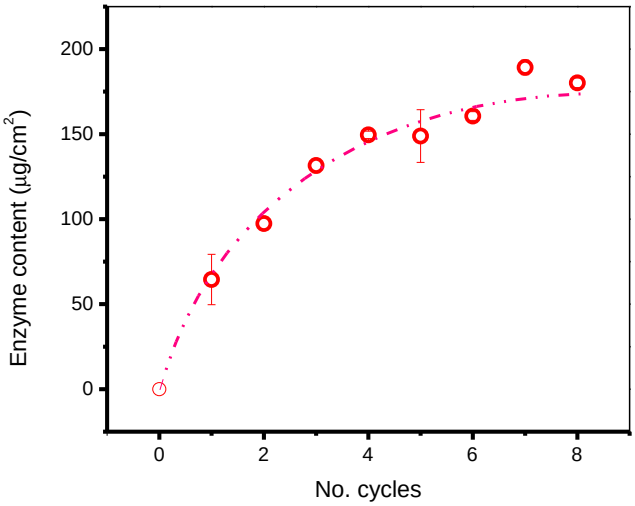

(a)

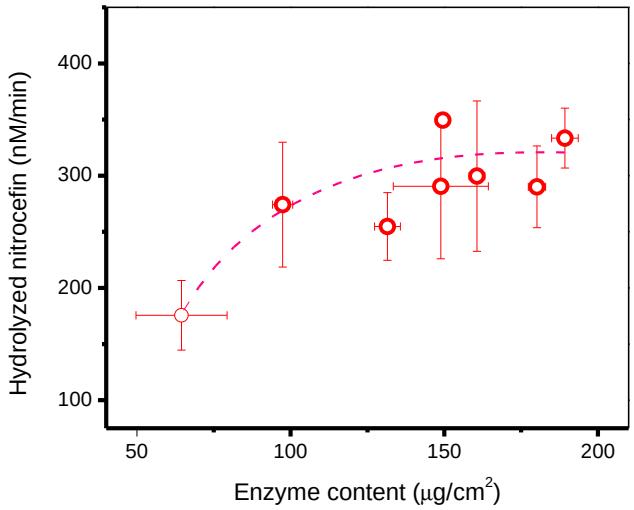

(b)

Figure 3.11: Effect of confinement for filled pores (chitosan/β-lactamase)$_n$: (a) amount of enzyme as a function of the number of cycles and (b) rate of hydrolysis *vs* β-lactamase content in 1cm^2 of PCm. The largest rate of hydrolysis was found at the point where pore saturation started (n = 4). Error bars correspond to the range of values measured on a sample series prepared and analyzed in parallel.

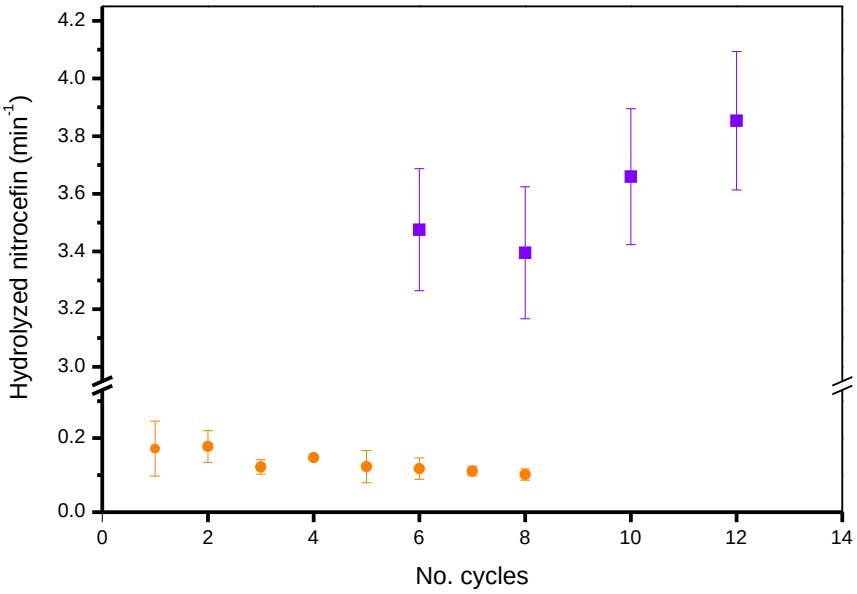

Figure 3.12: Rate of nitrocefin hydrolysis for the films (chitosan/β-lactamase)$_n$ flat films(■) and filled pores (○). Units: mol of product per mol of enzyme per minute. Error bars are unusually large for flat films, since their activities were estimated.

of β-lactamase in a flat film with n = 3, is close to 1/10 of the activity for the same amount of enzyme in solution. This result demonstrates that the diffusion of nitrocefin in and out of the films decreases considerably the rate of hydrolysis.

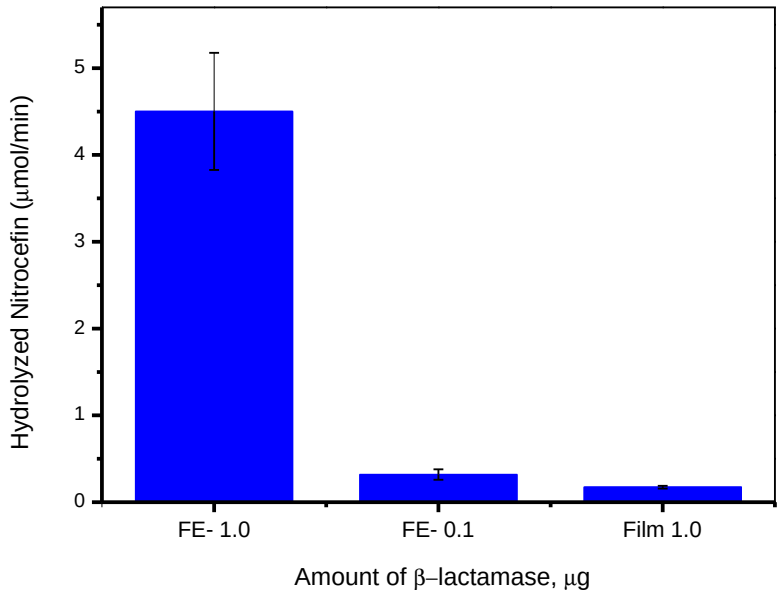

Figure 3.13: Activity of the free enzyme (FE) vs. a (chitosan/β-lactamase)$_3$ multilayered flat film. Error bars represent the range of activity values measured, with triplicates for each sample.

3.4 Conclusion

In this chapter, (chitosan/β-lactamase) films were successfully obtained by LbL. Different growth regimes were revealed and contrasted for multilayer films deposited on flat surfaces *vs* the pores of PCm. A special attention was paid to the chemical composition at different stages of LbL process in open or in confined geometries to achieve a better understanding of biocatalytic processes. First of all, the results corroborate the protein-friendly properties of chitosan, as β-lactamase preserves some enzymatic activity in both kinds of films. Secondly, it was found that the adsorption of bioactive polyelectrolytes by LbL in confined media could give very active surfaces with a very few number of LbL cycles. However, the diffusion of the substrate is slower in a porous membrane and a dense packing of enzymes may decrease the specific activity of the material.

To the knowledge of the author, this is the first report that determines the amount of enzyme in flat surfaces and filled pores by direct analysis. Moreover,

it is an attempt to establish a correlation between the load of enzyme and the bioactivity of thin films prepared by LbL in nanostructured materials.

3.5 Supporting Information IR

The infrared spectra of the films (chitosan/β-lactamase)$_n$ was collected in Transmittance mode using directly the silicon wafer with the coating on top of it, and compared to the components in KBr (Figure 3.14).

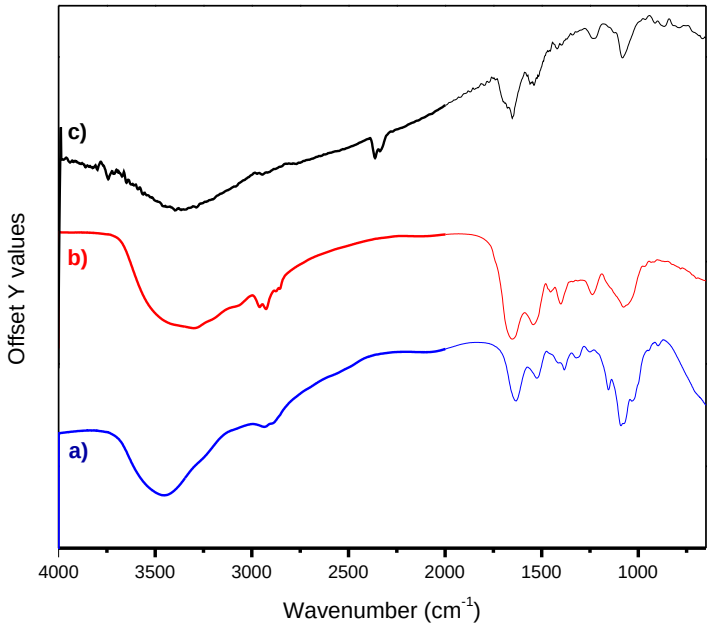

Figure 3.14: FTIR spectra (transmittance mode) of the polyelectrolytes involved on LbL buildup a) chitosan, b) β-lactamase, and c) (chitosan/β-lactamase)$_{16}$ film.

ATR and transmittance mode were compared to analyze multilayered flat films as powder or a film, respectively (Figure 3.15). In both cases, the film is a sum of the pure components and even both spectra are very similar. Although ATR spectrum has a better resolution.

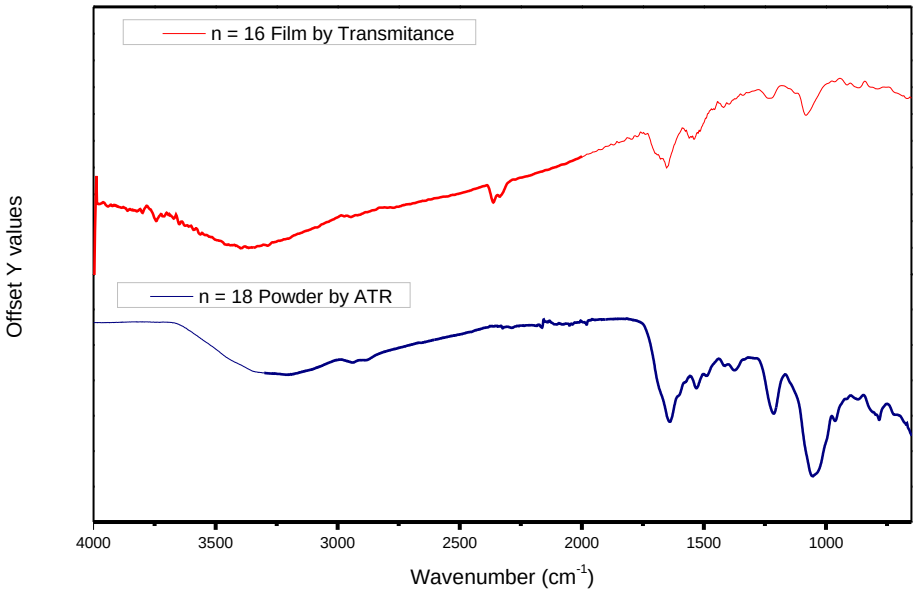

Figure 3.15: Infrared spectra of (chitosan/β-lactamase)$_n$ film by Transmission *vs.* Attenuated Total Reflectance mode.

3.6 Supporting Information NMR

In this section, experimental results describing the working conditions for solid-state ^{1}H fast MAS NMR spectra collection are presented and briefly discussed.

3.6.1 Pure polyelectrolyte spectra

The ^{1}H fast MAS NMR spectra of the as received polyelectrolytes (chitosan and β-lactamase), as well as the spectra of the support for the nanotubes were collected with a single pulse experiment (with baseline correction). For the sake of reproducibility, parameters of data collection such as temperature (K) and MAS spinning rate (kHz) were studied by launching a series of experiments for one sample (Figures 3.16). Sharper signals at larger spinning speed result from more efficient averaging of the homonuclear dipolar coupling on the spectra.

It is well known that improved resolution usually occurs at highest spinning rates. However, it is also well known that increasing spinning rate also increases the temperature in the body of the rotor (sometimes with gradients of tem-

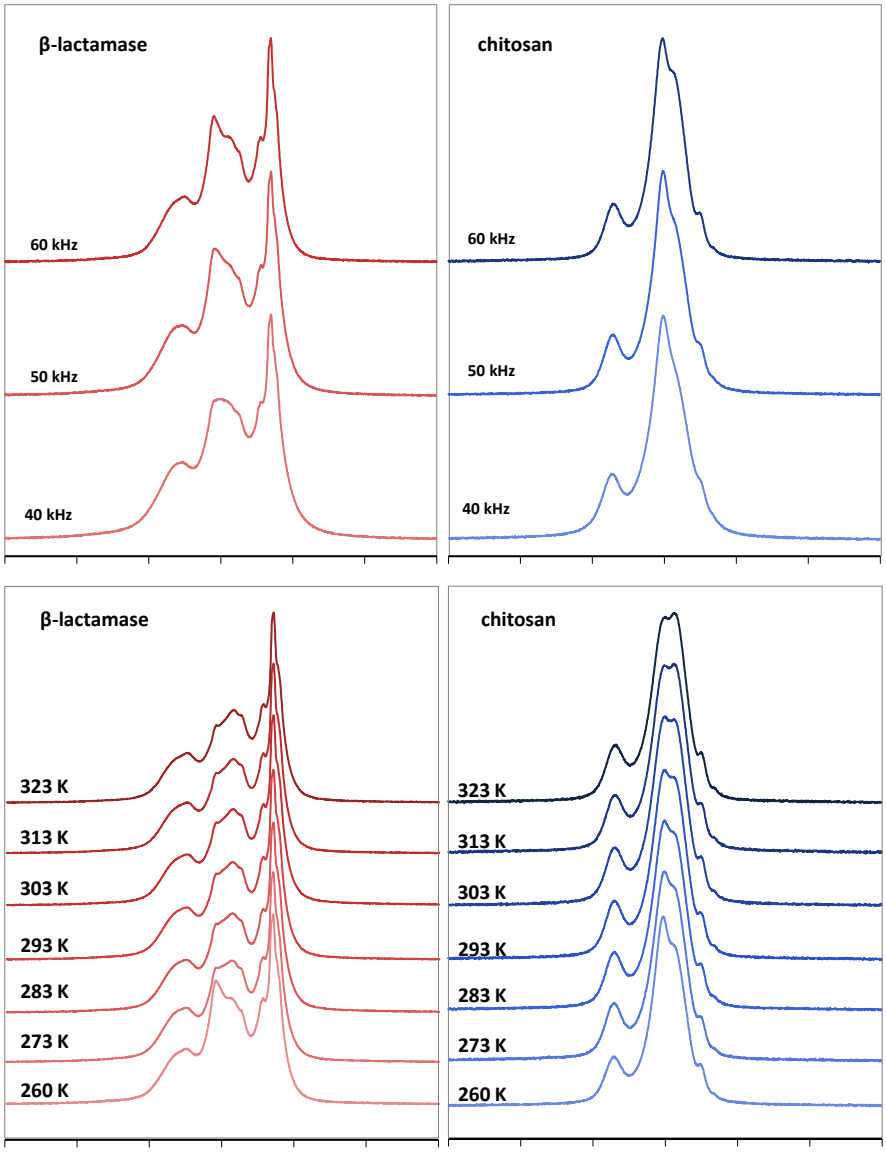

Figure 3.16: Effect of spinning rate (TOP, kHz) and temperature (BOTTOM, K) on chitosan and β-lactamase ^{1}H fast MAS NMR spectra.

perature). Even when the Bruker BCU Xtreme unit is working to control the temperature, there is a difference between the setup and the true temperature of the sample spinning (Fig. 3.17). Consequently, the temperature set up was fixed to the lowest possible (260 K) to guarantee that β-lactamase is far from denaturation as most of the studies we collected at 40, 50 and 60 kHz. In order

to stabilize the signal, we waited 10 min before data collection at every step.

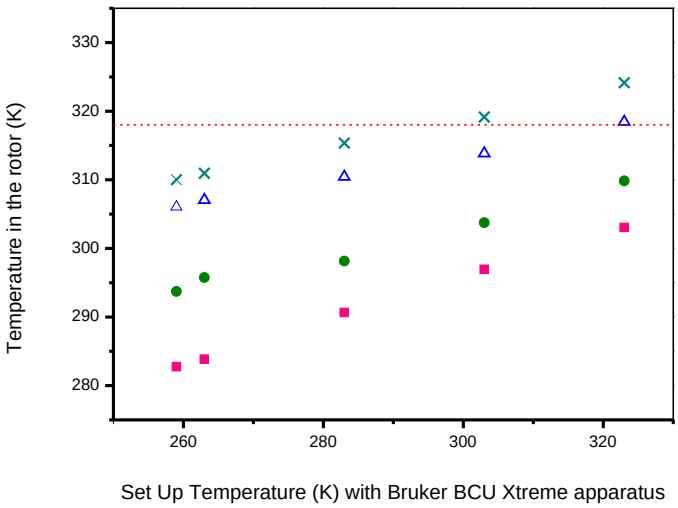

Figure 3.17: True temperature in the body of the rotor. As the temperature setup increases in the control unit, is also important to consider spinning rate: 40 kHz - ■, 50 kHz - ●, 60kHz - ▲, 65 kHz - ×. The red dotted line represents the temperature at which β-lactamase starts unfolding [49].

3.6.2 Spectra of the LbL nanotubes

The nanotubes (chitosan/β-lactamase) obtained by LbL were almost insensible to changes in temperature or spinning rate, Figure 3.18. While the nanotubes do not show any kind of evolution, their components (chitosan and β-lactamase) did. We think that this result could be a consequence of the sample preparation, since the collection of the nanotubes involves contact with dichloromethane and drying. On the contrary, chitosan and β-lactamase were analyzed "as received", and both of them were stored in the fridge before analysis.

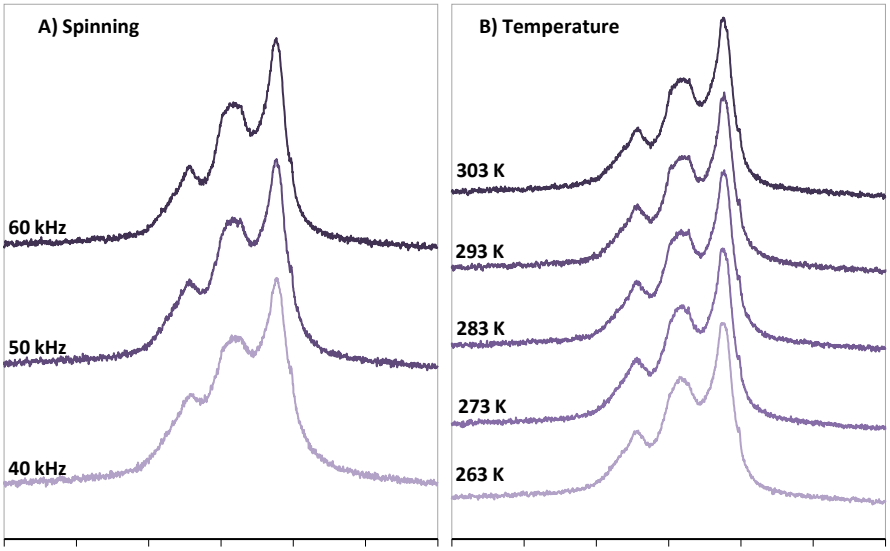

Figure 3.18: ^{1}H fast MAS NMR spectra of nanotubes (chitosan/β-lactamase) at different temperatures and spinning rates.

References

[1] Eva Blomberg and Maria Lundin. *Layer-by-Layer Assembly of Biomacromolecules*, chapter 262, pages 1–14. Taylor & Francis, 2011. doi: 10.1081/E-ESCS-120045969.

[2] Zhiyong Tang, Ying Wang, Paul Podsiadlo, and Nicholas A Kotov. Biomedical applications of layer-by-layer assembly: From biomimetics to tissue engineering. *Advanced Materials*, 18(24):3203–3224, 2006.

[3] Thomas Boudou, Thomas Crouzier, Kefeng Ren, Guillaume Blin, and Catherine Picart. Multiple functionalities of polyelectrolyte multilayer films: new biomedical applications. *Advanced Materials*, 22(4):441–467, 2010.

[4] Omar S Sakr and Gerrit Borchard. Encapsulation of enzymes in layer-by-layer (LbL) structures: Latest advances and applications. *Biomacromolecules*, 14(7):2117–2135, 2013.

[5] Gero Decher and Johannes Schmitt. Fine-tuning of the film thickness of

ultrathin multilayer films composed of consecutively alternating layers of anionic and cationic polyelectrolytes. In *Trends in Colloid and Interface Science VI*, volume 89, pages 160–164. Springer, 1992.

[6] Patrick Bertrand, Alain M. Jonas, André Laschewsky, and Roger Legras. Ultrathin polymer coatings by complexation of polyelectrolytes at interfaces: suitable materials, structure and properties. *Macromolecular Rapid Communications*, 21(7):319–348, 2000.

[7] Erell Leguen, Armelle Chassepot, Gero Decher, Pierre Schaaf, Jean-Claude Voegel, and Nadia Jessel. Bioactive coatings based on polyelectrolyte multilayer architectures functionalized by embedded proteins, peptides or drugs. *Biomolecular Engineering*, 24(1):33–41, 2007.

[8] Nicholas Stephanopoulos, Julia H Ortony, and Samuel I Stupp. Self-assembly for the synthesis of functional biomaterials. *Acta Materialia*, 61(3):912–930, 2013.

[9] Yuri Lvov, Katsuhiko Ariga, Izumi Ichinose, and Toyoki Kunitake. Assembly of multicomponent protein films by means of electrostatic layer-by-layer adsorption. *Journal of the American Chemical Society*, 117(22):6117–6123, 1995.

[10] Katsuhiko Ariga, Qingmin Ji, Taizo Mori, Masanobu Naito, Yusuke Yamauchi, Hideki Abe, and Jonathan P Hill. Enzyme nanoarchitectonics: organization and device application. *Chemical Society Reviews*, 42(15):6322–6345, 2013.

[11] Gero Decher. Fuzzy nanoassemblies: Toward layered polymeric multicomposites. *Science*, 277(5330):1232–1237, 1997.

[12] Teruyuki Komatsu. Protein-based nanotubes for biomedical applications. *Nanoscale*, 4(6):1910–1918, 2012.

[13] Thomas D Lazzara, KH Aaron Lau, Ahmed I Abou-Kandil, Anne-Marie Caminade, Jean-Pierre Majoral, and Wolfgang Knoll. Polyelectrolyte layer-

by-layer deposition in cylindrical nanopores. *ACS nano*, 4(7):3909–3920, 2010.

[14] Omar Azzaroni and KH Aaron Lau. Layer-by-layer assemblies in nanoporous templates: nano-organized design and applications of soft nanotechnology. *Soft Matter*, 7(19):8709–8724, 2011.

[15] Halima Alem, Françoise Blondeau, Karine Glinel, Sophie Demoustier-Champagne, and Alain M Jonas. Layer-by-layer assembly of polyelectrolytes in nanopores. *Macromolecules*, 40(9):3366–3372, 2007.

[16] Cécile J Roy, Christine Dupont-Gillain, Sophie Demoustier-Champagne, Alain M Jonas, and Jessem Landoulsi. Growth mechanism of confined polyelectrolyte multilayers in nanoporous templates. *Langmuir*, 26(5):3350–3355, 2010.

[17] Aimin Yu, Zhijian Liang, and Frank Caruso. Enzyme multilayer-modified porous membranes as biocatalysts. *Chemistry of materials*, 17(1):171–175, 2005.

[18] Barbara Krajewska. Application of chitin-and chitosan-based materials for enzyme immobilizations: a review. *Enzyme and microbial technology*, 35(2): 126–139, 2004.

[19] Thomas Crouzier, Thomas Boudou, and Catherine Picart. Polysaccharide-based polyelectrolyte multilayers. *Current Opinion in Colloid & Interface Science*, 15(6):417–426, 2010.

[20] João Borges, José M Campiña, Hiléia KS Souza, Maria P Gonçalves, and A Fernando Silva. Aggregation-induced conformational transitions in bovine β-lactoglobulin adsorbed onto open chitosan structures. *Soft Matter*, 8(4): 1190–1201, 2012.

[21] Sarah M Drawz and Robert A Bonomo. Three decades of β-lactamase inhibitors. *Clinical microbiology reviews*, 23(1):160–201, 2010.

[22] Dominique Massiot, Franck Fayon, Mickael Capron, Ian King, Stephanie Le Calve, Bruno Alonso, Jean-Olivier Durand, Bruno Bujoli, Zhehong Gan, and Gina Hoatson. Modelling one-and two-dimensional solid-state NMR spectra. *Magnetic Resonance in Chemistry*, 40(1):70–76, 2002.

[23] Q6W9J1. β-lactamase TEM-1. `http://www.uniprot.org/uniprot/Q6W9J1`, 2004. Accessed on 06-03-2014.

[24] Claudine Porcel, Philippe Lavalle, Vincent Ball, Gero Decher, Bernard Senger, Jean-Claude Voegel, and Pierre Schaaf. From exponential to linear growth in polyelectrolyte multilayers. *Langmuir*, 22(9):4376–4383, 2006.

[25] Thomas D Lazzara, Ingo Mey, Claudia Steinem, and Andreas Janshoff. Benefits and limitations of porous substrates as biosensors for protein adsorption. *Analytical chemistry*, 83(14):5624–5630, 2011.

[26] Xue Qu, Gang Lu, Eishun Tsuchida, and Teruyuki Komatsu. Protein nanotubes comprised of an alternate layer-by-layer assembly using a polycation as an electrostatic glue. *Chemistry-A European Journal*, 14(33):10303–10308, 2008.

[27] Christian Jelsch, Lionel Mourey, Jean-Michel Masson, and Jean-Pierre Samama. Crystal structure of Escherichia coli TEM-1 β-lactamase at 1.8 å resolution. *Proteins: Structure, Function, and Bioinformatics*, 16(4):364–383, 1993.

[28] Teruyuki Komatsu, Hiromi Terada, and Nao Kobayashi. Protein nanotubes with an enzyme interior surface. *Chemistry-A European Journal*, 17(6):1849–1854, 2011.

[29] Jorge Almodovar, Laura W Place, Jarrod Gogolski, Kristin Erickson, and Matt J Kipper. Layer-by-layer assembly of polysaccharide-based polyelectrolyte multilayers: a spectroscopic study of hydrophilicity, composition, and ion pairing. *Biomacromolecules*, 12(7):2755–2765, 2011.

[30] Teresa Cerchiara, Barbara Luppi, Federica Bigucci, and Vittorio Zecchi. Chitosan salts as nasal sustained delivery systems for peptidic drugs. *Journal of pharmacy and pharmacology*, 55(12):1623–1627, 2003.

[31] Andreas Barth. Infrared spectroscopy of proteins. *Biochimica et Biophysica Acta (BBA)-Bioenergetics*, 1767(9):1073–1101, 2007.

[32] Determination of secondary structure in proteins by Fourier Transform Infrared Spectroscopy (FTIR). Jena Library of Biological Macromolecules. `http://jenalib.fli-leibniz.de/ImgLibDoc/ftir/IMAGE_FTIR.html#Aminoacidsidechainvibrations`, 2005. Accessed on 12-02-2014.

[33] Marc Lavertu, Zhicheng Xia, Alessio N Serreqi, Mohammed Berrada, Accio Rodrigues, D Wang, Michael D. Buschmann, and Ajay Gupta. A validated ^{1} H NMR method for the determination of the degree of deacetylation of chitosan. *Journal of Pharmaceutical and Biomedical Analysis*, 32(6):1149–1158, 2003.

[34] Pierre-Yves Savard, Alejandro Sosa-Peinado, Roger C Levesque, Marvin W Makinen, and Stéphane M Gagné. Letter to the editor: ^{1}H, ^{13}C and ^{15}N backbone resonance assignments for TEM-1, a 28.9 kda β-lactamase from E. coli. *Journal of Biomolecular NMR*, 29(3):433–434, 2004. ISSN 0925-2738.

[35] Toshiaki Hattori, Rhee Hallberg, and Paul L Dubin. Roles of electrostatic interaction and polymer structure in the binding of β-lactoglobulin to anionic polyelectrolytes: measurement of binding constants by frontal analysis continuous capillary electrophoresis. *Langmuir*, 16(25):9738–9743, 2000.

[36] A Basak Kayitmazer, Daniel Seeman, Burcu Baykal Minsky, Paul L Dubin, and Yisheng Xu. Protein–polyelectrolyte interactions. *Soft Matter*, 9(9): 2553–2583, 2013.

[37] Christo Christov, Sven Gabriel, Boris Atanasov, and Jörg Fleischhauer. Calculation of the cd spectrum of class a β-lactamase from escherichia coli (tem-1). *Zeitschrift für Naturforschung Section AA Journal of Physical Sciences*, 56(11):757–760, 2001.

[38] Christo Christov, Frederik Tielens, and Miroslav Mirazchiiski. Modeling study of the influences of the aromatic transitions and the local environment on the far-UV rotational strengths in tem-1 β-lactamase. *Journal of molecular modeling*, 12(4):411–416, 2006.

[39] Marc Vanhove, Xavier Raquet, and Jean-Marie Frère. Investigation of the folding pathway of the TEM-1 β-lactamase. *Proteins: Structure, Function, and Bioinformatics*, 22(2):110–118, 1995.

[40] Francesco Secundo. Conformational changes of enzymes upon immobilisation. *Chemical Society Reviews*, 42(15):6250–6261, 2013.

[41] Steffi Grohmann, Holger Rothe, and Klaus Liefeith. Investigations on the secondary structure of polypeptide chains in polyelectrolyte multilayers and their effect on the adhesion and spreading of osteoblasts. *Biointerphases*, 7 (1-4):1–13, 2012.

[42] Ling Zhang, Bingyun Li, Zheng-liang Zhi, and Donald T Haynie. Perturbation of nanoscale structure of polypeptide multilayer thin films. *Langmuir*, 21(12):5439–5445, 2005.

[43] Mitsuhiko Onda, Katsuhiko Ariga, and Toyoki Kunitake. Activity and stability of glucose oxidase in molecular films assembled alternately with polyions. *Journal of bioscience and bioengineering*, 87(1):69–75, 1999.

[44] Frank Caruso and Corinna Schüler. Enzyme multilayers on colloid particles: assembly, stability, and enzymatic activity. *Langmuir*, 16(24):9595–9603, 2000.

[45] Shifeng Hou, Jiahai Wang, and Charles R Martin. Template-synthesized protein nanotubes. *Nano letters*, 5(2):231–234, 2005.

[46] Joey N Talbert and Julie M Goddard. Enzymes on material surfaces. *Colloids and Surfaces B: Biointerfaces*, 93:8–19, 2012.

[47] Ulf Hanefeld, Lucia Gardossi, and Edmond Magner. Understanding enzyme immobilisation. *Chemical Society Reviews*, 38(2):453–468, 2009.

[48] Kenan P Fears and Robert A Latour. Assessing the influence of adsorbed-state conformation on the bioactivity of adsorbed enzyme layers. *Langmuir*, 25(24):13926–13933, 2009.

[49] Xiaojun Wang, George Minasov, and Brian K Shoichet. Noncovalent interaction energies in covalent complexes: TEM-1 β-lactamase and β-lactams. *Proteins: Structure, Function, and Bioinformatics*, 47(1):86–96, 2002.

Chapter 4

Brushes of self-assembled enzyme-based nanotubes for biocatalysis

In this chapter, we report two different strategies explored for the fabrication of brushes of self-assembled nanotubes containing active enzyme (β-lactamase) layers. The successful strategy that we report makes use of a combination of layer-by-layer assembly, hard-templating and chemical crosslinking techniques. By this method, core-shell LbL nanotube brushes with the biocatalytic component included either in the core or in the shell part of the nanotubes were prepared. Kinetic studies reveal that both types of systems are bioactive but, that the activity is significantly better preserved when β-lactamase is incorporated in the core of the nanotubes.

4.1 Introduction

In the last 15 years, biomaterials and nanoscience research have joined efforts to mimic cellular environments. One of the features that has attracted a lot of attention is the compartmentalization and confinement of cellular components in small compartments, which enable cells to control the sequential manner of biochemical reactions to maximize their precision and efficiency [1]. From the point of view of materials design and synthesis, some spherical elements as polymer vesicles, micelles and inorganic microparticles have been studied to act as artificial organelles [2].

Microvilli are nanofinger-shaped protrusions that are found at the surface of a large variety of cell types (Figure 4.1). They offer a large increase of surface area for the plasma membrane and contribute to diverse biological functions (i.e. absorption, secretion, mechanotransduction and adhesion), yet their structure is quite similar. In essence, a microvillus is a collection of crosslinked actin filaments, packed in a specific way to dictate the binding of other proteins [3]. Motivated by the range of applications of microvilli structures, we studied the potential of self-assembled enzyme-based nanotube arrays for biocatalysis. Instead of actin filaments, we used polyelectrolyte multilayers to synthesize tubular structures and as a first approach, we immobilized these tubes on planar solid substrates.

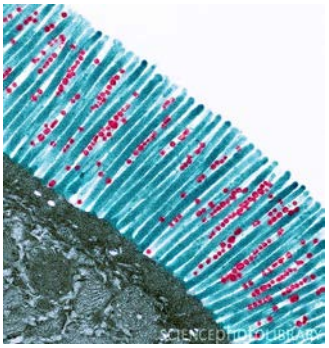

Figure 4.1: TEM images of intestinal microvilli [4]. The cells secrete enzymes and aid in the absorption of nutrients from the intestines into the blood by providing a large surface area.

Layer-by-layer assembly (LbL) is one of the most powerful tools to control film properties at nanoscale level, and it has also been used to prepare a variety of

biocatalytic thin films, including nanotube structures [2, 5]. Since LbL coatings can be deposit on any kind of charged surface, the use of membranes with submicron size pores open the door for polyelectrolyte nanotube fabrication. Early in the 2000s, the first self-assembled nanotubes were made of poly(allylamine hydrochloride) and poly(acrylic acid) [6]. Later on, the same polyelectrolyte couple was used to prepare the first LbL nanotube arrays with pH responsive properties [7]. Based on the same principle but varying the polyelectrolyte couple, the group of Komatsu started the study of protein nanotube arrays with human serum albumin and poly-L-arginine to functionalize surfaces for biotin capture [8, 9].

In this chapter, we report the synthesis of brushes of nanotubes containing β-lactamase layers and the bioactivity of the resulting surfaces. The nanotubes were prepared by LbL assembly within polycarbonate membranes, using two different pairs of polyelectrolytes to get a core-shell structure. The main idea of using two polyelectrolyte couples was to integrate 1) mechanical stability and 2) bioactivity. In a second stage, we tried two different strategies to anchor the nanotubes onto a planar surface. The first strategy involved the fabrication and use of supported track- etched membranes as templates. The second strategy made use of covalent crosslinking as adhesive to attach the nanotubes on a solid support. Pros and cons of both methods are discussed in detail.

4.2 Experimental methods

4.2.1 Fabrication of track-etched supported templates

Materials. Single-side polished silicon wafers (Si, <100> orientation, ACM), polycarbonate bisphenol A (Lexan 145, General Electric), n-decyldimethylchlorosilane (Gelest), chloroform, methanol and dichloro-methane (Sigma-Aldrich, ACS reagent > 99.5%) were used as received without further purification.

Supported templates of polycarbonate were prepared by track-etching method following the procedure reported by Ferain and Legras [10], Figure 4.2. Silicon wafers, used as supports, were first cleaned by piranha solution and further silanized with n-decyl dimethyl chlorosilane to improve their hydrophobic-

ity. Then, a polycarbonate solution in chloroform (90 mg mL^{-1}) was spin-coated at 4000 rpm during 30 s on top of the Si wafer ($\sim$ 1 μm film thickness) and annealed during 4 h at 190 °C prior to irradiation. Heavy-ion irradiation of polycarbonate films on silicon was carried out at the cyclotron with Ar^{9+} at 220 MeV and $1 \times 10^{8} \cdot cm^{-2}$ ion density followed by 1h of UVB irradiation to enhance the track selectivity during etching. Finally, the samples were immersed in a solution 1:1 methanol: sodium hydroxide 0.5 N at 50 °C to etch the tracks and create nanoporous supported thin films. The pore size depends on etching time, 30 min in NaOH gave a mean pore size of 200 nm.

4.2.2 Layer-by-Layer Assembly

Polyelectrolytes. Chitosan chloride (chit, DDA> 90%, Mw$\sim$ 270k, Novamatrix) and poly(allylamine hydrochloride) (PAH, Mw 15000 or Mw 58000, Sigma-Aldrich) were used as polycations. β-lactamase (TEM-1 from *Enterobacter cloacae*, Sigma-Aldrich), poly(acrylic acid, sodium salt) (PAA, Mw 15000 or Mw 100000, Sigma-Aldrich), carboxymethylpullulan (CMP, Mw$\sim$ 220000, DS$\sim$ 97%) and sodium hyaluronate (HA, Mw 176 kDa - 350 kDa from LifeCore) were used as polyanions. All polyelectrolytes were dissolved in buffer solution to keep a concentration of 1mg. mL^{-1}, in buffer MES (100 mM, pH 6.5) or sodium acetate buffer (0.1 N, pH 4.6).

Templates. Track-etched polycarbonate membranes (PCm) of 200 nm pore size, 21 μm thickness and $2 \times 10^{8} \cdot cm^{-2}$ pore density, were kindly provided by it4ip and used as received.

Crosslinking agents. 1-Ethyl-3-(3-dimethylaminopropyl) carbodiimide (EDC) and N-hydroxysuccinimide (NHS) were purchased from ThermoScientific and used in aqueous solution with a concentration of 6 and 3.5 mM respectively.

Build-up. Polyelectrolyte multilayers were deposited by dipping the template (either PCm or supported membranes) in a polycation solution for 30 min, rinsing it twice in buffer solution (2 min each) and then dipping the same template in a polyanion solution for 30 min, followed by two rinsing steps of 2 min in fresh buffer. The process was repeated n times to produce $(\text{polycation/polyanion})_n$

Figure 4.2: Scheme of track-etching process to prepare supported templates: 1) Starting material: virgin Si wafer, 2) Piranha cleaning, 3) Functionalization with n-decylsilane, 4) Deposition of a continuous polycarbonate film by spin-coating, 5) Heavy ion irradiation to create tracks in the polymer film, 6) Chemical etching by NaOH to create nanopores and, 7) Final supported nanoporous template.

films. Since the polyelectrolytes are also adsorbed outside of the pores, a "de-crusting step" was performed to remove these layers. Three different de-crusting methods were tested: *i)* a cotton swab with basic solution (3M NaCl pH$\sim$ 12) of high ionic strength (3M NaCl), *ii)* alumina powder (1 μm) in a polishing plate, or *iii)* oxygen plasma etching. The performance of each method varied with the nature of the polyelectrolyte pair that has to be removed.

Core-shell nanotubes. Core-shell nanotubes were prepared by LbL assembly of two different pairs of polyelectrolytes in the pores of a polycarbonate membrane. The polyelectrolyte couple that played the role of the shell was first adsorbed as [shell (+)/ shell (-)]$_{\mathrm{m}}$, and the bioactive core of the nanotubes made of (chit/β-lactamase)$_{\mathrm{n}}$ layers, were deposited in a second step. In this way, the external surface of the nanotubes is the polycation of the shell. De-crusting of the top and bottom layers was done after the deposition of the last polyanion shell layer. Immediately after de-crusting the pores from shell layers, the membrane was dipped in a crosslinking solution EDC/NHS (6 and 3.5 mM respectively) for 30 min at room temperature and rinsed twice for 5 minutes in fresh buffer before starting the adsorption of the first chitosan layer.

4.2.3 Nanotube brushes by adhesive crosslinking

Templates. Track-etched polycarbonate membranes (PCm) of 300 nm pore size, 5 μm thickness and 2 $\times$ $10^{8}\cdot$ cm^{-2} pore density, were also provided by it4ip and used as received.

Brushes preparation (Figure 4.3). Brushes of nanotubes were prepared following the protocol reported by Chia et al. [7] with some modifications. LbL assembly of (PAH/PAA)$_n$ was performed in PC membranes at pH 4.6 in acetate buffer 0.1 N. The adsorption process started with a polycation layer (PAH) deposition and ended with a polyanion layer (PAA) adsorption. No intermediate de-crusting was done until this point, as the layers that cover one of the external membrane surfaces will further be used as anchoring layer. A droplet of EDC/NHS (6, 3.5 mM) crosslinking solution was placed on top of an amine-functionalized silicon wafer (1 $\times$ 1 cm^2) and then a piece of PCm with (PAH/PAA)$_n$ filled pores was extended over it. The LbL assembly on the wafer

was then heated at 60 °C for 30 min (at least, and maximum 60 min) to allow the reaction between the amine groups present at the silicon surface and the carboxylic acid groups present on the last LbL layer (PAA). The upper side of the membrane was then de-crusted by 1 min polishing with alumina microparticles (1 μm) and further rinsed with deionized water in an ultrasonic bath (3 times, 1 min each rinsing step) before drying. Finally, the supported membrane was immersed five times in fresh dichloromethane to dissolve the polycarbonate (10, 10, 2, 2 and 1 min) and reveal the nanostructure array.

4.2.4 Gas-Flow Porometry Measurements

Pore diameter of the polycarbonate membranes (PCm) was determined by gas-flow porometry measurements on air-dried samples before and after LbL assembly, using the method explained in detail in section 3.2.4. Briefly, a piece of PCm was hold perpendicularly to a nitrogen flux with a known pressure ranging between 10^4 -10^5 Pa, then the flux downstream from the sample was measured (mL/min) using a flowmeter (Agilent). At least ten flow measurements were averaged and the pore size was calculated using a program based on Knudsen diffusion and the Hagen-Poiseuille flow.

4.2.5 Electron Microscopy

The nanotubes prepared by LbL were collected on a copper grid after the PCm template was dissolved in dichloromethane and imaged by a LEO 922 TEM microscope at 200 kV. Brushes and films on Si wafers were air-dried and imaged by a field-effect gun digital scanning electron microscope FE-SEM (either DSM 982 Gemini from LEO at 1kV or JEOL 7600F at 5kV).

4.2.6 Activity assay

Kinetics of nitrocefin hydrolysis were followed for the PCm and nanotube brushes containing β-lactamase by UV/Vis spectrophotometry (Agilent Cary 50) using the method fully described in Chapter 3, Section 3.2.7. A nitrocefin solution (2mL, 50μM in 100 mM MES buffer pH 6.5) was added on a 1cm^2 sample of either

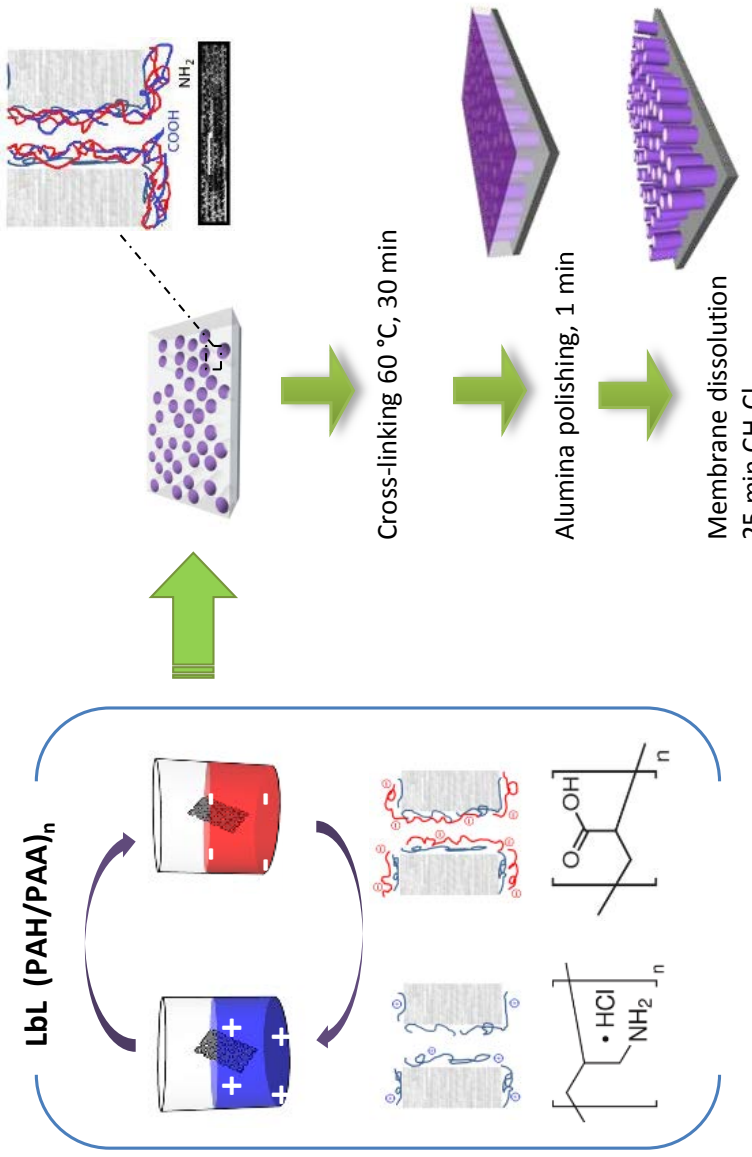

Figure 4.3: Preparation of nanotube brushes by LbL and crosslinking.

filled pores of PCm or of (chit/β-lactamase)$_n$ nanotube brushes on Si wafers. The samples were stirred at 150 rpm and aliquots were taken at different time intervals. Absorbance of hydrolyzed nitrocefin was detected at 485 nm in standard cuvettes with 1.0 cm pathlength and converted to molar concentration using Lambert-Beer law and an extinction coefficient ϵ_{485} = 16700 $M^{-1}cm^{-1}$.

A single value of activity reported for a (chitosan/β-lactamase)$_n$ film or nanotube brush represents the average of triplicates, and all the samples were prepared and analyzed in parallel.

4.2.7 Contact Angle Measurements

Droplets of deionized water (6 μL) were placed on the surface of the samples with the help of a 500 μL syringe. The contact angle was determined by a sessile drop technique using a camera coupled to a OCA/SCA software from Future Digital/Scientific Co.

4.2.8 Atomic Force Microscopy

Atomic force imaging was performed using a Bruker Dimension ICON microscope. The cantilevers employed have a spring constant of 0.2 $N.m^{-1}$, and the apparatus operated in contact mode with 300 mV as set-up with a scanning frequency of 0.3 Hz.

4.3 Results and Discussion

4.3.1 Elaboration of core-shell nanotubes

Polyelectrolyte nanotubes and, in particular, nanotubes made of proteins can be extremely soft and flexible. Consequently, is not straightforward to prepare a brush of this kind of nanotubes standing vertically aligned on a surface. To overcome this issue, we decided to prepare nanotubes with a core-shell architecture (Figure 4.4: TOP scheme), the shell being a pair of crosslinked polyelectrolytes to improve the rigidity of the nanotubes and protect the inner layers containing the enzyme from external aggressions. Two different pairs of weak polyelectrolytes were studied as a shell. The first one is the most studied synthetic polyelectrolyte couples,(PAH/PAA), and the second one is a couple of semi-natural polyelectrolytes (chit/CMP). Three bilayers of shell polyelectrolyte couple (either PAH/PAA or chit/CMP) were adsorbed within the pores of PCm samples, de-crusted with a basic solution of high ionic strength, and then crosslinked by EDC/NHS. Then a biocatalytic core was built-up by adsorbing three bilayers of chit/ β-lactamase. At the end of the assembly, the top and bottom layers deposited on the membrane were removed using the same basic solution (3M NaCl, pH 12). The bioactivity of the two different sets of samples [(PAH/ PAA)$_3$ + (chit/β-lactamase)$_3$] and [(chit/CMP)$_3$ + (chit/β-lactamase)$_3$] was studied and compared to a system without shell, (chit/β-lactamase)$_3$. As shown on Figure 4.4, only a weak difference (maximum 10% of activity loss) in catalytic performance was observed for the sample with a (chit/β-lactamase)$_3$ shell on the day of samples preparation, as well as two weeks later. This result suggests that there is nearly no influence of the shell on the enzyme activity retention. In Table 4.1, we gathered the thicknesses of the various LbL films built-up within the pores at different stages of the construction. These thickness values were calculated as half of the difference in pore diameter (determined from gas flow porometry measurements) after the shell built-up (central column) and after the active core deposition (right column). As it can be observed, the film (PAH/PAA)$_3$ is thicker than (chit/CMP)$_3$ before and especially after the core (chit/β-lactamase)$_3$ was built. Therefore, the core layers (chit/β-lactamase)$_3$ are thinner in the array with

a shell (chit/CMP)$_3$, implying that less enzyme has been loaded in the polysaccharide shell nanotubes. This result is of particular interest because the enzyme did not show preferential adsorption or stability in the (chit/CMP) array, which was expected for layers fully made of polysaccharides [11]. Maybe working at lower pH for the adsorption of (chit/CMP), could lead to more stable and thicker films allowing further deposition of a higher enzyme content. The group of Komatsu prepared nanotubes with an enzyme interior and demonstrated that a single layer of enzyme α-D-glucosidase works as a supported catalyst [12]. However, the rate of reaction was significantly lower (1/38) compared to the free enzyme in solution even when they used a polypeptide assembly to preserve the bioactivity of the enzyme.

To determine if there was or not a difference on stiffness, the nanotubes with and without shell layers were imaged by TEM (Figure 4.5) after membrane dissolution in dichloromethane. Though the nanotubes with a PAH/PAA shell appear flattened under vacuum, they are straighter than the tubes made only of chitosan/β-lactamase which tend to twist more often. On the contrary, the tubes with a shell chit/CMP seem even more flexible. Up to now, we can thus conclude that a polyelectrolyte shell layer can be prepared prior to adsorbing the enzyme in the pores and that PAH/PAA shell layer improves the linearity of the nanotubes without modifying significantly the enzyme bioactivity.

Table 4.1: Thickness of core-shell adsorbed layers in the PCm pores, calculated from gas flow porometry measurements.

Sample	Shell (nm)	Core + Shell (nm)
(PAH/PAA)$_3$ + (chit/β-lactamase)$_3$	33 $\pm$3	59 $\pm$ 2
(chit/CMP)$_3$ + (chit/β-lactamase)$_3$	21 $\pm$ 3	34 $\pm$ 2
(chit/β-lactamase)$_3$	—	23 $\pm$ 3

* Error corresponds to the range of wall thickness calculated for two independent experiments.

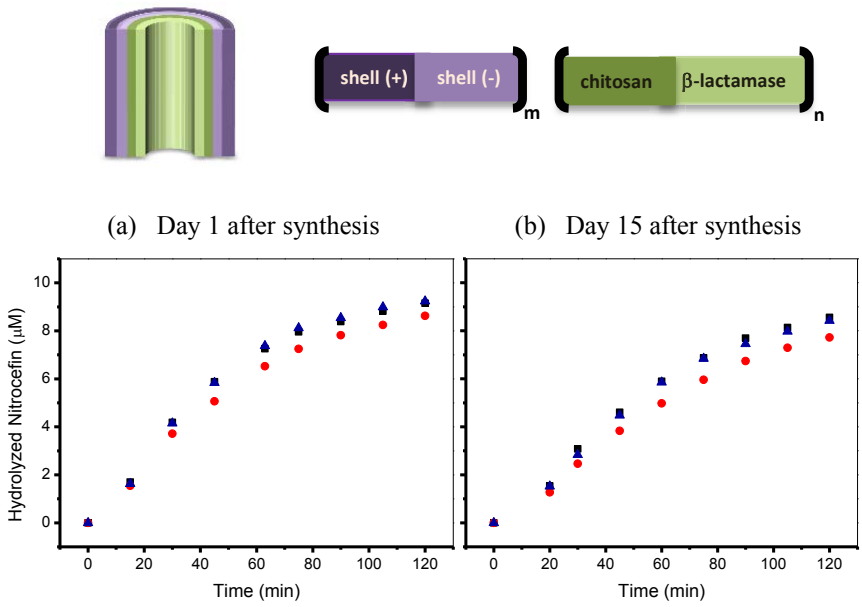

Figure 4.4: TOP: Schematic representation of core-shell nanotubes. BOTTOM: Activity assay in filled pores: [(PAH/PAA)$_3$ + (chit/β-lactamase)$_3$]-■, [(chit/CMP)$_3$ + (chit/β-lactamase)$_3$]-●, (chit/β-lactamase)$_3$-▲Remark: These data is not directly comparable to the graphs presented in Chapter 3, because the stirring speed is smaller ($\approx$ 100 rpm), and the batch of enzyme was different and older.

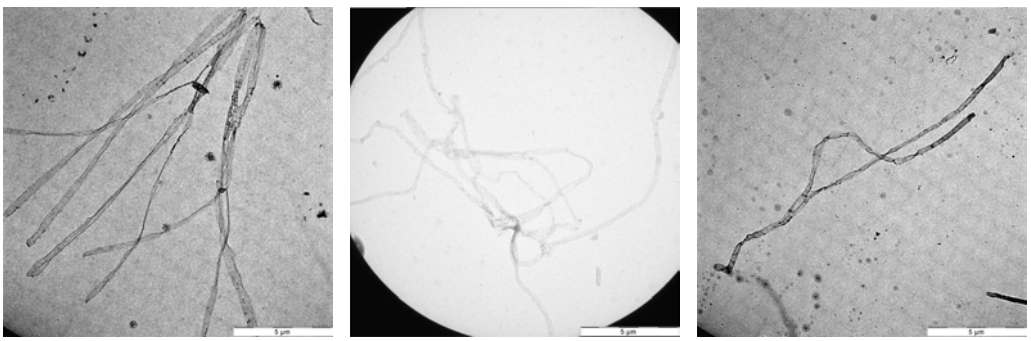

(a) (b) (c)

Figure 4.5: TEM images of the nanotubes with and without shell layers: (a) (PAH/PAA)$_3$+(chit/β-lact)$_3$, (b) (chit/CMP)$_3$+(chit/β-lact)$_3$, (c) (chit/β-lactamase)$_3$. The scale bar is 5 μm.

4.3.2 Strategy 1 to prepare nanotube brushes: Use of supported membranes on Si wafers

The first approach tested to obtain brushes of nanotubes consisted in using supported nanoporous membranes as templates. In this method, LbL assembly is directly performed within the pores of the supported membrane and the array of nanotubes is simply revealed by removing the template. For this purpose, silicon wafers were used as support and a continuous polycarbonate film was deposited on top of them by spin-coating. The porosity was then created by the track-etching process. At first, silicon wafers were silanized with n-decyldimethylchlorosilane to improve the hydrophobicity of the surface and consequently, facilitate the adhesion of polycarbonate. The functionalization was confirmed by an increase in water contact angle, from 59° to 90°± 2° and a thickness increase, from 1.5 nm to 3.5 ± 0.3 nm, determined by ellipsometry. Then, a polycarbonate solution was spin-coated and annealed to get a continuous film of approximately 1 μm thickness. The precise thickness of the polycarbonate films used in this work was estimated by ellipsometry as 844 ± 8 nm. To obtain porous templates, the polycarbonate films were submitted to heavy ion irradiation in a cyclotron. This treatment leads to the creation of tracks in the polymer films. UV irradiation was then applied to increase the sensitivity of the tracks towards chemical etching. Finally, the samples were immerged in a CH_3OH/NaOH solution to reveal the tracks and create pores. The time of chemical etching allows controlling the pore size and the final thickness of the PC film, given that the base attacks the whole polymer film but the hydrolysis reaction could be twice faster along the tracks. Typically, we used a chemical etching time of 30 min which leads to fairly uniform pore size of 200.0 nm ± 4.9 nm as observed by SEM (Figure 4.6a). Prior to LbL adsorption in the pores, the silane present at the bottom of the pores was removed by short exposure of the supported templates to oxygen plasma. This treatment was performed to avoid any potential interference between the silane molecules and the polyelectrolytes adsorption. Two different polyelectrolyte pairs were adsorbed in these supported templates: (chit/HA) and (PAH/PAA), and the samples were characterized by SEM after dissolution of the template in dichloromethane. As shown on Figure 4.6, we did not observe any

polyelectrolyte nanotube brushes, but only found circular traces of polymer on the silicon wafer, possibly the borders of the nanotubes. This result indicates that the nanotubes formed into the membrane pores are not firmly anchored onto the silicon surface and consequently, pull away from the surface when the template is dissolved. As all attempts to prepare nanotube brushes by this strategy were unsuccessful, we decided to develop another approach.

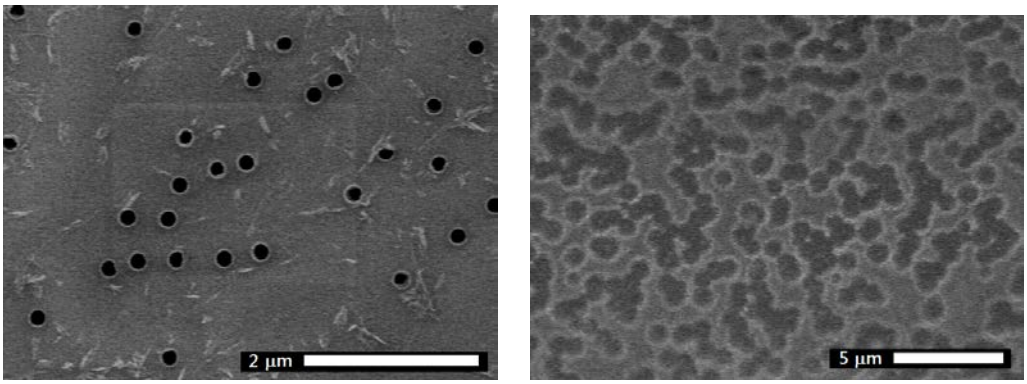

(a) (b)

Figure 4.6: SEM images of (a) the surface of supported PC membrane (200 nm pore size), (b) the surface after template dissolution of a supported PC membrane filled by LbL deposition of $(PAH/PAA)_6$.

4.3.3 Strategy 2 to prepare nanotube brushes: Covalent crosslinking used as LbL nanotube adhesive

The second strategy developed to prepare brushes of nanotubes consists in filling, by LbL deposition, the pores of a polycarbonate template and further, fixing it onto a planar surface. A first possibility to fix the filled membrane onto a solid support reported in the literature [13] is the use of resin superglue. But in our case we did not want to use this strategy as it was shown that the glue is easily adsorbed by capillarity into the pores, which could be very dedrimental to the enzyme activity. Therefore, we tried another method based on chemical crosslinking, presented by Rubner et al. [7]. For this purpose, twelve bilayers of a polysaccharide polyelectrolyte couple $[(chit/HA)_{12}]$ or a synthetic polyelec-

trolyte pair [$(PAH/PAA)_{12}$] were assembled into the pores of a PCm. In both cases, the last layer adsorbed borne carboxylic acid groups that can react with amine groups present on a functionalized Si wafer. After LbL deposition and crosslinking, the upper side of the membrane was polished with alumina powder to remove the top polyelectrolyte layer that clogs the pores. Finally, the PC template was dissolved in dichloromethane and the samples were characterized by SEM. Figure 4.7 shows the resulting brushes of nanotubes made of $(chit/HA)_{12}$. The dimensions of the nanotubes correspond to the dimensions of the pores in the membrane: 300 nm diameter and approximately 5 μ m height. However, most of the nanotubes look very flexible regardless the number of layers and the crosslinking step. Some of the nanotubes are twisted and/or completely lying on the silicon wafer, instead of standing perpendicular to it. On the contrary, nanotubes composed of $(PAH/PAA)_{12}$ appear much more rigid (Figures 4.8a and 4.9) and stand vertically aligned onto the surface, though they tend to form small groups leaning against each other. The fact that polysaccharide-based nanotube brushes were not stiff enough to stand vertically aligned might come from their only partial derivatization (so, lower content of amino- or carboxylic acid groups than synthetic polyelectrolytes) and consequently, weaker crosslinking and/or it might come from an earlier saturation of the pores leading to thinner or less dense nanotube walls compared to synthetic polyelectrolytes like PAA and PAH.

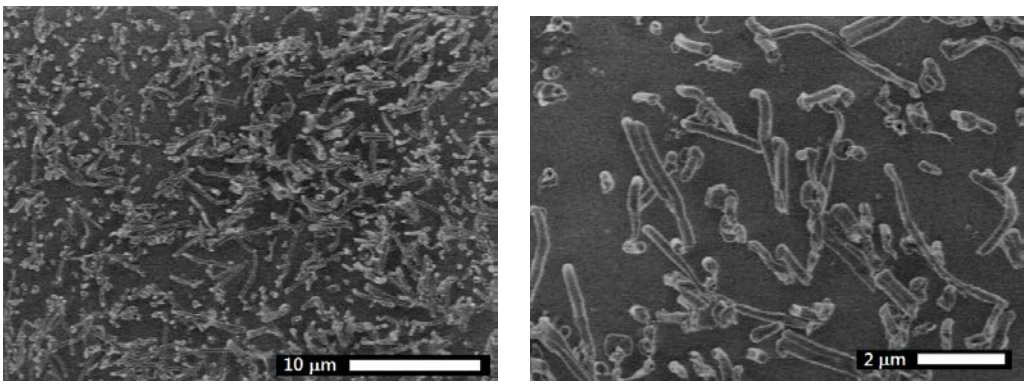

(a) (b)

Figure 4.7: SEM pictures of a brush of $(chit/HA)_{12}$ nanotubes prepared by LbL deposition combined with hard-templating and crosslinking.

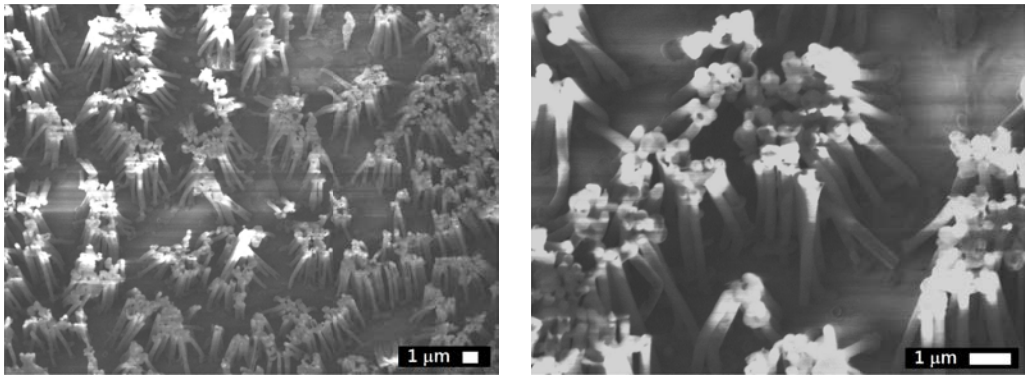

(a) (b)

Figure 4.8: SEM images of brushes of nanotubes $(PAH/PAA)_{12}$ prepared by LbL deposition combined with hard-templating and crosslinking. The samples were decrusted by polishing with alumina powder.

Originally, we tried de-crusting the pores by oxygen plasma, as described by Rubner et al. [7] but we faced some problems (Figure 4.10). Plasma treatment produced highly heterogeneous surfaces, where only some areas presented nice nanotubes, while other regions were still covered by a layer of polyelectrolytes. Increasing the time of irradiation did not solved this problem but strongly damaged the areas that were already uncovered at the beginning of the process. De-crusting with a basic solution also affected the nanotubes and led to tangled nanostructures. We, therefore, used a mechanical decrusting method using 1 μm alumina particles, as they cannot penetrate the pores (300 nm) to polish the membrane surface. This method gives good results (Figure 4.8) though, some small areas still present a crust top layer. This is probably due to irregular hand pressure during the polishing of the samples.

4.3.4 Bioactive enzyme-based nanotube brushes

With the aim of creating bioactive nanotube brushes, a few active layers composed of (chit/β-lactamase) were deposited either inside or outside of $(PAH/PAA)_{12}$ nanotube brushes as illustrated on Figure 4.11. By this way, two different systems were obtained: either nanotube brushes with a bioactive core, or nanopillar arrays

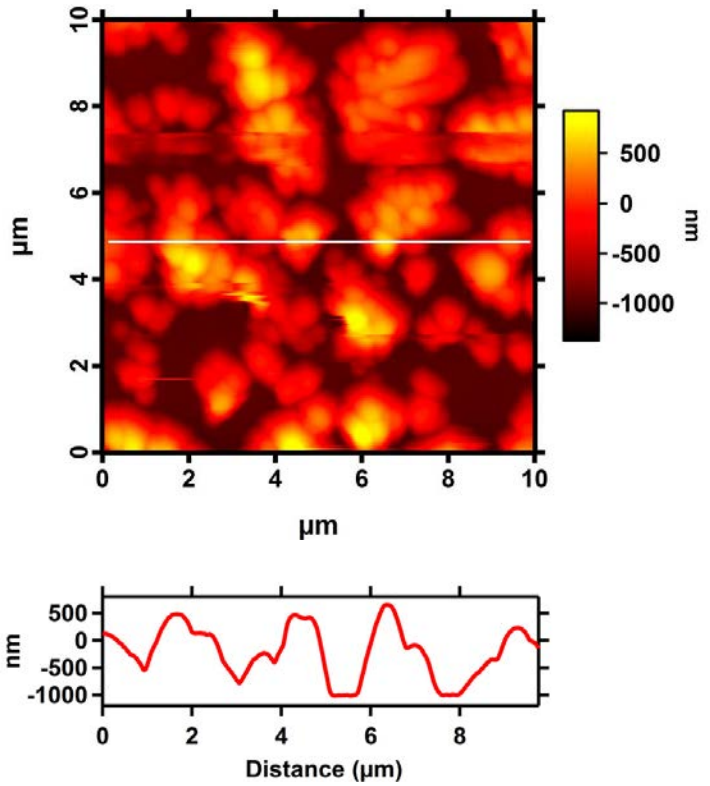

Figure 4.9: AFM image of the nanotube brush $(PAH/PAA)_{20}$ prepared by LbL deposition combined with hard-templating and crosslinking. The height of the features founded by this technique is shorter than expected (height profile), probably the tubes were damaged due to Al polishing.

coated with enzyme.

Here it is important to note that the characteristic dimensions of the PC template (5 μm thick, 300 nm pore size) and the brush were chosen in view to favor the synthesis of standing nanotubes while keeping a large aspect ratio. More important was the selection of the number of (PAH/PAA) adsorbed layers, since they define the new pore diameter in the tubes. For the assembly of 12 PAH/PAA bilayers in a 300 nm external diameter without intermediate decrusting, an internal pore diameter of ca. 180 nm was observed by SEM. And, considering the results from the previous chapter (Section 3.3.4), 4 bilayers of chitosan and β-lactamase in a starting pore of 180 nm are enough to reach the

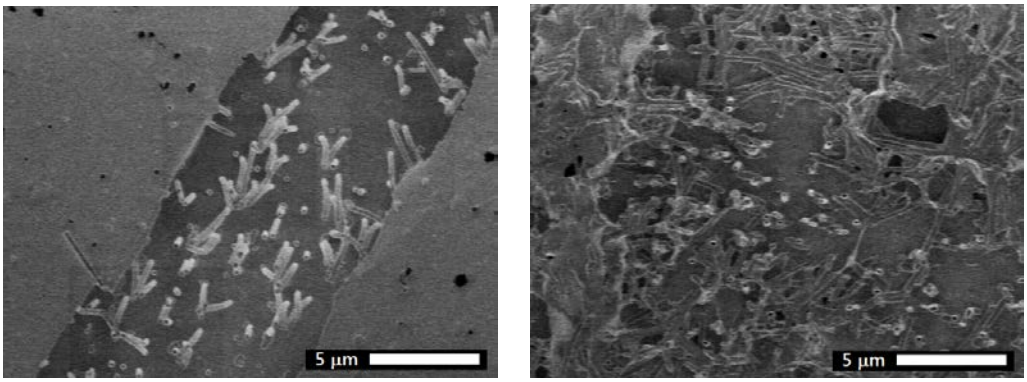

(a) (b)

Figure 4.10: SEM pictures of $(PAH/PAA)_{12}$ nanotube brushes, decrusted by (a) oxygen plasma treatment and, (b) a basic solution.

largest activities.

To incorporate the enzyme within the nanotubes, the PC template was kept after crosslinking of the shell $(PAH/PAA)_{12}$ layers and dipped alternatively into chitosan and β-lactamase solutions to complete four LbL cycles. Then, the template was dissolved in fresh dichloromethane. Conversely, to adsorb the enzyme on top of the nanopillars, the template was removed prior to the LbL deposition of four (chit/β-lactamase) bilayers. This last step has to be performed very carefully to avoid any damage to the nanostructures.

At the end of the entire assembly, the activity of β-lactamase in the different samples was tested by following nitrocefin hydrolysis and the results were compared to those obtained on flat $(chit/\beta\text{-lactamase})_4$ films (Figure 4.12a). The faster rate of nitrocefin hydrolysis is obtained for the system where the enzyme is adsorbed on the outer part of the $(PAH/PAA)_{12}$ pillars. But, the gain of bioactivity (by a factor close to 2) compared to the corresponding flat system is much lower than what could be expected based on the increase of surface area. Indeed, a sample of 1 cm^2 presenting $2 \times 10^8 \cdot$ vertically aligned nanotubes of 5 μm height would provide an increase of the surface area by a factor of 10. This observed difference certainly comes from the fact that $(PAH/PAA)_{12}$ nanotubes are not perfectly vertical-aligned and that some areas of the sample are partially damaged. For the system where the enzyme is adsorbed within the pores, a

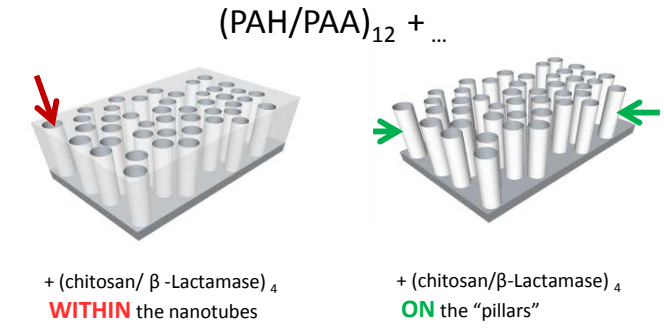

Figure 4.11: Schematic representation of the two methods used to incorporate enzyme layers in the PAH/PAA nanotube brush systems. (Left) adsorption of enzyme layers WITHIN the tubes or (right) adsorption of enzyme layer ON the pillars.

lower bioactivity than the one obtained on flat (chit/β-lactamase)$_4$ film is observed, while the theoretical available surface area should be around 5 cm^2. This probably results from the limited diffusion of nitrocefin within the nanotubes to interact with β-lactamase and the limited diffusion of hydrolyzed nitrocefin out of the nanotubes after reaction, which increases the complexity of the kinetics. Moreover, the contact of the multilayererd samples with dichloromethane also reduces the enzymatic activity of β-lactamase (Supporting Information 4.5).

One interesting feature of the brush of nanotubes with biocatalytic core is, however, its very good enzyme activity retention. Indeed, only a negligible loss of bioactivity is noticed after keeping the samples for 1 month in the fridge (Figure 4.12), while an almost 30 % of enzyme activity loss is observed, in similar conditions, for the system where the enzyme is adsorbed on the pillars. This last finding is in good agreement with previous reports pointing out the fact that LbL confinement can improve enzyme properties, enhancing stability under operation and in stock [14, 15, 16]. Moreover, the selective deposition of (chit/β-lactamase)$_4$ inside or outside of the nanotubes might define the interaction of the brush with the surrounding environment. For example, Rubner et al. recently demonstrated that the most external layers on polyelectrolyte nanotubes define the way the nanotubes orient themselves on cell surfaces [17].

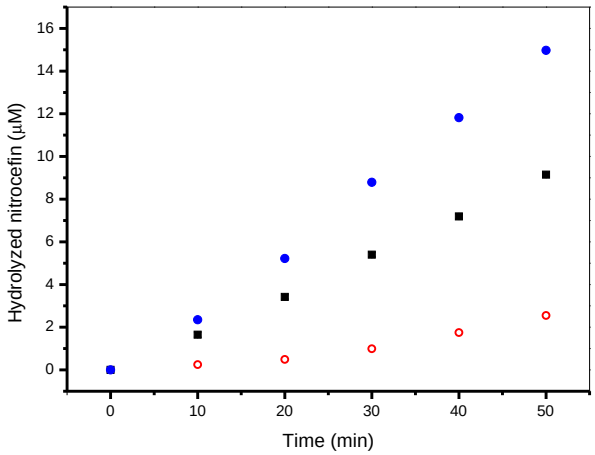

(a)

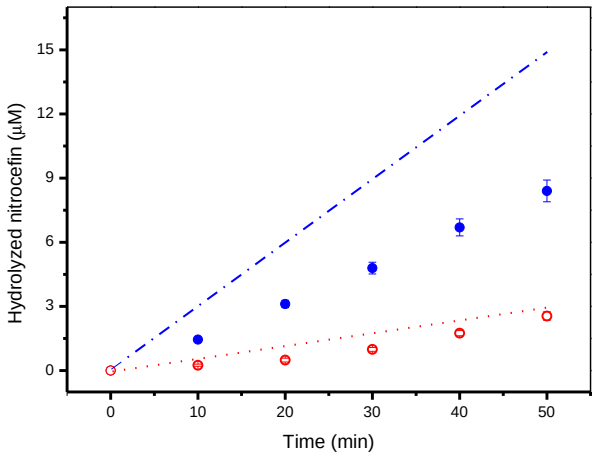

(b)

Figure 4.12: Nitrocefin hydrolysis by the nanotubes brushes $(PAH/PAA)_{12}$ with $(chit/\beta\text{-lactamase})_4$ layers WITHIN the tubes (○) or ON the tubes(●). (a) Also compares the activity with $(chit/\beta\text{-lactamase})_4$ flat film (■), and (b) graph shows the activity after 1 month of preparation. Dashed and dotted lines indicate the original activity values, one day after the brushes were prepared.

4.4 Conclusion

Two different strategies, based on LbL-assisted templating method, were explored to fabricate brushes of self-assembled bioactive nanotubes containing β-lactamase.

In the first approach, track-etched PC membranes supported on silicon wafers were used as templates. Though the LbL deposition within the nanopores was efficient, the anchorage of the resulting nanotubes onto the solid surface after template removal was too weak for obtaining nanotube brushes. (PAH/PAA)-based nanotube brushes were, however, successfully fabricated by the second explored strategy, consisting in filling the pores of a self-supported PC membrane by LbL deposition of polyelectrolytes and fixing it onto a functionalized solid surface by covalent crosslinking prior to template removal. Ultimately, bioactivity was imparted to these nanotube brushes by depositing (chit/β-lactamase)$_4$ layers on the inner or on the outer part of the nanotubes. Interestingly, it was shown that when the enzyme is included in the core of the nanotubes, its biocatalytic activity is better preserved than when the enzyme is deposited on top of the PAH/PAA nanopillars.

4.5 Supporting Information.

Loss of enzymatic activity due to dichloromethane. The influence of CH_2Cl_2 on the activity of β-lactamase molecules was investigated in flat films (chitosan/β-lactamase)$_3$.

For this test, a set of 8 samples (chitosan/β-lactamase)$_3$ were prepared in parallel and their rate of hydrolysis was determined by UV/Vis spectroscopy. After rinsing the samples, 4 of them were exposed to CH_2Cl_2 (2 during 5 min, and other 2 for 30 min), whereas 4 samples were kept in MES buffer solution all the time. After rinsing again the samples in MES buffer, the nitrocefin colorimetric test was repeated. The loss of activity found between the first and the second test is summarized in the Figure 4.13.

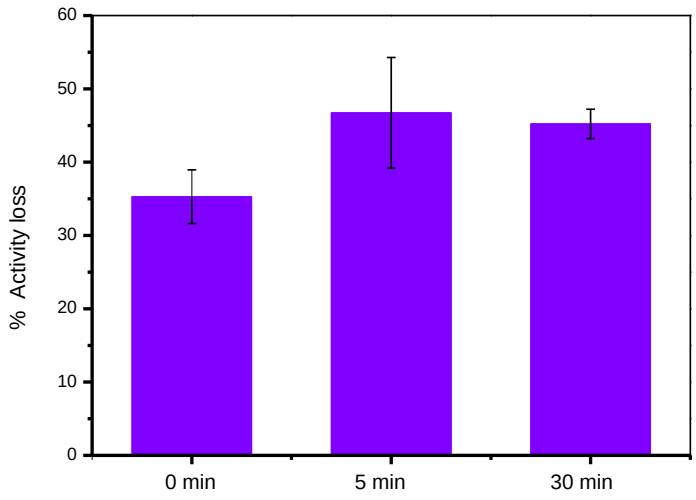

Figure 4.13: Activity loss for multilayered films (chit/β-lactamase)$_3$ from the 1st to the 2nd activity test. The samples were rinsed in MES buffer between the analyses and brought in contact with dichloromethane during 0, 5 and 30 minutes.

It seems that the contact with dichloromethane decreases an extra 10-15 % of the activity between the first and the second test. Moreover, 5 or 30 minutes contact has a very similar influence.

References

[1] Kyoung Taek Kim, Silvie A Meeuwissen, Roeland JM Nolte, and Jan CM van Hest. Smart nanocontainers and nanoreactors. *Nanoscale*, 2(6):844–858, 2010.

[2] Katsuhiko Ariga, Qingmin Ji, Taizo Mori, Masanobu Naito, Yusuke Yamauchi, Hideki Abe, and Jonathan P Hill. Enzyme nanoarchitectonics: organization and device application. *Chemical Society Reviews*, 42(15):6322–6345, 2013.

[3] Evelyne Friederich and Daniel Louvard. Microvilli. In *Encyclopedic Reference of Genomics and Proteomics in Molecular Medicine*, pages 1116–1121. Springer Berlin Heidelberg, 2006. ISBN 978-3-540-44244-8.

[4] Intestinal microvilli, TEM (p520/0194). `http://www.sciencephoto.com/media/310080/view`, 2013. Accessed on 30-03-2014.

[5] Omar. S. Sakr and Gerrit Borchard. Encapsulation of enzymes in layer-by-layer (LbL) structures: Latest advances and applications. *Biomacromolecules*, 14(7):2117–2135, 2013.

[6] Sufen Ai, Gang Lu, Qiang He, and Junbai Li. Highly flexible polyelectrolyte nanotubes. *Journal of the American Chemical Society*, 125(37):11140–11141, 2003.

[7] Khek-Khiang Chia, Michael F. Rubner, and Robert E. Cohen. pH-responsive reversibly swellable nanotube arrays. *Langmuir*, 25(24):14044–14052, 2009.

[8] Ryunosuke Kato and Teruyuki Komatsu. Protein nanotube arrays immobilized on solid substrates: Molecular trap in aqueous medium. *Chemistry Letters*, 40(12):1338–1339, 2011.

[9] Shun Goto, Yusuke Amano, Motofusa Akiyama, Christoph Bottcher, and Teruyuki Komatsu. Gold nanoparticle inclusion into protein nanotube as a layered wall component. *Langmuir*, 29(46):14293–14300, 2013.

[10] Etienne Ferain and Roger Legras. Track-etch templates designed for micro- and nanofabrication. *Nuclear Instruments and Methods in Physics Research Section B: Beam Interactions with Materials and Atoms*, 208:115–122, 2003.

[11] Thomas Crouzier, Thomas Boudou, and Catherine Picart. Polysaccharide-based polyelectrolyte multilayers. *Current Opinion in Colloid & Interface Science*, 15(6):417–426, 2010.

[12] Teruyuki Komatsu, Hiromi Terada, and Nao Kobayashi. Protein nanotubes with an enzyme interior surface. *Chemistry A European Journal*, 17(6): 1849–1854, 2011.

[13] Shelley A Dougherty, Dawei Zhang, and Jianyu Liang. Fabrication of protein nanotubes using template-assisted electrostatic layer-by-layer methods. *Langmuir*, 25(22):13232–13237, 2009.

[14] Roger A Sheldon. Enzyme immobilization: The quest for optimum performance. *Advanced Synthesis & Catalysis*, 349(8-9):1289–1307, 2007. ISSN 1615-4169.

[15] Cesar Mateo, Jose M Palomo, Gloria Fernandez-Lorente, Jose M Guisan, and Roberto Fernandez-Lafuente. Improvement of enzyme activity, stability and selectivity via immobilization techniques. *Enzyme and Microbial Technology*, 40(6):1451–1463, 2007.

[16] Rafael C Rodrigues, Claudia Ortiz, Ángel Berenguer-Murcia, Rodrigo Torres, and Roberto Fernández-Lafuente. Modifying enzyme activity and selectivity by immobilization. *Chemical Society Reviews*, 42(15):6290–6307, 2013.

[17] Jonathan B Gilbert, Janice S O'Brien, Harini S Suresh, Robert E Cohen, and Michael F Rubner. Orientation-specific attachment of polymeric microtubes on cell surfaces. *Advanced Materials*, 25(41):5948–5952, 2013.

Chapter 5

Thermoresponsive thin films as tunable biocatalytic barriers

This chapter presents several strategies to prepare thermoresponsive thin films with different architectures on β-lactamase multilayer assemblies, in an effort to obtain thermoresponsive biocatalytic surfaces. The ability of these films to control substrate diffusion (*i.e.* nitrocefin) is evaluated by nitrocefin hydrolysis below and above the LCST.

5.1 Introduction

Stimuli-responsive behavior is one of the most important features present in living systems and desired for synthetic materials. It can be described as the ability to sense a change of one external factor (*e.g.* pH, light, temperature, ultrasonic waves, mechanical force), to display some conformational or chemical changes, and to reflect these changes at a larger scale or in a significant event. In some sense, stimuli-responsive materials interact smartly with their surroundings and they are of great interest for a diverse range of applications, such as drug delivery, tissue engineering, biosensors, microfluidic devices, etc.

Among a large spectrum of responsive materials, polymers that respond to temperature have attracted much attention, and poly(*N*-isopropylacrylamide) (PNIPAM) derivatives are probably the most studied in this category [1, 2]. The thermoresponse relies on a reversible and abrupt change of solubility at a critical temperature that is also called coil to globule transition. PNIPAM is very attractive for biomedical applications since its Lower Critical Solution Temperature (LCST) in water is 32 °C [3], and this temperature can be tuned by adding comonomer units to its structure. Another and more recently discovered thermoresponsive polymer is poly (2-(2-methoxyethoxy)ethyl methacrylate) ($PMEO_2MA$), which has a LCST of 26 °C in solution that increases to 33 °C when the polymer chains are grafted on a surface [4]. Hence, the critical temperature can be tuned by monomer composition and the set of constrains that limit the structural transformation. Moreover, the right selection of a synthesis method and monomer composition, depends on the specific application [5].

Thermoresponsive thin films offer shorter response times compared to their analogous bulk polymer, and can be synthesized by several strategies that lead to different architectures, including: a) grafted polymer chains, b) polymer networks, c) self-assembled polymer layers and multilayers [6]. The LCST has been exploited to prepare surfaces that modify their wettability, adhesivity or porosity. In the field of biomaterials, responsive hydrogels and microgels are reported as good alternative for drug/protein uptake and release [7], whereas grafted thermoresponsive brushes can give tunable antibacterial/antifouling surfaces [8] and reversible interfaces for cell sheet culture [9].

In this chapter, we investigate the anchorage of thermoresponsive thin films on enzyme multilayers and evaluate their ability to control biocatalytic performance. The enzyme multilayer assembly (chitosan/β-lactamase) plays the role of biocatalytic reservoir, onto which different thermoresponsive thin films are deposited in order to function as a membrane with responsive permeability, blocking or allowing substrate diffusion. The chemical structure of the thermoresponsive polymers and a schematic representation of the films prepared are given in the Figure 5.1. As a starting point, the biocatalytic behavior of the (chitosan/β-lactamase) films (Figure 5.1**(a)**) was studied at different temperatures to have a reference against the $PMEO_2MA$ or PNIPAM coated systems. The first responsive strategy presented is the grafting of polymer brushes from LbL layers. The functionalization of surfaces with polymer brushes has shown a good control for load/release of small particles [10]. In this study, $PMEO_2MA$ brushes (Figure 5.1**b**) were grafted from chitosan/β-lactamase biocatalytic layers, as was done by Advincula *et al.* [11] for PNIPAM brushes. The ATRP initiator was either adsorbed as a functionalized polymer (by electrostatic interactions) or reacted as a silane (by gas-phase silanization) (Figure 5.1**(b1, b2)**). As a second strategy, we investigate a more simple method which consists of the LbL adsorption of PNIPAM segments in a PAH/PAA-*b*-PNIPAM top multilayer (Figure 5.1**(c)**). Due to the fact that microgel particles have shown responsive properties applicable to drug release [7, 12, 13], we decided also to test microgel particles based on NIPAM and NIPAM-like monomers (Figure 5.1**(d1, d2)**). The microgels were adsorbed by LbL as negatively charged particles, using PAH as a polycation. As the 4th thermoresponsive strategy, spin-coating of ene functionalized PNIPAM hydrogel networks (PNIPAM*) was done over (chitosan/β-lactamase) flat films, and separately on nanotube brushes with (chitosan/β-lactamase) active core (Figure 5.1**(e1, e2)**).

The final goal of the strategies implemented is to achieve a thermo-responsive biocatalytic platform. Mechanically-triggered biocatalytic LbL assemblies have been successfully prepared by the group of Vogel and Lavalle [14, 15]. In their work, a $(PDADMAC/\ PSS)_n$ top multilayer controls substrate diffusion by changes in permeability, which result from the stretching of the whole film assembly supported on polydimethylsiloxane. In our case, it is expected that the coil-to globule

Figure 5.1: Chemical structure of the thermoresponsive polymers used herein (top), and schematic representation of the different architectures prepared (bottom). From left to right: (a) biocatalytic reservoir: chitosan/β-lactamase, (b1, b2) $PMEO_2MA$ brushes grafted from LbL using a macroinitiator layer or a silane initiator, (c) PNIPAM blocks in LbL, (d) microgel particles *M1* or *M2* in LbL, and finally (e1, e2) spin-coated PNIPAM* networks over flat films or brushes of nanotubes, respectively.

transition of the thermoresponsive barrier tunes the permeability of the films and controls substrate diffusion. Moreover, the idea behind testing several responsive film architectures is to compare them and find the "all in one" system that better preserves the activity of the enzyme and simultaneously displays the larger responsive behavior. As a matter of fact, one of the major challenges faced in this study was to adapt some synthesis pathways to protein-friendly conditions, so that we could evaluate the role of the responsive coatings on the activity response afterwards.

5.2 Experimental methods

5.2.1 Layer-by-Layer build-up

Polyelectrolyte multilayers were deposited by alternately dipping a charged surface (Si wafers or polymer films) in polycation and polyanion solutions. The build-up started typically with polycation adsorption (5 min), followed by two rinsing steps in MES buffer (2 min each) to remove loosely attached polyelectrolyte chains. Then, the surface with an excess of positive charge was dipped in the polyanion solution (also for 5 min) and rinsed twice to complete one LbL cyle. This process was repeated until the desired number of cycles (n) was achieved. All the polyelectrolytes were adsorbed from a 1 mg.mL^{-1} solution in MES 0.1 M pH 6.5, for 5 min unless stated otherwise. Some of the multilayer films were crosslinked by EDC/NHS at the end of the assembly.

Chemical crosslinking by EDC/NHS. 1-Ethyl-3-(3-dimethylaminopropyl) carbodiimide (EDC) and N-hydroxysuccinimide (NHS) were purchased from ThermoScientific and used in aqueous solution at a concentration of 6 and 3.5 mM respectively. To achieve partial chemical crosslinking between COOH and NH_2 groups, the multilayer films were immersed in the EDC/NHS solution for 30 min at room temperature and rinsed twice (5 min each) in fresh buffer.

5.2.2 Polymer brushes by ATRP

Materials. Poly(2-hydroxyethyl methacrylate) (PHEMA, Mn 11,600 g.mol^{-1}, PDI 1.09) from Polymer Source was used without further purification. Triethylamine (TEA, $\geq$ 99%), 4-(dimethylamino)pyridine (DMAP, $\geq$ 99%), 2-bromoisobutyryl bromide (BIBB, 98%), 2-sulfobenzoic acid cyclic anhydride (SBA, 95%), N,N'-dicyclohexyl-carbodiimide (DCC, 99%), hexanes ($\geq$95%) and dichloromethane ($\geq$99.8%) from Acros were used as received. 2-Hydroxyethyl 2-bromoisobutyrate (HEBIB, 95%), N,N-dimethylformamide (DMF, 99%), di(ethylene glycol) methyl ether methacrylate (MEO2MA) (95%), poly(acrylic acid) (Mw $\sim$100,000 g.mol^{-1}, 35 wt. % in H_2O), copper(I) chloride ($\geq$ 99.995%) ($Cu^{I}Cl$), copper(II) chloride ($\geq$ 99.999%) ($Cu^{II}Cl_2$) and 2,2'-bipyridyl (bipy, $\geq$99%), were purchased from Sigma-Aldrich and utilized without further purification. Milli-Q water (resistivity higher

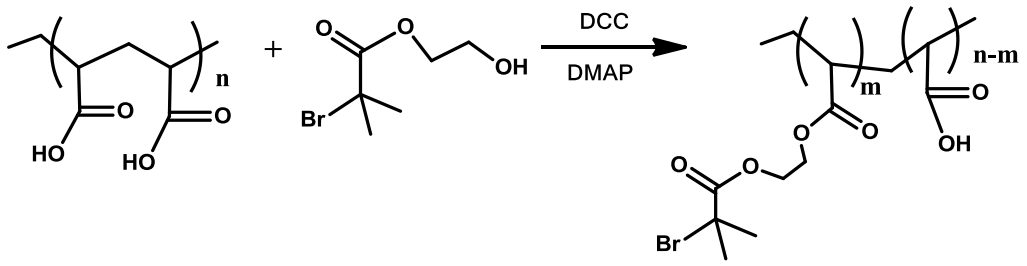

Figure 5.2: PAA functionalization with HEBIB to act as ATRP macroinitiator.

than 18.2 MΩ.cm) was obtained from a Millipore Simplicity 185 system. Single-side polished silicon wafers (Si, <100> orientation, ACM) were cleaned in piranha solution for at least 20 min, and then thoroughly washed with pure Milli-Q water prior to use.

Synthesis of PAA macroinitiator. A macroinitiator based on PAA was prepared using the method reported earlier by Advincula *et al.* [16] (Figure 5.2). Briefly, HEBIB (7.0 g, 31 mmol), PAA (24.4 mL, 135 mmol), and DMAP (100 mg, 0.8 mmol) were dissolved in dichloromethane (20 mL). DCC (6.386 g, 31 mmol) was dissolved in dichloromethane (10 mL) and added dropwise to the stirring solution at 0 °C, which was further stirred for 20 min. The solution was left to react for another 5 h and allowed to warm to room temperature, after which the solution was filtered to remove urea that had formed during the reaction. The solvent was removed by rotoevaporation, and the modified PAA polymer precipitated in hexanes. The PAA-alkyl bromide initiator was then dried at 50 °C in vacuum, yielding a white powder.

PAA macroinitiator layers. PAA macroinitiator (PAA_i) was adsorbed from 1 $mg.mL^{-1}$ solution in a methanol:water mixture, onto amine-functionalized Si wafers. To increase the load of macroinitiator per unit of area, we used poly(allylamine hydrochloride) (PAH) as a polycation and PAA_i as a polyanion, to prepare multilayer films. The first adsorbed layer was the macroinitiator, followed by n cycles of $(PAH/PAA_i)_n$ and ending by a PAA_i layer.

Functionalization of PHEMA as anionic macroinitiator. The functionalization with sulfobenzoic acid was done in two stages (Figure 5.3), following a previously reported method [17].

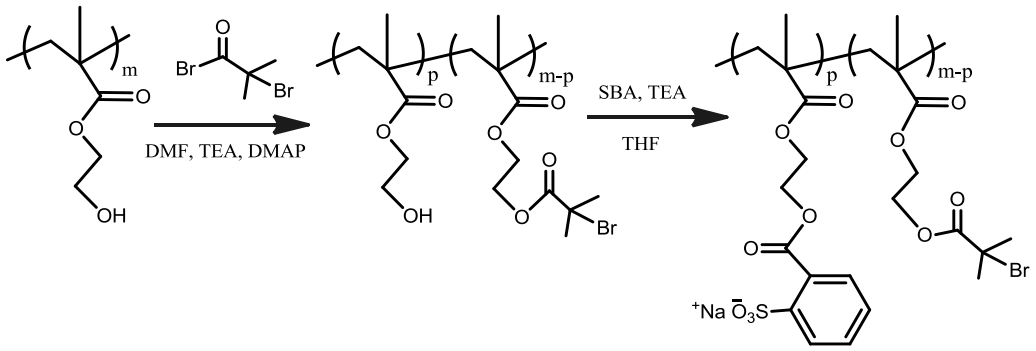

Figure 5.3: PHEMA esterification to prepare an anionic ATRP macroinitiator

i) PHEMA partial esterification with 2-bromoisobutyryl bromide. To start, PHEMA (1.0 g, 7.7 mmol of hydroxyl groups) was dissolved in dried DMF (2.5 mL) followed by the addition of TEA (0.10 g, 1 mmol) and DMAP (0.12 g, 1 mmol) at room temperature. The mixture was then cooled in an ice bath, and BIBB (0.33 mL, 2.7 mmol, 35 mol % relative to the hydroxyl groups of PHEMA) was added dropwise under dry nitrogen. The reaction mixture was allowed to reach room temperature and it was stirred for 24 h. The solvent was removed by rotoevaporation. The isolated product was redissolved in methanol and subsequently precipitated in excess deionized water (twice). The resulting solid (PHEMA-BIBB) was finally dried in vacuum to produce the partially esterified precursor (yield 0.7 g, 70%).

ii) Synthesis of PHEMA anionic macroinitiator from PHEMA-BIBB. The partially esterified precursor (PHEMA-BIBB, 0.70 g, 2.5 mmol of OH residues) was dissolved in anhydrous THF (8.75 mL), followed by the addition of TEA (1.05 mL, 7.5 mmol) and SBA (1.38 g, 7.5 mmol) under nitrogen. The reaction was allowed to proceed for 3 days at room temperature to allow the esterification of the remaining hydroxyl groups. The solvent was removed under vacuum and the isolated crude product was dissolved in deionized water. The aqueous resulting solution was purified by dialysis, replacing successive mother liquors with deionized water, prior to freeze drying to obtain PHEMA anionic macroinitiator (yield 0.80 g, 66%).

PHEMA macroinitiator adsorption from aqueous solution. The anionic macro-

initiator was adsorbed on top of amine-functionalized Si wafers from 1 mg.mL^{-1} aqueous copolymer solutions overnight at room temperature, similarly to the work reported by Edmonson *et al.* [18] (Figure 5.4). In this case, the amine-functionalized surfaces were either Si wafers previously functionalized with (3-aminopropyl)-dimethylethoxysilane (APDMS), either multilayered films terminated with amine groups; *i.e.* chitosan or poly(allylamine hydrochloride). Wafers were thoroughly rinsed with water and dried before use. Typical values of thickness increase observed by ellipsometry were: 1.5 ± 0.2 nm for the macroinitiator layer on APDMS functionalized wafer, 5.1 ± 0.5 nm for LbL films ending with PAH and 9.2 ± 1.0 nm for LbL films terminated with chitosan.

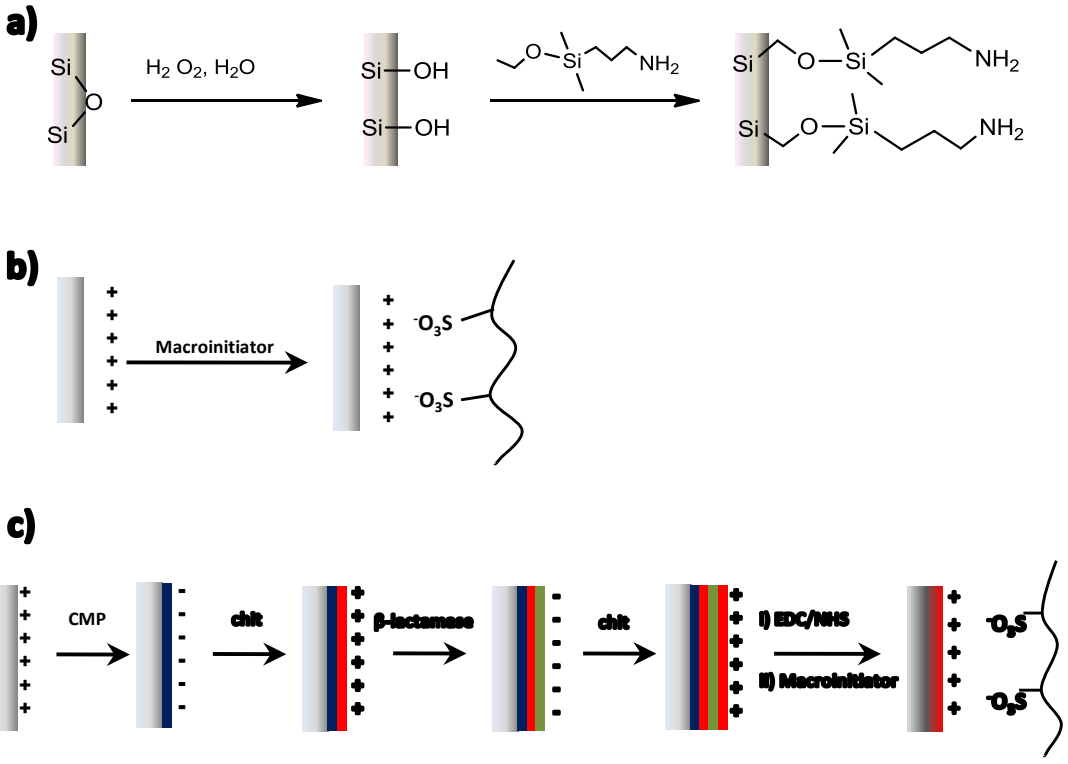

Figure 5.4: Schematic representation of the surface functionalization with PHEMA macroinitiator: (a) Amine functionalization on Si wafers and the subsequent macroinitiator adsorption on (b) Aminosilanized Si wafers, or (c) Multilayer assemblies terminated with amine functionalized polymers, *e.g.* chitosan.

Silane initiator. The ATRP silane initiator, 3-(chlorodimethylsilyl)propyl 2-

bromo-2-methylpropanoate, was previously synthesized as described elsewhere [4]. A monolayer of ATRP initiator silane was prepared on clean Si wafers by gas phase silanization. The substrates were placed on a teflon holder and placed in a Schlenk tube. Three cycles of argon/vacuum (5/15 min respectively) at 80 °C were performed on the system before injection of the silane mixture. After 2 h reaction, the thickness of the silane monolayer was 1.0 ± 0.2 nm as determined by ellipsometry. Surfaces functionalized by the ATRP initiator were used as reference samples in ATRP to compare with PAA or PHEMA macroinitiators. Alternatively, the ATRP initiator silane was reacted on top of LbL multilayers $(PAH/PAA)_n$ using the same protocol of gas phase silanization.

Surface-initiated ATRP. Polymer brushes were prepared on Si wafers from a macroinitiator layer (silane, PHEMA or PAA), similarly to the work of Jonas [4] and Advincula [11]. The monomer, MEO_2MA (8.3 mL, 42.5 mmol) was dissolved in a mixture of water (15 mL) and CH_3OH (7.5 mL) in a round-bottom flask sealed with a rubber septum. Bipy (2.5 mmol, 391 mg) and $Cu^{II}Cl_2$ (0.08 mmol, 11 mg) were added to this solution, which was stirred and degassed with a stream of nitrogen for one hour. $Cu^{I}Cl$ (0.8 mmol, 79.25 mg) was then added quickly to the solution. The solution was stirred and degassed for 45 further min. Meanwhile, the initiator-grafted Si wafers were sealed into Schlenk tubes and were degassed (4 vacuum/N_2 filling cycles). The polymerization solution was then extracted with a syringe and quickly transferred to the Schlenk tubes. After various polymerization times at room temperature under inert atmosphere in the absence of stirring, the samples were removed, washed with water then methanol and dried with a stream of N_2. For each kind of sample, one replica was stored under nitrogen and two others were stored in buffer solution prior to ellipsometry and UV bioactivity assay, respectively.

Bio-friendly surface-initiated ATRP. Polymer brushes were prepared in water, following almost the same protocol described above. In this case, there was no methanol, the monomer concentration was lower ($\sim$ 20%) and the molar ratios are according to Averick's work about protein-friendly ATRP [19] (Table 5.1).

Table 5.1: Stoichiometry of the reactants for Surface-Initiated ATRP reactions

Reference	MEO_2MA		Bipy	CuCl	$CuCl_2$	Solvent
	%v	mmol	mmol	mmol	mmol	-
Jonas [4]	28	594	31	10	1	CH_3OH:H_2O 1:2
Averick [19]	17	227	22	1	9	H_2O

5.2.3 Multilayers of PNIPAM block copolymers.

Materials. Poly(allylamine hydrochloride) (PAH, M_w 15000) was purchased from Sigma-Aldrich and used as received. The block copolymer poly(acrylic acid)-PAA-*b*-PNIPAM was synthesized by Reversible Addition-Fragmentation chain Transfer polymerization (RAFT) at the Center for Education and Research on Macromolecules, University of Liège, Belgium. The molar mass of the blocks is 13400 and 15400 $g.mol^{-1}$ for PAA and PNIPAM, respectively. Crosslinking agents: 1-ethyl-3-(3-dimethylaminopropyl) carbodiimide (EDC) and N-hydroxysuccinimide (NHS) were purchased from ThermoScientific and used without further purification.

Multilayer coatings $(PAH/PAA\text{-}b\text{-}PNIPAM)_n$ (Figure 5.1c) were prepared by LbL on top of the active films $(chitosan/\beta\text{-}lactamase)_m$. Traditionally, the assembly started by a few layers of chitosan and β-lactamase, also called "active" layers. Then the "responsive" layers $(PAH/PAA\text{-}b\text{-}PNIPAM)_n$ were adsorbed, following the LbL protocol. The first adsorbed layer was PAH and the last (and more external layer) was PAA-block-PNIPAM. Some of the samples were chemically crosslinked by EDC/NHS at the end of the assembly.

5.2.4 Crosslinked microgel nanoparticles

Microgels of crosslinked poly(*N*-isopropylacrylamide) (PNIPAM, M1) or based on copolymers *N,N*-propylacrylamide (NNPAM) and *N*-isopropylmethacrylamide (NIPMAM) (M2) were synthesized via precipitation polymerization by the group of Physical and Biophysical Chemistry from the University of Bielefeld, Germany. Both kind of microgels exhibit a Lower Critical Solution Temperature (LCST) [20, 21], and their responsive properties are summarized in Table 5.2. The micro-

Table 5.2: Properties of the responsive crosslinked microgel nanoparticles.

Sample name	M1	M2
Thermoresponsive monomer	NIPAM	NNPAM:NIPMAM[i]
LCST (°C)	33	30
R_h in fully swollen state (nm)	125	130
R_h in fully collapsed state (nm)	56	58

[i] 60%mol NNPAM, 40%mol NIPMAM.
[ii] R_h stands for hydrodynamic radius.

gel surface is slightly negatively charged due to the persulfate initiator used for the synthesis, and this charge is important to achieve a LbL assembly.

In order to prepare a responsive film, the microgel suspension was diluted to give a working solution of 5 mg.mL^{-1} in MES 0.1 M at pH 6.5. Amine-functionalized wafers (either aminosilanized or coated by LbL active films), were dipped in the microgel solution for about 30 min to promote the microgel adsorption, then the wafers were rinsed twice in MES buffer (10 minutes in total). To increase the load of microgel particles per unit of area, we also prepared multilayer assemblies using poly(allylamine hydrochloride) as a polycation to obtain $(PAH/M1)_n$ or $(PAH/M2)_m$ films by LbL.

5.2.5 Spin-coated PNIPAM* hydrogels

Materials. Poly(diallyldimethylammonium chloride) solution (20% in water, Mw $\leq$ 100,000 g.mol^{-1}, PDADMAC), poly(sodium 4-styrenesulfonate) (Mw $\sim$ 70,000 g.mol^{-1}, PSS) and 2,2-dimethoxy-2-phenylacetophenone (99%, DMPA) from Sigma-Aldrich were used as received. Dithioerythritol (DTE) and the PNIPAM ene-functionalized hydrogels (PNIPAM*) were kindly provided by the Laboratory of Soft Matter Science and Engineering, ESPCI-ParisTech, France and used as received.

PNIPAM* responsive coatings were prepared over active films (chitosan/β-lactamase) by a thiol-ene reaction (Figure 5.5). To anchor PNIPAM* hydrogels atop the active films, (chitosan/β-lactamase) was sandwiched between PAH/PAA layers, spincoated by PNIPAM* and the crosslinking agents and exposed to UV irradiation afterwards:

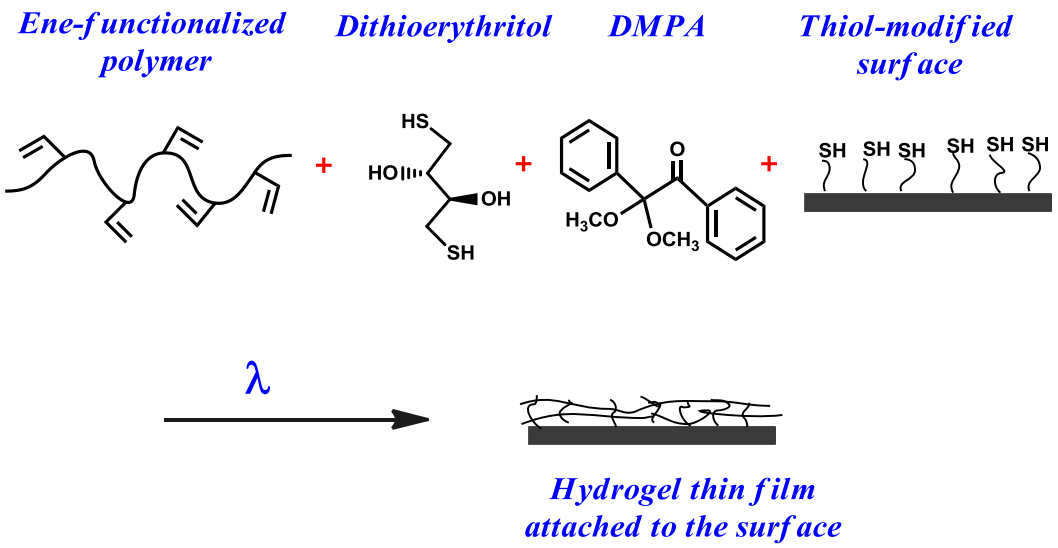

Figure 5.5: Schematic representation of PNIPAM* and the thiol-ene reaction to prepare hydrogels atop a structured multilayer film containing β-lactamase.

1. The first part involved the adsorption of "active" enzyme layers sandwiched by "stabilizing" layers. To that end, a few layers of poly(acrylic acid), poly(allylamine hydrochloride) $(PAA/PAH)_{2.5}$ were adsorbed on aminosilanized Si wafers. The first and last adsorbed layer were PAA to have a negatively charged film. Then 4 "active" LbL cycles of (chitosan/β-lactamase) were adsorbed, and finally three more "stabilizing" layers (PAH/PAA/PAH), to get a positively charged surface.

2. One layer of PNIPAM* was adsorbed from solution (5 $mg.mL^{-1}$ in MES 0.1 M, pH 6.5) for 30 min, then rinsed in MES buffer (5 min, twice). The whole multilayer assembly was crosslinked by EDC/NHS in solution for 30 min, rinsed and dried prior to spin-coating.

3. PNIPAM* (20 mg), DTE (3 mg) and DMPA (5 mg) were dissolved in 1 mL of methanol:butanol mixture 1:1 v:v. The mixture was spin-coated at 3000 rpm for 30 s. Immediately after, the films were exposed to UVA irradiation (365 nm) at 3.3 $mW.cm^{-2}$ for 3 h to crosslink the film through reaction of thiol groups of DTE with the ene groups of PNIPAM copolymer. Finally,

the samples were rinsed to remove loosely attached polymer chains and residual chemicals and then rehydrated in MES buffer prior to the test of activity.

Spin-coated hydrogels on active brushes. PNIPAM* hydrogels were also spin-coated atop [$(PAH/PAA)_{12}$ + $(chitosan/\beta\text{-lactamase})_4$] nanotubes brushes (Figure 5.6).

1. The brushes were prepared by hard-templating, LbL assembly and adhesive crosslinking, following the protocol described in section 4.2.3 to obtain nanotubes 5 μm in height and 300 nm in external diameter.

2. A thin layer of PNIPAM* was adsorbed on the brushes from a 5 $mg.mL^{-1}$ solution in MES 0.1 M pH 6.5 for 30 min, prior to spin-coating. The same spin-coating parameters (2% PNIPAM in methanol/butanol, 3000 rpm, 30 s) and same irradiation conditions as were used for the films (3h at 365 nm and 3.3 $mW.cm^{-2}$)

3. A polyelectrolyte layer (either PDADMAC/PSS or PAH/PSS) was adsorbed on top of the brushes and PNIPAM* coating for some of the spin-coated samples. The LbL assembly was done in MES buffer 0.1 M, pH 6.5 at 38 °C, so the gel was collapsed. Besides working at higher temperature, all the working conditions of LbL assembly were maintained (polyelectrolyte concentration of 1 $mg.mL^{-1}$, 5 min polyelectrolyte adsorption, rinsing twice before changing polyelectrolyte).

5.2.6 Ellipsometry

The thickness of flat films deposited on Si wafers was measured by ellipsometry. We used a spectroscopic ellipsometer Uvisel from Horiba-Jobin-Yvon at an incidence angle of 70° in a wavelength range from 400 to 800 nm, for dry film measurements. Ellipsometric data were fitted using the DeltaPsi 2 software with a three layered model: silicon (bulk), native silicon oxide (1.5 nm thickness), and a polymer film. The refractive index of the multilayer films was modeled by a

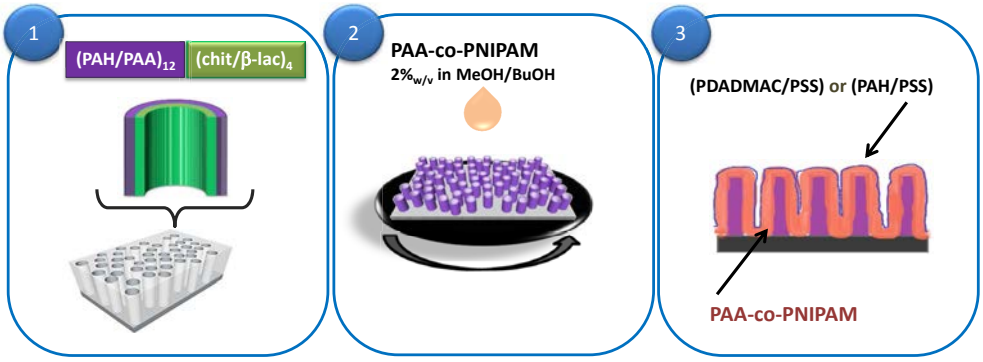

Figure 5.6: Illustration of the basic steps to prepare [PNIPAM* + (PDADMAC/PSS)] coated polyelectrolyte nanotubes brushes: (1) Brush assembly by LbL and hard-templating, (2) Spin-coating PNIPAM* hydrogels, (3) PDADMAC/PSS LbL assembly.

transparent Cauchy layer and the measurement was carried out three times at different points on the substrate to obtain an average.

The film thickness in water medium was determined using an ellipsometer EP3 (from Accurion, Germany), equipped with a liquid cell and a thermo-regulated bath. The system uses a combination of auto nulling ellipsometry and microscopy.

5.2.7 Activity assay

Kinetics of nitrocefin hydrolysis were followed for the samples containing β-lactamase by UV/Vis spectrophotometry (Agilent Cary 50) using the method fully described in Chapter 3, Section 3.2.7. A nitrocefin solution (2 mL, 50 μM in 100 mM MES buffer pH 6.5) was added on a 1 cm^2 sample. The samples were stirred at 300 rpm at constant temperature (25 °C), unless stated otherwise, and aliquots taken at different time intervals. For the response assay, the same protocol was followed, first at 25 °C and then at 40 °C with an intermediate rinsing step (in MES buffer) while the new temperature was reached and stabilized (approx. 15 min). Absorbance of hydrolyzed nitrocefin was detected at 485 nm in standard cuvettes with 1.0 cm pathlength and converted to molar concentration using Lambert-Beer law and a extinction coefficient ϵ_{485} = 16700 M^{-1}cm^{-1}.

A single value of activity reported for a (chitosan/β-lactamase)$_n$ film repre-

sents the average of duplicates, and all the samples compared in each Figure were prepared and analyzed in parallel. It is important to note that any disagreement of activity values reported in previous chapters is due to a faster stirring (300 rpm).

5.2.8 Atomic Force Microscopy

Atomic force imaging was performed using a Bruker Dimension ICON equipped with a Nanoscope V controler and a liquid cell Bruker. The cantilevers employed have a spring constant of 0.01 Nm^{-1}, and the apparatus operated in contact mode with 360 mV as set-up with a scanning frequency of 0.5 Hz.

5.3 Results and Discussion

5.3.1 Biocatalysis and temperature dependence

Since our objective is to control the activity of β-lactamase-based multilayers by changes in temperature, it is important to know how the activity of the enzyme is affected while free in solution or embedded in (chitosan/β-lactamase)$_n$ films (Figure 5.1**a**). Thus, nitrocefin hydrolysis by β-lactamase was studied at 20 °C and also at 40 °C, to guarantee we were below and above the LCST of the thermo-responsive polymers studied. For the free enzyme kinetics, an aliquot of enzyme solution (120 μL of 1 μ.mL^{-1}) was added to nitrocefin and the amount of hydrolyzed nitrocefin was followed by UV-spectrophotometry. Figure 5.7 shows that the hydrolysis by the free enzyme starts slightly faster at 40 °C. However, a larger amount of hydrolyzed nitrocefin was obtained at 20 °C for a larger period of time (more than 1 h). The fact that increasing temperature increases the probabilities of collision explains the higher initial rate at 40 °C. Still, the total amount of hydrolyzed nitrocefin is smaller at 40 °C after 1 h of reaction, which might be a result of the thermal denaturation of β-lactamase. According to the literature, a full unfolded state can be achieved for some classes of β-lactamases above 60 °C, but any temperature above 45 °C could already diminish the activity of the free enzyme [22]. Here this effect appears at slightly lower temperature.

To extend the study to LbL assemblies, a series of (chitosan/β-lactamase)$_4$ films were prepared and brought into contact with nitrocefin at different temperatures to compare their activity. All the samples gave a linear-like evolution of hydrolyzed nitrocefin *vs.* time after 30 min of reaction, and therefore the slopes were taken as initial rates and compared (Figure 5.8). The temperature-activity curve is broad and does not have a clear maximum, the activity values are rather close from 20 to 40 °C, then a clear drop of activity was found at 45 °C and above, as expected [22]. Given that the optimum working temperature reported for β-lactamase in solution is 25 °C [23], it seems that the enzyme won certain resistance to small temperature changes. In fact, the target of enzyme immobilization in many cases is to obtain a more stable enzyme in a broader temperature spectrum [24].

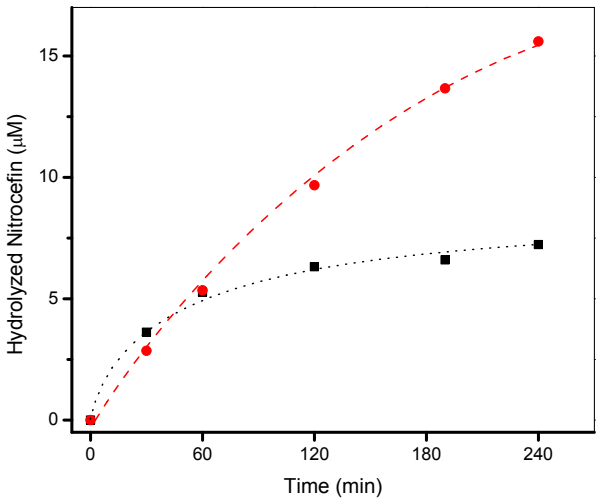

Figure 5.7: Nitrocefin hydrolysis by free β-lactamase in MES 0.1 M pH 6.5, at 20 °C (●) or 40 °C (■).

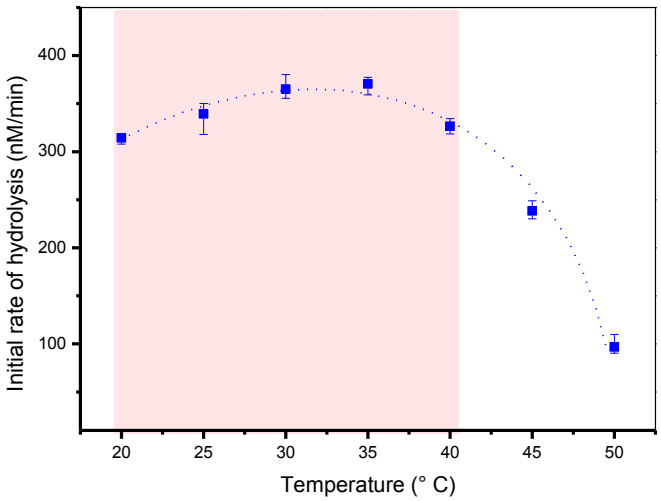

Figure 5.8: Temperature - activity curve of nitrocefin hydrolysis by (chitosan/β-lactamase)$_4$ films in MES 0.1 M pH 6.5. The red area considers the range of working temperatures for thermo-responsive films. Error bars correspond to the range of values measured on triplicates.

Another important fact to consider is the change of enzymatic activity due to the repeated exposure to different cycled temperatures. Hence, a series of (chitosan/β-lactamase)$_4$ films were prepared and used to hydrolyze nitrocefin at 26 and 40 °C for three "thermal cycles" (1 hour at 26 °C, rinsing for 20 min and 1 hour at 40 °C). Intermediate rinsing steps were done between assays to remove unreacted nitrocefin and to allow the samples to be stabilized at the new working temperature. Figure 5.9 shows that the largest loss of activity occurs after the 1st thermal cycle, whereas the average activity at both temperatures tends to be close. The first result might be related to 1) partial enzyme desorption or 2) annealing of the film (i.e. conformational changes and interface smoothing), similar to what Klitzing *et al.* reported for PAH/PSS [25]. It is logical to expect that a minimal amount of enzymes that are loosely attached could desorb after rinsing and stirring. Also, the thermal cycling could promote some conformational changes in the films, resulting in more dense packing and leading to slower nitrocefin diffusion. On the other hand, since the film displays close activity values at 26 and 40 °C along 3 temperature cycles, this suggests that the immobilized enzyme gains some thermal stability at 40 °C compared to the free enzyme. To avoid data misinterpretation, we always compare the PNIPAM or PMEO$_2$MA coated films to reference (chitosan/β-lactamase)$_4$ films without any thermo-responsive layers processed in an identical way.

5.3.2 Polymer brushes by ATRP

We first attempted to provide thermoresponsiveness to the β-lactamase layers by growing a thermoresponsive polymer brush above the multilayer compartment. The polymer brush growth was started either from a macroinitiator layer adsorbed on top of (chitosan/β-lactamase)$_n$ films or from a silane initiator directly reacted on the active films (Figure 5.1 **b1, b2**). The thickness of the macroinitiator films and the grafted PMEO$_2$MA brush was determined by ellipsometry. More important, the activity of the enzyme for nitrocefin hydrolysis in the assembly was surveyed by UV spectrophotometry after every step of surface modification.

First, a **PAA macroinitiator (PAA$_i$)** was prepared following the protocol reported by Fulghum *et al.* [16]. However, our PAA$_i$ product exhibited low sol-

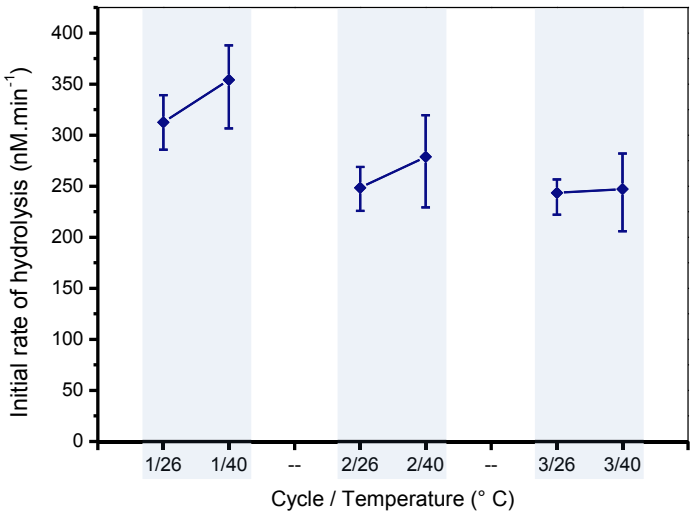

Figure 5.9: Observed activity of (chitosan/β-lactamase)$_4$ films for nitrocefin hydrolysis. Each one of the darker areas represents one thermal cycle.

ubility in water at pH 5.5, 6.5 or 7, contrary to the published report. This issue was probably due to the higher molar mass (100000 g.mol^{-1} *vs.* 60000 g.mol^{-1}) or a different functionalization degree. After the incorporation of the bromine molecule (BIBB) on PAA was confirmed by ^{1}H NMR, we decided to work with it using different mixtures of water and organic solvents (*i.e.*, isopronanol, ethanol, methanol, DMSO, DMF) to improve solubility. The mixture water/methanol (90/10, v/v) showed the highest affinity with the product and it made possible to prepare multilayer assemblies by LbL, using PAH as a polycation. Films (PAH/PAA$_i$)$_n$ were prepared over aminosilanized Si wafers and their growth was monitored by ellipsometry (Figure 5.10). The thickness of the films follows a linear trend, similarly to the PAH/PAA films (with 100% of COOH functionalization along the chain).

The (PAH/PAA$_i$)$_n$ assemblies were then used to grow PMEO$_2$MA polymer chains by ATRP. We observed the growth of an extra layer on the surface after a few hours of reaction: an unstable gel was formed (Figure 5.11). However, this PMEO$_2$MA gel was partially destroyed by air-drying and gave irreproducible results for ellipsometry measurements. The formation of this gel suggests that

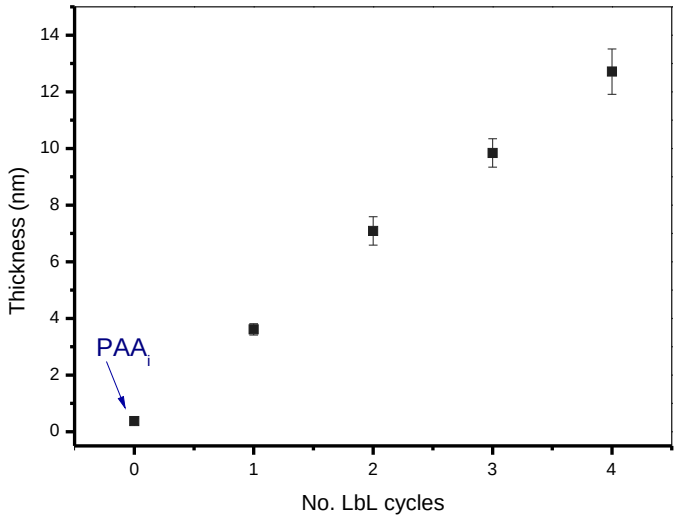

Figure 5.10: Growth of PAA_i + $(PAH/PAA_i)_n$ detected by ellipsometry on aminosilanized Si wafers. The fist and last layer adsorbed was PAA_i.

$(PAH/PAA_i)_n$ layers might partially dissolve during the reaction. Moreover, when the ATRP was initiated from $(PAH/PAA_i)_n$ layers adsorbed on top of (chitosan/β-lactamase) films, we observed a large loss of activity after grafting the brushes. To find more about this inactivation of the enzyme, the samples $(\text{chitosan}/\beta\text{-lactamase})_4$ + $(PAH/PAA_i)_4$ were brought into contact with the ATRP solution mixture for a short time (30 min), rinsed, air-dried and rehydrated on MES buffer for 2h prior to nitrocefin assay. The activity of the films that went through 30 min of contact with the SI-ATRP mixture was equivalent to 5% of the activity of the initial $(\text{chitosan}/\beta\text{-lactamase})_4$ samples, indicating that something in the reaction medium was inhibiting the activity of the enzyme.

It has been reported that the use of polar organic solvents can cause protein unfolding [26], and we used methanol to adsorb the responsive layers as well as in the reaction medium. Therefore, we decided to investigate the effect of methanol on the activity of β-lactamase. Hence, nitrocefin was dissolved in three different solution mixtures with MES buffer 0.1 mM pH 6.5 and CH_3OH. Then, β-lactamase (250 ng) was added to the solutions and stirred, taking aliquots at different time intervals to follow the kinetics of hydrolysis (Figure 5.12). As it can

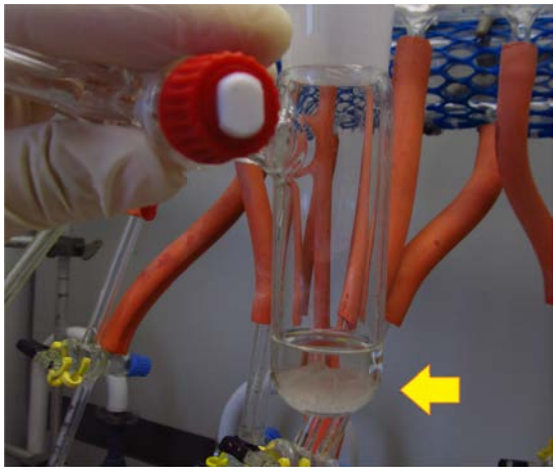

Figure 5.11: Picture of the gel-like structure found on the Si wafers after 1h of SI-ATRP, using PAA_i layers and water/methanol as medium for reaction.

be observed, the contact of β-lactamase with methanol decreases the initial rate of hydrolysis and also the total amount that the enzyme can hydrolyze, suggesting a partial or total unfolding of the enzyme. Because methanol was required for the deposition of $(PAH/PAA_i)_n$ layers, we discarded the use of PAA_i layers to graft responsive brushes.

Therefore, in order to obtain a system fully compatible with water, a **PHEMA anionic macroinitiator** (Mi) was synthesized in the lab. The functionalized polymer contains 30% of BIBB groups and 65% of SBA, in good agreement with the structure reported by Vo *et al.* [17]. More important, the purified macroinitiator Mi was soluble in water and easily adsorbed on top of amine-functionalized surfaces. The thickness of a single Mi layer varied depending on the surface where it was adsorbed: *e.g.* 1.5 ± 0.2 nm on top of aminosilanized Si wafers, 5.1 ± 0.3 nm on *(PAH/PAA)*$_4$ *+ PAH* or, 8.5 ± 1.0 nm on top of *(chit/β-lac)*$_4$ *+ chit*. After confirming the adsorption of the macroinitiator, the surfaces were reacted by ATRP with MEO_2MA monomer in a mixture water:methanol. However, it was difficult to determine the thickness of the polymer brushes prepared by SI-ATRP by ellipsometry, because the films appeared to be quite heterogeneous. In fact, the $PMEO_2MA$ brushes on LbL were partially detached from the surface when air-stream drying, as it occurred with PAA_i macroinitiator.

Since the water/methanol medium showed repeatedly unstable films by SI-

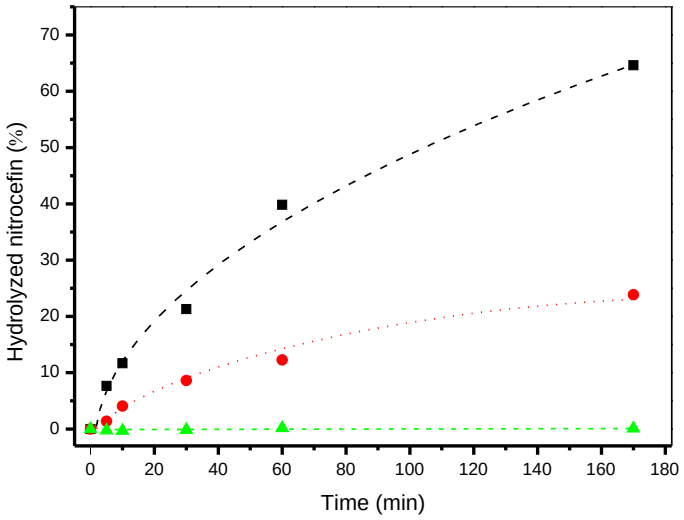

Figure 5.12: Kinetics of nitrocefin hydrolysis by free β-lactamase in different reaction medium: (a) 100% MES 0.1 M pH 6.5 –(■), (b) 90% MES, 10% CH_3OH –(●), and (c) 10 % MES, 90% CH_3OH –(▲).

ATRP on LbL and decreased enzymatic activity, we tried pure water as reaction medium. Also the molar ratios of the controlling agents were adapted to work in a protein-friendly environment, similarly to Matyjaszewski *et al.* [19]. Again, a layer of Mi was adsorbed on a series of (chitosan/β-lactamase)$_4$ prior to polymerization. The films were reacted for 3 h by ATRP in the protein-friendly medium and the thickness and activity of the films were monitored after reaction (Table 5.3). The thickness increase demonstrates the adsorption of the macroinitiator and the growth of polymer brushes. Moreover, the $PMEO_2MA$ anchored on LbL films were stable even without crosslinking the films to the Si wafers and using a single layer of PHEMA macroinitiator. The right column in Table 5.3 presents the activity loss percentage, considering the initial rate of reaction exhibited by (chit/β-lac)$_4$ films as a zero loss reference. A clear activity decrease (55% loss) was observed after Mi adsorption and almost full inactivation after $PMEO_2MA$ grafting. This result might be a consequence of several factors; first of all, the material deposited above β-lactamase layers represents a physical barrier and it slows down nitrocefin diffusion. Furthermore, some transfer agents (ATRP) could

lead to protein denaturation [19]. In fact, we used the same molecular ratios and reaction conditions reported by Matyjaszewski [19] as favorable for bovine serum albumin (BSA)-polymer hybrids. Nevertheless, a BSA friendly medium is not necessarily preserving β-lactamase activity. Considering that a single Mi adsorbed layer causes a large drop of activity, we explored a different method to load an ATRP initiator in the β-lactamase based films.

Table 5.3: Thickness increase after PHEMA macroinitiator adsorption and grafting of P(MEO_2MA) brushes on polyelectrolyte multilayers.

Sample description	Thickness nm	Activity loss %[a]
(chit/β-lac)$_4$ + chit	34.3 ± 2.0	0
(chit/β-lac)$_4$ + (chit/Mi)	42.9 ± 1.0	55
(chit/β-lac)$_4$ + (chit/Mi) + Brush	158.1 ± 1.4	98

[a] Activity loss is considered zero for the film(chit/β-lac)$_4$.

At last, we tried the direct reaction of an **ATRP silane initiator** over the LbL films (Figure 5.1 **c2**) to prepare P(MEO_2MA) brushes in aqueous medium. Gas-phase silanization was performed on Si wafers with (PAH/PAA)$_4$ multilayer films at 80 °C during 2 h. The resulting multilayers loaded with macroinitiator, (PAH/PAA)$_4$-Br, were then tested for SI-ATRP and the thickness increase determined by ellipsometry. Table 5.4 shows that the wafers impregnated with the silane initiator are capable to promote the growth of P(MEO_2MA) brushes. It is also clear that the thickness increase of the grafted brushes was smaller on (PAH/PAA) multilayers compared to the aminosilanized Si wafer. The last result could be explained by a lower density of macroinitiator at the surface, or the presence of buried initiator molecules in the LbL assembly.

Before testing the silane initiator over β-lactamase multilayer films, the silanization process was slightly modified by trial-error, to protect the activity of the enzyme. Hence, the softer silanization conditions we found were: 30 °C, 1 h exposure and more air-vacuum cycles with shorter time before silanization (5 cycles, 3 min each step). A series of [(chit/β-lac)$_4$ + (PAH/PAA)$_4$] was then prepared on aminosilanized Si wafers, crosslinked by EDC/NHS and reacted with the silane initiator. Ellipsometry measurements revealed a thickness increase of

Table 5.4: Thickness increase after reacting silane initiator at 80 °C on $(PAH/PAA)_4$ multilayers and the grafting of $P(MEO_2MA)$ brushes.

Sample description	After Silanization nm	After SI-ATRP nm
Si wafer	1.0 ± 0.1	80.5 ± 0.3
Si + $(PAH/PAA)_4$	0.7 ± 0.4	34.1 ± 2.0
Si + aminosilane + $(PAA/PAH)_4$	0.8 ± 0.2	36.8 ± 2.0

0.50 ± 0.15 nm after silanization, and of 12.30 ± 1.00 nm after 3 h of SI-ATRP in aqueous medium. Unfortunately, a negligible amount of nitrocefin was hydrolyzed by [(chit/β-lac)$_4$ + $(PAH/PAA)_4$ + $PMEO_2MA$] multilayer assembly at room temperature. In consequence, we decided to investigate the effect of the ATRP aqueous solution on the bioactivity of β-lactamase based multilayers. A set of (chitosan/β-lactamase)$_5$ films were prepared; one of them was kept in MES buffer all the time, another one was dipped in the ATRP solution mixture (H_2O, MEO_2MA, $CuCl_2$, CuCl, bipyridyne) for 30 minutes, and a third sample was exposed to extreme conditions (heated at 120 °C during 5 min, dipped in methanol for 5 min and dried). The activity of all the films was surveyed by nitrocefin hydrolysis (Figure 5.13). The sample exposed to extreme conditions and the sample dipped in the ATRP solution mixture showed a similar activity loss. In fact, both sample treatments retain about 5% of the initial activity of the β-lactamase film. This dramatic loss of activity after contact with the ATRP solution might be caused by unspecific inhibition of the enzyme by the copper ions, which have been reported as possible inhibitors [27], or by the monomer. With this last result we decided to discard SI-ATRP (Cu mediated) of $PMEO_2MA$ brushes, considering the large activity loss of β-lactamase based multilayer films in the reaction medium.

5.3.3 Polyelectrolyte multilayers with PNIPAM segments

Due to the extreme sensitivity of β-lactamase enzyme to the ATRP conditions, we switched to a more innocuous system, allowing the deposition of thermoresponsive segments in conditions fully compatible with LbL processing. To im-

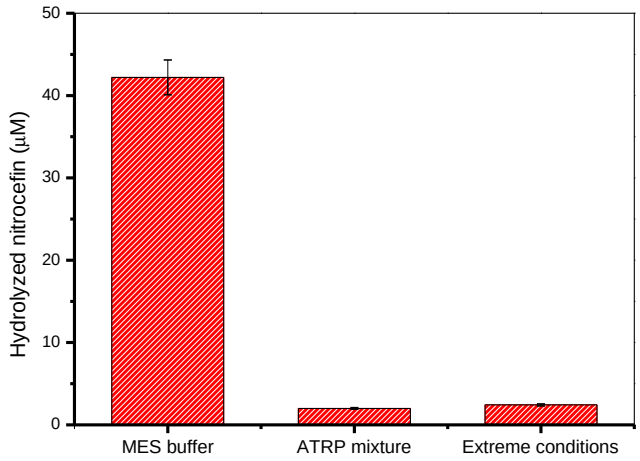

Figure 5.13: Activity of (chitosan/β-lactamase)$_5$ films exposed to different environments prior to nitrocefin assay: MES buffer, ATRP solution or extreme heating and drying conditions. Error bars correspond to the range of values measured on duplicates.

plement this strategy, we used a PAA-*b*-PNIPAM copolymer (Figure 5.1**(c)**). A previous study in our group found a LCST of 35 °C for this particular diblock copolymer in solution [28], and also its ability to adsorb as negatively charged species. Taking these results as a starting point, we adsorbed layers of PAH and PAA-*b*-PNIPAM from MES buffer on top of (chitosan/β-lactamase)$_4$ films, following the LbL protocol. A thickness increase of 29.0 ± 1.0 nm was observed by ellipsometry on dry films after 4 bilayers (PAH/PAA-*b*-PNIPAM) were deposited on top of 4 bilayers (chitosan/β-lactamase) (28.0 ± 0.5 nm). The enzymatic activity at 20 and 40 °C was compared for the PAA-*b*-PNIPAM coated films (crosslinked or not), using the β-lactamase-terminated film as a reference (Figure 5.14). PAA-*b*-PNIPAM coated films show lower initial rate *vs.* (chitosan/β-lactamase)$_4$ films. Since the "responsive layers" function as a physical barrier, the diffusion of nitrocefin is slower and decreases the observed activity on the PNIPAM coated films. It is also clear that all the systems react faster at 40 °C. The last result suggests that the layers of PAA-*b*-PNIPAM never stopped nitrocefin diffusion to the (chitosan/β-lactamase)$_4$ films. Contrariwise, the non

crosslinked PNIPAM layers seem to react faster at higher temperature, which might be related to the instability of the film. In the best scenario, crosslinked (PAH/PAA-*b*-PNIPAM) layers caused a smaller gain on activity at 40 °C *vs.* 20 °C, but not a reverse effect (*i.e.* higher activity at lower temperature). A similar trend was observed for the active films coated with (PAH/PAA-*b*-PNIPAM)$_n$, for 1$\leq$ n $\leq$ 4 (data not shown). The minimum blockage of nitrocefin at 40 °C might be a result of the interpenetration between the PNIPAM segments and the polyelectrolytes, which prevents a full response to the thermal stimulus, as some authors have hypothesized for PAA-*block*-PNIPAM [2, 29].

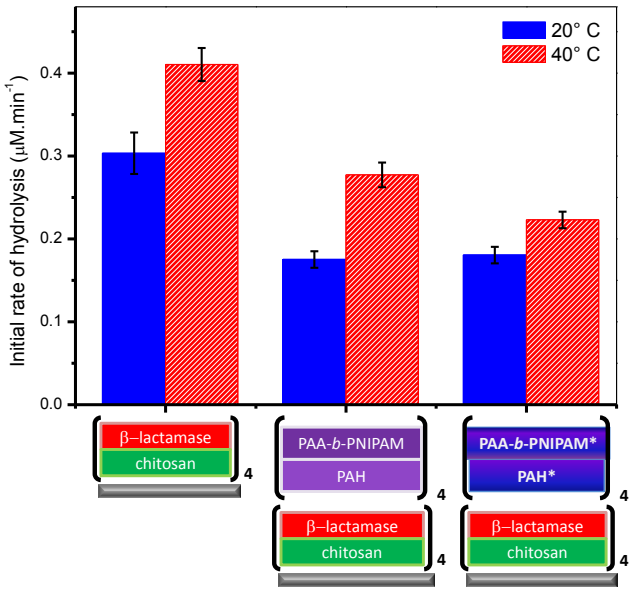

Figure 5.14: Influence of (PAH/PAA-*b*-PNIPAM) multilayers on the activity of (chitosan/β-lactamase)$_4$ films at 20 and 40 °C. Starred systems indicate chemical crosslink by EDC/NHS. Error bars correspond to the range of values measured on duplicates.

5.3.4 Crosslinked microgel nanoparticles

Since PNIPAM microgels have demonstrated a stronger and reversible phase transition (compared to block copolymers) [29], we then decided to prepare multilayers incorporating PNIPAM microgel particles on the active layers (Figure 5.1

(d)). PNIPAM microgel particles (M1) were received as colloidal suspensions in water and they were diluted in MES buffer to achieve a concentration of 5 $mg.mL^{-1}$. As a first experiment, the particles were adsorbed from solution on top of a PAH layer, and a thickness increase of 11.4 ± 0.6 nm was observed by ellipsometry. Then we proceeded to adsorb a bilayer (PAH/M1) or (PAH/M2) on top of (chitosan/β-lactamase) films to observe whether or not these coatings can modulate nitrocefin hydrolysis at different temperatures. The microgel adsorption was confirmed by a thickness increase of 46 ± 1.0 nm for M1. However, the M2 thickness gain could not be quantified by ellipsometry, because the film turned whitish after the microgel adsorption. Both kind of films were in contact with a nitrocefin solution during 30 min, first at 20 °C and after at 40 °C, with intermediate rinsing steps. Figure 5.15 shows that the activity of the microgel coated films (M1 or M2) increases with temperature, similarly to the active layers "(chitosan/β-lactamase)$_4$ + PAH". In addition, no slowing down of hydrolysis rate was observed, suggesting that M1 and M2 top layers are very permeable.

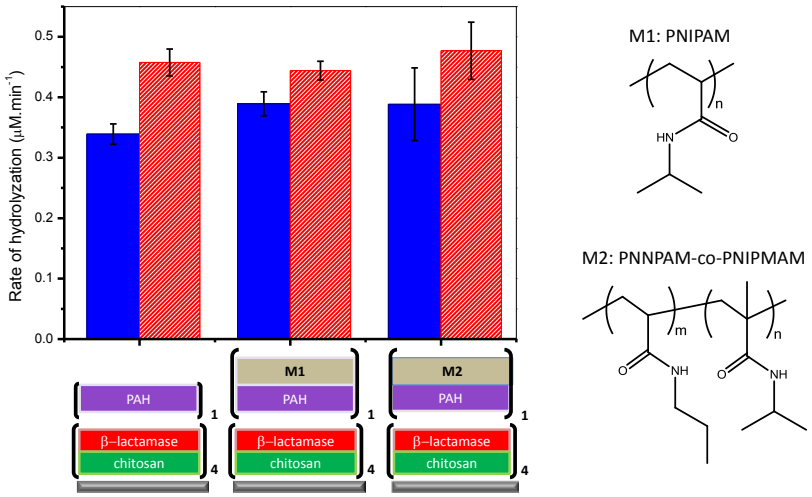

Figure 5.15: Influence of a single (PAH/microgel) layer (M1 or M2) on the activity of (chitosan/β-lactamase)$_4$ films at 20 and 40 °C. Error bars correspond to the range of values measured on duplicates.

As a single microgel layer did not affect the temperature response, we decided to prepare samples stacking a few more microgel bilayers. To that end, we chose the NNPAM/NIPMAM based particles (M2) to prepare (PAH/M2)$_n$

multilayers on a Si wafer, due to their lower LCST (30 °C for M2 *vs.* 33 °C for M1). A close to linear thickness increase was observed (Figure 5.16) for the M2 terminated films (**n** integer), and a small thickness decrease was observed after the adsorption of PAH layers (**n.5**). This result could be explained by desorption of some loosely attached microparticles when the sample is dipped in the polycation solution. Also, we noticed that the adsorption of the microgel particles causes a large thickness increase, which corresponds approximately to one tenth of their fully swollen hydrodynamic radius (130 nm). The latter result is in good agreement with the relationship *thickness/hydrodynamic radius* reported for crosslinked PNIPAM-co-PAA microgel particles adsorbed on planar surfaces [30].

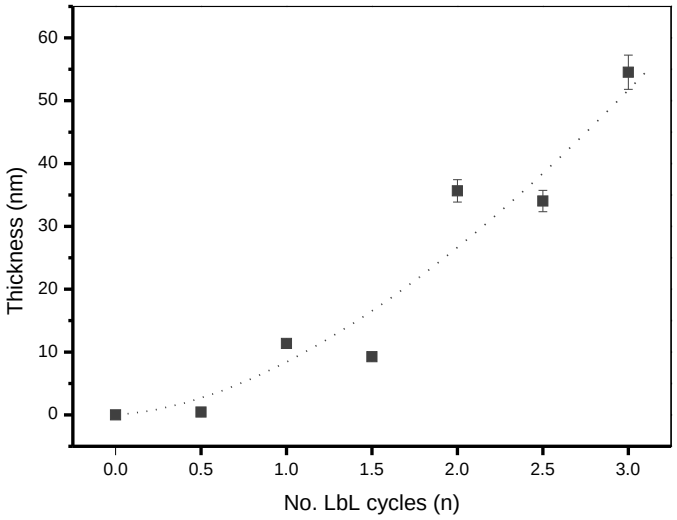

Figure 5.16: Evolution of film thickness as a function of the number of cycles $(PAH/M2)_n$ on aminosilanized Si wafers. The dashed line is a guide to the eye.

For the activity assay, (chitosan/β-lactamase)$_4$ + $(PAH/M2)_4$ films were then prepared by LbL. The active (chitosan/β-lactamase)$_4$ layers were 23 ± 1 nm thick, but we could not determine the film thickness for the microgel layers on top due to the whitish color obtained (scattering of light). Nevertheless, we could assume that they are thicker than 55 nm ($(PAH/M2)_3$ thickness, Figure 5.16). Nitrocefin hydrolysis was conducted at 20 °C and 40 °C for two thermal cycles, holding

the temperature of the medium for 1 h periods while the assay was done and rinsing between changes of temperature. Figure 5.17 shows the rate of hydrolysis observed for the samples (chitosan/β-lactamase)$_4$ + (PAH/M2)$_4$, as well as β-lactamase-terminated films. Both kinds of multilayer films lose activity from the 1st to the 2nd thermal cycle, and also hydrolyze nitrocefin faster at 40 °C. The films covered by M2 layers have 14 ± 3% of activity increase in the first thermal cycle, and a 48 ± 5% gain in the 2nd cycle. The larger gain is in fact closer to the response of β-lactamase terminated films, meaning that the (PAH/M2) layers had a small effect on the 1st cycle but no effect on the second cycle. It is also important to note that (PAH/M2)$_4$ coated films displayed consistently smaller activities in all the assays, indicating that the particles act as a physical barrier and that they were stable at least for 2 thermal cycles. Despite the fact that the LCST of the microgel particles (M1, M2) is proven in solution [21], the microgels adsorbed on the multilayers were not able to stop nitrocefin diffusion at 40 °C. To understand this result we bring to mind that the swelling ratio of the microgel particles in solution is about ∼2, and also that their swelling ratio might have decreased after the adsorption on planar surfaces. As a matter of fact, a 38% reduction of swelling ratio was observed for PAA-PNIPAM microgel particles after adsorption on a PEI layer [20]. If this was the case for our samples, we could think of small nitrocefin molecules passing through the interstices in M2 layers at both temperatures (Figure 5.17. right scheme).

5.3.5 Spin-coated PNIPAM hydrogels

The last thermo-responsive strategy presented in this chapter is the preparation of a thin responsive hydrogel network atop the enzymatic compartment (Figure 5.1**e**). The advantage of this network over the microgel particles is the continuity of the film, which in theory provides a less permeable coating. PNIPAM* hydrogel films of submicron thickness (called *PNIPAM** thereafter) were spin-coated and anchored on polyelectrolyte multilayers assembled by LbL (called *PEMA* thereafter). Two crosslinking strategies were employed to prepare stable hydrogel layers: 1) -COOH groups of the PAA block reacted with -NH_2 groups present in the LbL assembly and, 2) a small fraction of the PAA of the triblock copolymer

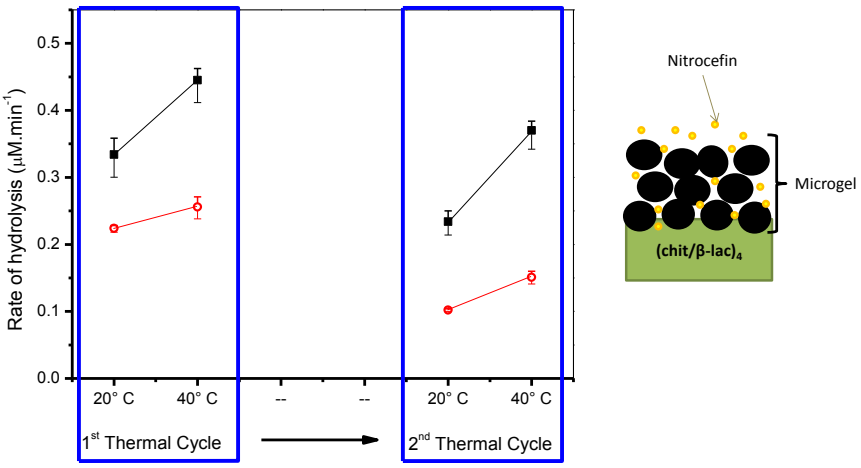

Figure 5.17: Left: Activity of (chit/β-lac)$_4$ –(■), and [(chit/β-lac)$_4$ + (PAH/M2)$_4$]–(●) films along two temperature cycles. Right: Schematic representation of microgels on the active films. Error bars correspond to the range of values measured on duplicates.

was "ene" functionalized to react with thiols loaded in the spin-coating solution. The carboxyl-to-amine crosslinking step is frequently used in LbL films and it has a minimal effect on the activity of the enzyme. On the other hand, the thiol-ene crosslinking requires thermal or photoactivated initiation, which might be detrimental to the activity of β-lactamase (more information in Section 5.5). After a detailed study of the right wavelength, intensity and time of irradiation, the PNIPAM* films were crosslinked at 365 nm (3.3 mW.cm^{-2}) during 3h. The samples were rinsed in deionized water overnight after irradiation, and their thickness loss (before/after rinsing) was around 10% (*e.g.* from 238 to 217 nm). Moreover, it was important to keep an active enzyme and the samples were compared by nitrocefin hydrolysis. After the anchorage of a PNIPAM* film 120 nm thick on a 45 nm active PEMA, the initial rate of hydrolysis decreased by 45%. Since longer or more aggressive irradiation conditions will lead to higher activity loss, we decided to work under the mentioned conditions (365 nm, 3.3 mW.cm^{-2}, 3h).

In order to investigate the temperature-response, the thickness of PEMA and PNIPAM* coated films was determined in air (at room temperature) and in water (at 26 and 40 °C) by ellipsometry (Figure 5.18). The PEMA film doubles

its thickness when immersed in water, and it shows a negligible temperature response. In contrast, the *PEMA + PNIPAM** film has a dry thickness of 232 nm, and exhibits a strongly temperature-dependent thickness in water, *i.e.* 858 nm at 26 °C and 321 nm at 40 °C. This means that the PNIPAM* layer is ∼ 194 nm thick in the dry state, and its swelling ratio is *ca.* 4.0 at 26 °C and approximately 1.2 at 40 °C.

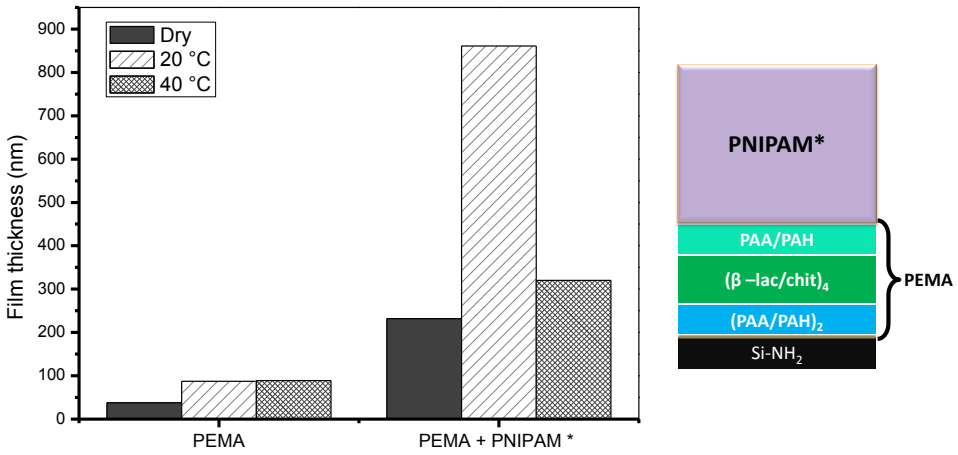

Figure 5.18: PEMA film thickness in air, and in water at 20 °C and 40 °C. (Left) Before and (right) after PNIPAM* incorporation.

Once we confirmed that the PNIPAM* hydrogels swell and deswell on the PEMA depending on the temperature of the medium, we proceeded to evaluate their influence on bioactivity. Thus, a series of samples containing (chitosan/β-lactamase)$_4$ multilayers were prepared. Some of the samples kept β-lactamase as the most external layer and some of them were coated with PNIPAM* (samples labelled A and B, respectively). Dry film thickness was determined by ellipsometry (Table 5.5) and the amount of hydrolyzed nitrocefin after 1 hour of reaction was compared at different temperatures (Figure 5.19). β-lactamase-terminated (A) and PNIPAM*-terminated (B) samples hydrolyzed larger amounts of nitrocefin at higher temperatures, and all of them hydrolyzed less substrate when the number of thermal cycles increased. In addition, PNIPAM*-covered samples have

a decreased activity, which implies that PNIPAM* film slows down the diffusion at all temperatures. However, the PNIPAM* film is not able to stop nitrocefin molecules even when it collapses, since the films display the same relative activity at 40 °C and 20 °C, independent of whether they are covered by PNIPAM* or not.

Table 5.5: Thickness of the PEMA and PNIPAM* coated samples on Si wafers.

Sample	Description	Thickness, nm
A	NH_2-$(PAA/PAH)_{2.5}$ - $(chit/\beta\text{-lac})_4$	44.5 ± 2.0
B	... + PAH/PAA/PAH - PNIPAM*	158.3 ± 2.6
C	... + (PDADMAC/PSS)	178.5 ± 0.5

Considering that PNIPAM* gels swell and collapse but do not stop nitrocefin, we added a last polyelectrolyte couple that has shown tunable permeability under stress: (PDADMAC/PSS) [14, 31] (sample C). We speculated that the stress generated by the swelling of the underlying PNIPAM* gel layer may affect the permeability of the (PDADMAC/PSS) layer and therefore control nitrocefin diffusion by changes in temperature. The adsorption of this extra layer caused a 20 nm thickness increase (Table 5.5), and exhibited 40% of activity retention (compared to the reference sample **A**, Table 5.5) in the first assay at 26 °C (Figure 5.19). Interestingly, this sample **C** displayed lower activity at 40 °C during the first thermal cycle, and really close activities at both temperatures in the subsequent cycles. This shows that, as we speculated, this added layer might strongly change the thermal behavior of the multilayer system. Given that the lower response at higher temperature was observed only during the first cycle, one could speculate that (PDADMAC/PSS) formed a denser impermeable layer at 40 °C but that the film suffered some cracks after, due to the dimensional change of the gel. As a consequence, [*PNIPAM* + (PDADMAC/PSS)*] act together like a barrier that avoids faster hydrolysis at 40 °C, yet is not able to control nitrocefin hydrolysis along several temperature cycles.

Motivated by the potential of [*PNIPAM* + (PDADMAC/PSS)*] barrier, we considered how to amplify the effect of PNIPAM* tunable swelling on the (PDADMAC/PSS) layer. Hence, we also deposited the same coating on top of self-

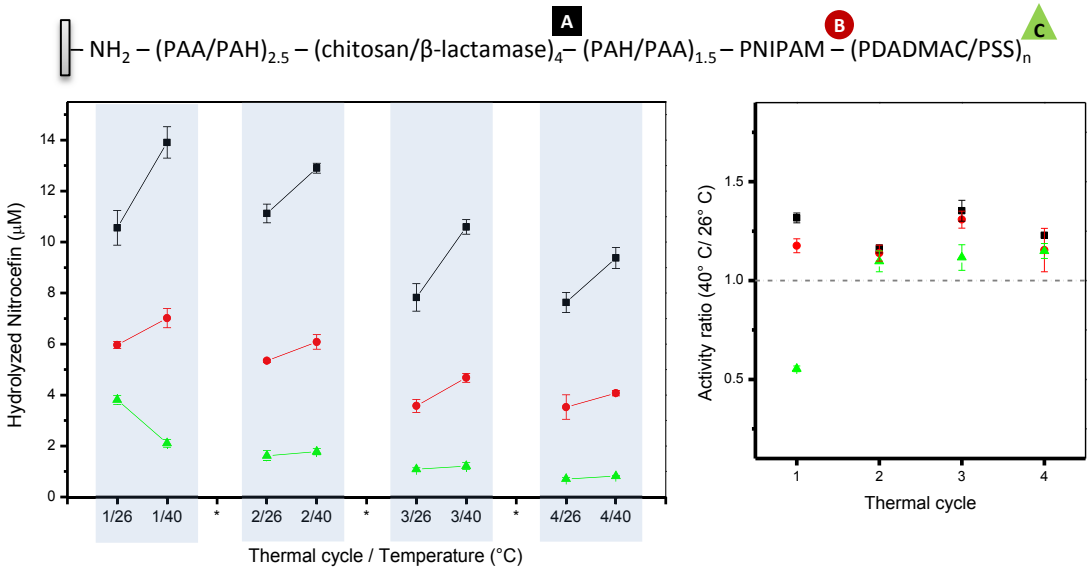

Figure 5.19: Influence of PNIPAM* on the activity of (chitosan/β-lactamase)$_4$ films at 26 and 40 °C, along 4 thermal cycles. Left: Activity response. Right: Ratio of activity response (Activity at 40 °C/activity at 26 °C). Error bars correspond to the range of values measured on duplicates.

assembled nanotube brushes with the structure: [(PAH/PAA)$_{12}$ + (chit/β-lac)] (Figure 5.20), (PAH/PAA) being the most external layer of the tubes. The change of geometry of the gel layer now results in an amplified stretching of the (PDADMAC/PSS) film: when PNIPAM* swells it now stretches (PDADMAC/PSS) film biaxially, which resembles the mechanical stretching of responsive biocatalytic films prepared by Lavalle *et al.* [14, 15]. Due to the intricate nature of the brushes, an aminosilanized silicon wafer was used as a reference to evaluate the thickness of PNIPAM* and the polyelectrolyte layers on top by ellipsometry (Table 5.6). For the polyelectrolyte couple adsorbed over PNIPAM*, we chose (PDADMAC/PSS) (labelled **Y**) and (PAH/PSS)$_3$ (labelled **Z**), and tried to work with similar film thicknesses (12.2 *vs.* 9.3 nm thickness increase on PNIPAM*).

Figure 5.21 shows that the activity of the nanotube brushes is lower than the activity of the films. This phenomena was also observed in Chapter 4 (Section 4.3.4) and it was attributed to the rather low accessibility of the enzyme in the brush structure. Now, if we look in detail at the different sample treatments, we can observe that:

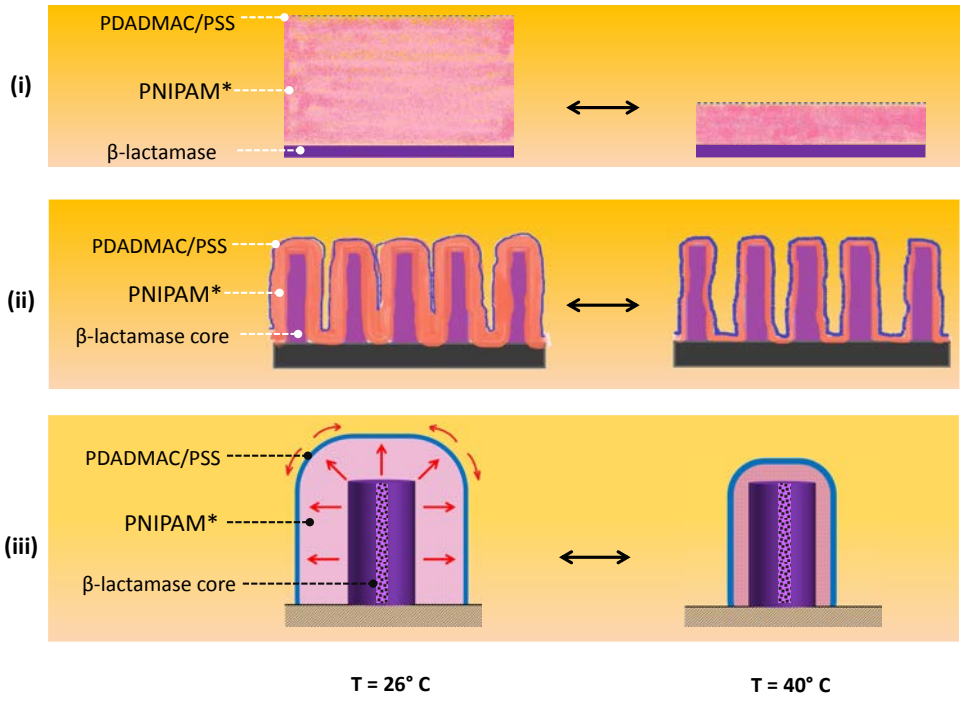

Figure 5.20: Schematic representation of the spin-coated hydrogels on PEMA containing β-lactamase and their expected behavior. (i) Planar films, (ii) Brushes of self-assembled nanotubes, (iii) PNIPAM* swells and stretches biaxially PDADMAC/PSS at 26°C on the nanotubes.

- All the coated samples (X, Y, Z) exhibit an activity ratio $\cong$ 1 on the 1st thermal cycle, while the nanotube brush **W** has an activity ratio $\geq$ 1.0. This result indicates that **X, Y, Z** hydrolyze nitrocefin at the same rate at 26 or 40 °C, while **W** brush reacts faster at 40 °C. Consequently, the PNIPAM* barrier is partially effective but is out of equilibrium. It looks like PNIPAM* is annealing along the first thermal cycle to reach equilibrium. In fact, the samples **W** and **X** follow the same trend of response on the 2nd and 3rd cycles.

- The (PDADMAC/PSS) barrier leads to activity ratios farther from 1.0 in all the thermal cycles and it acts alike $(PAH/PSS)_3$ during the 2nd and 3rd cycles. However, the activity loss in the samples **Y** is really large since the beginning, leading to low amounts of hydrolyzed nitrocefin and large error

Table 5.6: Thickness increase after the sample treatment X,Y,Z measured over an aminosilanized Si wafer.

Sample	Description	Thickness increase, nm
X	+ PNIPAM*	144.7 ± 0.6
Y	+ $(PDADMAC/PSS)_1$	12.2 ± 2.1
Z	+ $(PAH/PSS)_3$	9.3 ± 0.7

bars. Therefore, is difficult to evaluate the thermal response of **Y** under these conditions.

- $(PAH/PSS)_3$ barrier (**Z**) keeps an activity ratio ≥ 1.0 from cycle 2 to cycle 5, even though this effect decreases after the 3rd cyle. Thus, **Z** brushes display a modest yet real variation from the uncoated nanotube brushes **W**. At the same time, the coating $(PAH/PSS)_3$ clearly possess higher activities than a single bilayer (PDADMAC/PSS), suggesting that they are more permeable.

- **Y** and **Z** coated nanotube brushes seem to favor nitrocefin hydrolysis at higher temperature, which implies that the mechanical effect expected is not controlling nitrocefin diffusion.

To confirm the swelling/deswelling of the hydrogels, we spin-coated PNIPAM* on $(PAH/PAA)_{20}$ nanotube brushes and imaged the topography by AFM in water at 20 and 40 °C. Figure 5.22 shows that we can observe more defined structures at higher temperature, when the gel is in collapsed state. In the height profiles we can appreciate groups of objects as tall as 1 μm, forming wider groups at lower temperature. Which implies that PNIPAM* responds to the change in temperature when it is anchored on the nanotube brushes. The difference between the expected height (5 μm) and the height observed by AFM might be related to the fact that the nanotubes can be damaged at some areas and are not perfectly homogeneous.

At this stage, it is useful to recapitulate our observations, and to draw conclusions. Among the different methods we used to deposit a responsive barrier atop the β-lactamase enzymatic compartment, the spin-coating of a crosslinkable PNIPAM gel layer is undoubtedly the best, since it gives rise to a relatively thick

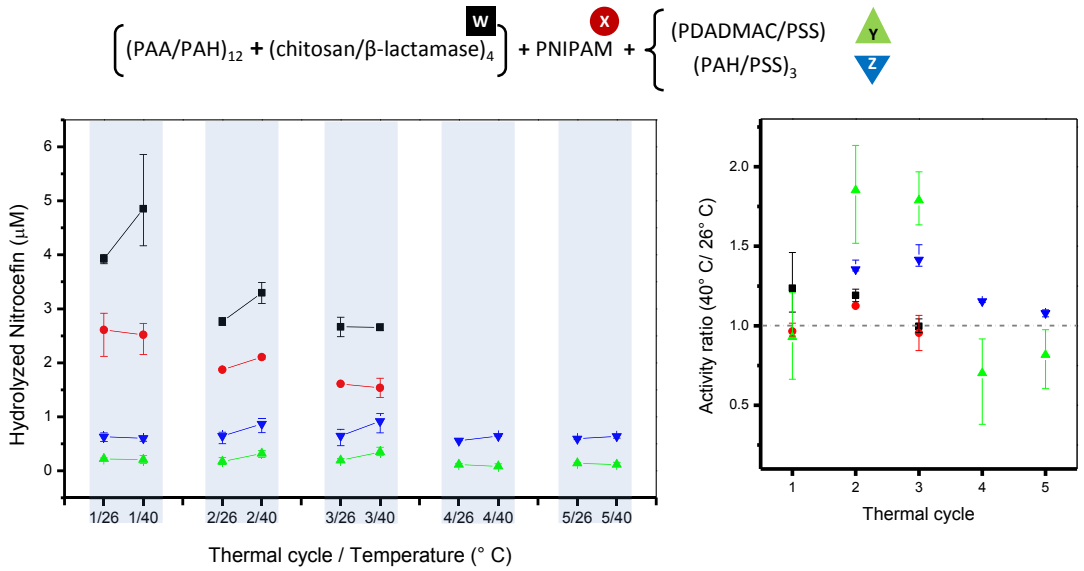

Figure 5.21: Influence of PNIPAM* on the activity of the nanotube brushes at 26 and 40 °C, along 5 thermal cycles. Left: Activity response. Right: Ratio of activity response (Activity at 40 °C/activity at 26 °C). Error bars correspond to the range of values measured on duplicates.

continuous responsive film without destroying the enzyme. Despite the strong thermoresponse it possesses, this barrier is not capable to modulate thermally the enzymatic reaction. Instead, it reduces the enzymatic rate by a factor that is essentially independent of temperature. This shows that the diffusion of nitrocefin through this barrier is independent on the swelling/deswelling of PNIPAM*. This observation, which was not expected, can be understood by realizing that the efficiency of the diffusion barrier is controlled by two factors, which neutralize each other when temperature varies across the LCST. The first factor is the barrier thickness, which decreases from below to above the LCST and should thus favor diffusion at higher temperatures. The second is the intrinsic permeability of the gel, which is increased with swelling, and therefore decreases from below to above to LCST. Overall, the two effects cancel out, leading to a quasi uniform permeability independent of temperature.

Therefore, we have added a new component to the barrier, consisting of a thin polyelectrolyte multilayer, whose function is to respond to the dimensional changes of the gel layer and thereby to amplify its response. This barrier is

deposited above the LCST, when the gel is collapsed. Then, the system is cooled to 20 °C, which swells the gel and forces the polyelectrolyte layer to adapt to these new conditions, resulting in a given value of permeability. Upon reheating to 40 °C, the polyelectrolyte barrier anneals again, leading to a decreased value of permeability, as desired. However, once this is done, the system is stabilized, with a loss of thermal response in subsequent thermal cycles.

Similar observations were also made on the nanotube brush, for two different polyelectrolyte barriers. However, contrary to our expectations, the thermoresponse was not amplified by the roughness provided by the nanotube brush, indicating that the tuning of permeability in the first thermal cycle is not related to the mechanical deformation of the polyelectrolyte layer by the underlying gel. This supports our interpretation that the decreased permeability in the first thermal cycle is due to irreversible reorganizations occurring in the polyelectrolyte layer, triggered by the different degrees of swelling of the gel layer. Once reorganized, the polyelectrolyte multilayer just serves to decrease in a thermally-independent way the global permeability, except maybe for the PDADMAC/PSS systems in the 4th and 5th cycles, although this is difficult to judge due to imprecision of the measurements.

Figure 5.22: AFM images and their height profiles (below) of the nanotube brushes $(PAH/PAA)_{20}$ coated by PNIPAM* at **(a)** 20 °C and **(b)** 40 °C in water. Height measurements were done along the white line on the top image.

5.4 Conclusion

In this chapter, we prepared different thin coatings with thermoresponsive polymers and studied their ability to control nitrocefin diffusion towards β-lactamase reservoirs.

- $PMEO_2MA$ brushes were grafted from (PAH/PAA) polyelectrolyte multilayers by ATRP in water, using either a silane initiator loaded in the multilayers or an anionic macroinitiator (PEMA) adsorbed on top. However, the extreme sensitivity of the enzyme limited the application of this method of synthesis to cover (chitosan/β-lactamase) multilayers: indeed, the enzyme lost activity after being in contact with the monomer and the transfer agents.

- Multilayer thin films (PAH/PAA-*b*-PNIPAM) were then successfully prepared over (chitosan/β-lactamase) multilayers and the activity of the enzyme was well preserved. Unfortunately, we did not observe an effect on the bioactivity below or above the LCST. The interdigitation between adjacent layers and the block copolymer might have decrease the swelling ratio.

- PNIPAM and PNIPAM-like microgel particles were then adsorbed on positively charged surfaces, to prepare one layer or multilayer assemblies using PAH as polycation. The microgel adsorption results in a minimal loss of activity, yet a poor control over nitrocefin diffusion is again observed. Further studies on the swelling ratio of the microgels in LbL would be relevant to understand these results.

- PNIPAM* hydrogel networks were then successfully synthesized and anchored on top of (chitosan/β-lactamase) multilayers and brushes. The enzyme was still active after the synthesis and the LCST on the films was confirmed by ellipsometry. However, the PNIPAM* gel barrier was not capable to modulate the permeation of nitrocefin, and therefore we added a new component polyelectrolyte barrier to the system. This approach provided good results, albeit limited to the first thermal cycle. For subsequent cycles, the reorganization of the polyelectrolyte barrier resulted in a loss of

thermal modulation of the permeability. This suggests that one way to go further would be to crosslink this barrier either at 40 °C just after deposition, or at 20 °C just after the first cooling. To apply this strategy, other polyelectrolytes should be selected (*e.g.* PAA and PAH), and the crosslinking degree should be tuned for optimal response. This experiment was not done here, given the limited timeframe of this thesis.

5.5 Supporting Information

Loss of enzymatic activity: drying and UV irradiation.

Since the insertion layers atop chitosan/β-lactamase film often involved a drying step, and UVA irradiation for PNIPAM* films, it is important to determine the impact these treatments on enzymatic activity. To this end, a set of samples (chitosan/β-lactamase)$_4$ was prepared and then exposed to (a) drying, (b) UVA irradiation in air, or (c) UVA irradiation under water, for 2, 4, and 6 hours. At the end of the treatment (a, b, c), the samples were re-hydrated in MES buffer (overnight) before following a nitrocefin colorimetric test. The activity loss was calculated as a difference on the rate of hydrolysis, and the results are summarized in the Figure 5.23.

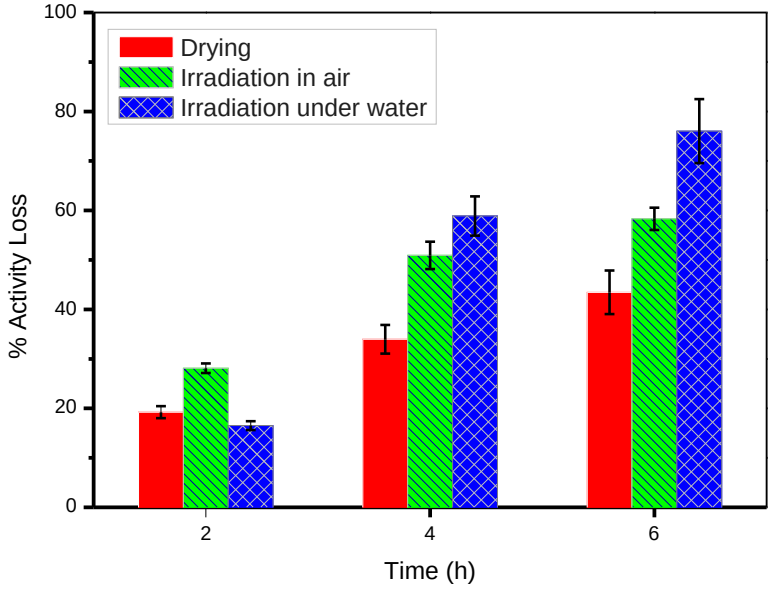

Figure 5.23: Activity loss percentage after drying and UVA irradiation (365 nm), for a series of (chitosan/β-lactamase)$_4$ samples.

References

[1] Carolina de las Heras Alarcón, Sivanand Pennadam, and Cameron Alexander. Stimuli responsive polymers for biomedical applications. *Chemical Society Reviews*, 34(3):276–285, 2005.

[2] Karine Glinel, Christophe Déjugnat, Michelle Prevot, Björn Schöler, Monika Schönhoff, and Regine v Klitzing. Responsive polyelectrolyte multilayers. *Colloids and Surfaces A: Physicochemical and Engineering Aspects*, 303(1): 3–13, 2007.

[3] Howard G. Schild. Poly(N-isopropylacrylamide): experiment, theory and application. *Progress in Polymer Science*, 17(2):163–249, 1992.

[4] Alain M Jonas, Karine Glinel, Ron Oren, Bernard Nysten, and Wilhelm TS Huck. Thermo-responsive polymer brushes with tunable collapse temperatures in the physiological range. *Macromolecules*, 40(13):4403–4405, 2007.

[5] Hidenori Kuroki, Ihor Tokarev, and Sergiy Minko. Responsive surfaces for life science applications. *Annual Review of Materials Research*, 42:343–372, 2012.

[6] Martien A Cohen Stuart, Wilhelm TS Huck, Jan Genzer, Marcus Müller, Christopher Ober, Manfred Stamm, Gleb B Sukhorukov, Igal Szleifer, Vladimir V Tsukruk, Marek Urban, et al. Emerging applications of stimuli-responsive polymer materials. *Nature Materials*, 9(2):101–113, 2010.

[7] John F Quinn and Frank Caruso. Facile tailoring of film morphology and release properties using layer-by-layer assembly of thermoresponsive materials. *Langmuir*, 20(1):20–22, 2004.

[8] Karine Glinel, Alain M Jonas, Thierry Jouenne, Jérôme Leprince, Ludovic Galas, and Wilhelm TS Huck. Antibacterial and antifouling polymer brushes incorporating antimicrobial peptide. *Bioconjugate Chemistry*, 20(1):71–77, 2008.

[9] Martin A Cole, Nicolas H Voelcker, Helmut Thissen, and Hans J Griesser. Stimuli-responsive interfaces and systems for the control of protein–surface and cell–surface interactions. *Biomaterials*, 30(9):1827–1850, 2009.

[10] Michał Szuwarzynski, Leszek Zaraska, Grzegorz D Sulka, and Szczepan Zapotoczny. Pulsatile releasing platform of nanocontainers equipped with thermally responsive polymeric nanovalves. *Chemistry of Materials*, 25(3):514–520, 2013.

[11] Nicel C. Estillore and Rigoberto C. Advincula. Stimuli-responsive binary mixed polymer brushes and free-standing films by LbL-SIP. *Langmuir*, 27 (10):5997–6008, 2011. doi: 10.1021/la200089x.

[12] Michael J Serpe, Kristen A Yarmey, Christine M Nolan, and L Andrew Lyon. Doxorubicin uptake and release from microgel thin films. *Biomacromolecules*, 6(1):408–413, 2005.

[13] Zhichen Zhu and Svetlana A Sukhishvili. Temperature-induced swelling and small molecule release with hydrogen-bonded multilayers of block copolymer micelles. *ACS nano*, 3(11):3595–3605, 2009.

[14] Damien Mertz, Cédric Vogt, Joseph Hemmerlé, Jérôme Mutterer, Vincent Ball, Jean-Claude Voegel, Pierre Schaaf, and Philippe Lavalle. Mechanotransductive surfaces for reversible biocatalysis activation. *Nature Materials*, 8(9):731–735, 2009.

[15] Cedric Vogt, Damien Mertz, Karim Benmlih, Joseph Hemmerle, Jean-Claude Voegel, Pierre Schaaf, and Philippe Lavalle. Layer-by-layer enzymatic platform for stretched-induced reactive release. *ACS Macro Letters*, 1(7):797–801, 2012.

[16] Timothy M Fulghum, Derek L Patton, and Rigoberto C Advincula. Fuzzy ternary particle systems by surface-initiated atom transfer radical polymerization from layer-by-layer colloidal core-shell macroinitiator particles. *Langmuir*, 22(20):8397–8402, 2006.

[17] Cong-Duan Vo, Andreas Schmid, Steven P. Armes, Kenichi Sakai, and Simon Biggs. Surface ATRP of hydrophilic monomers from ultrafine aqueous silica sols using anionic polyelectrolytic macroinitiators. *Langmuir*, 23(2):408–413, 2007. doi: 10.1021/la063003j.

[18] Steve Edmondson, Cong-Duan Vo, Steven P. Armes, and Gian-Franco Unali. Surface polymerization from planar surfaces by atom transfer radical polymerization using polyelectrolytic macroinitiators. *Macromolecules*, 40(15): 5271–5278, 2007. doi: 10.1021/ma070876r.

[19] Saadyah Averick, Antonina Simakova, Sangwoo Park, Dominik Konkolewicz, Andrew J. D. Magenau, Ryan A. Mehl, and Krzysztof Matyjaszewski. ATRP under biologically relevant conditions: Grafting from a protein. *ACS Macro Letters*, 1(1):6–10, 2012.

[20] Stephan Schmidt, Michael Zeiser, Thomas Hellweg, Claus Duschl, Andreas Fery, and Helmuth Möhwald. Adhesion and mechanical properties of PNIPAM microgel films and their potential use as switchable cell culture substrates. *Advanced Functional Materials*, 20(19):3235–3243, 2010.

[21] Bastian Wedel, Michael Zeiser, and Thomas Hellweg. Non NIPAM based smart microgels: systematic variation of the volume phase transition temperature by copolymerization. *Zeitschrift fur Physikalische Chemie*, 226(7): 737, 2012.

[22] Xiaojun Wang, George Minasov, and Brian K Shoichet. Noncovalent interaction energies in covalent complexes: TEM-1 β-lactamase and β-lactams. *Proteins: Structure, Function, and Bioinformatics*, 47(1):86–96, 2002.

[23] EC 3.5.2.6 - β-lactamase. `http://www.brenda-enzymes.info`, 2004. Accessed on 22-03-2014.

[24] Rafael C Rodrigues, Claudia Ortiz, Ángel Berenguer-Murcia, Rodrigo Torres, and Roberto Fernández-Lafuente. Modifying enzyme activity and selectivity by immobilization. *Chemical Society Reviews*, 42(15):6290–6307, 2013.

[25] Roland Steitz, Vincent Leiner, Klaus Tauer, Victor Khrenov, and Regine v Klitzing. Temperature-induced changes in polyelectrolyte films at the solid–liquid interface. *Applied Physics A*, 74(1):s519–s521, 2002.

[26] Carla Mattos and Dagmar Ringe. Proteins in organic solvents. *Current Opinion in Structural Biology*, 11(6):761–764, 2001.

[27] Steven J Cartwright and Stephen G Waley. β-lactamase inhibitors. *Medicinal Research Reviews*, 3(4):341–382, 1983.

[28] Thomas Caliaro. Design and characterization of surfaces with thermoresponsive properties for cell culture applications. Master's thesis, Université catholique de Louvain, 2011.

[29] Anna Burmistrova, Roland Steitz, and Regine von Klitzing. Temperature response of PNIPAM derivatives at planar surfaces: Comparison between polyelectrolyte multilayers and adsorbed microgels. *ChemPhysChem*, 11(17): 3571–3579, 2010.

[30] Stephan Schmidt, Hubert Motschmann, Thomas Hellweg, and Regine von Klitzing. Thermoresponsive surfaces by spin-coating of PNIPAM- co-PAA microgels: A combined AFM and ellipsometry study. *Polymer*, 49(3):749–756, 2008.

[31] Damien Mertz, Joseph Hemmerlé, Jérôme Mutterer, Sophie Ollivier, Jean-Claude Voegel, Pierre Schaaf, and Philippe Lavalle. Mechanically responding nanovalves based on polyelectrolyte multilayers. *Nano Letters*, 7(3):657–662, 2007.

Chapter 6

Conclusion and Perspectives

In the present study we went from the assembly of enzyme-based multilayer films to the building of biocatalytic nanostructures for surface modification and addressed the challenges of temperature-responsive integration. Aiming to mimic physiological cell functions that are controlled by temperature, we demonstrated the synthesis of enzyme-based nanotube brushes and also discussed the phenomena underlying the integration of bioactive molecules in nano-sized features. Layer-by-layer (LbL) combined with hard templating and crosslinking techniques appeared as green, versatile and robust techniques for nanofabrication in the overall picture.

In the first place, the influence of surface geometry and confinement was highlighted for the synthesis of (chitosan/β-lactamase)$_n$ multilayer films by LbL. While the enzyme preserves its activity after adsorption on flat surfaces and in nanoporous membranes, the restrictions imposed in a geometrically confined environment favor activity at low enzyme loading. Conversely, flat surfaces perform better as the load of enzyme increases with the number of layers ($\boldsymbol{n}$). The growth of the flat films in the nanopores proceeds similarly to the one of synthetic polyelectrolytes[1]. However, the adsorption of a different enzyme in smaller/larger pore diameters and the follow up of stoichiometry variations will help to improve our understanding of the consequences of geometrical confinement on biocatalysis.

[1]Roy, C. J.; Dupont-Gillain, C.; Demoustier-Champagne, S.; Jonas, A. M.; Landoulsi, J. Langmuir 2009, 26, 3350.

In a second stage, a "core-shell" nanotube structure was defined and proven effective to enhance the storage stability of β-lactamase-based films in porous membranes. Furthermore, this approach was key to prepare biocatalytic nanotube brushes by modifying (PAH/PAA) nanotubes and inserting biocatalytic multilayers at the interior or exterior surface of the nanotubes. Indeed, both options showed to be useful in different ways, as β-lactamase layers adsorbed on top of (PAH/PAA) nanotube brushes displayed faster rates of reaction, and the enzyme layers within the nanotubes preserved better the activity. One question that remains unsolved is how the activity of free nanotubes compares to the activity of filled pores in the membranes and/or to the nanotube brushes. In order to answer this question, complementary studies to avoid the aggregation of the nanotubes after template removal are necessary. Albeit, fully soluble nanotubes are best carriers and we could expect better performance in flow, while the target of a brush is to act upon circulating substrates, as an interface.

While the nanotube brush structure was achieved and the activity of the enzyme was detected, some processing conditions can be further optimized (*e.g.* the minimal number of PAH/PAA shell layers to achieve standing tubes) to improve the biocatalytic response. In this sense, is important to remark that the layers that contribute to maintain the tubular structures perpendicular to the surface also slow down substrate diffusion when the enzyme is in the core. Therefore, the nanotube brush structure with enzymatic core could be useful for specific applications where a sustained and small catalytic effect is desired for a long time (*e.g.* prostheses functionalization). Another alternative to increase efficiency of the brushes is to have structural layers that act as co-factors for biocatalysis, for instance, nanoparticles of late transition metals (*e.g.* platinum, palladium, gold).

In Chapter 5, we compared several thermo-responsive coatings to control nitrocefin diffusion towards β-lactamase layers beneath. While different film architectures with PNIPAM and $PMEO_2MA$ were efficiently anchored, the biocatalytic response obtained was not LCST/VPTT dependent and repeatable. One main issue was the sensitivity of β-lactamase enzyme to ATRP monomer and transfer agents, which led to activity loss. If a different enzyme preserves its activity under these conditions, then grafted polymer brushes prepared by ATRP could be evaluated to block substrate diffusion. The second challenge we faced was the small

size of the substrate which apparently passed through PNIPAM coatings, without reflecting the expected temperature effect. As we realized, the collapse-transition is not able to control the diffusion of a small substrate by itself, and it might be linked to the fact that the permeability and the thickness of the gel react in opposite directions, canceling each other. Besides this fact, we found promising results in more complex structures. The addition of polyelectrolyte layers atop PNIPAM hydrogel on the active films showed a partial effect, that was however, lost after temperature cycling. Further investigation of this last scenario (PNIPAM* hydrogel) with more stable (crosslinked) polyelectrolyte layers might result in truly thermo-responsive biocatalytic valves. It is important to mention that stacking several elements to obtain thermo-response reduces the performance of the surface and the enzyme itself has already an optimum working temperature. Thus, thermoresponsive barriers on biocatalytic films are limited for applications where the protection of the enzyme is critical in a given environment.

It comes to our attention that the fabrication of self-assembled nanotube brushes is just starting and that their use for biocatalysis involves a variety of complex phenomena waiting to be investigated before we can successfully integrate them for real-life applications. Nonetheless, this study has presented some elements that may pave the way towards the design of biocatalytic and three-dimensionally nanostructured surfaces.

The tools of synthesis presented in this study are all relevant for nanotechnology and in progress. While it is known that enzyme immobilization in LbL can enhance stability and activity, each particular enzyme-polyion couple presents different properties and even the multilayer assembly can give unpredictable results. Thereupon, the careful selection of a biocompatible polyion is recommended, as well as the choice of a robust enzyme with practical applications. Between the areas that could exploit the strategies presented in this work, biomedical research is possibly the most interesting for the preparation of surface mediated enzyme therapy, surface drug activation and tissue engineering. As an example, enzymes for lysosomal storage diseases can be loaded in prosthesis to avoid the high doses to reach some organs or tissues (*e.g.* heart, cartilage and bones).

The combination of LbL and hard templating to produce arrays of soft nanostructures is unique and certainly has a wide range of applications. It is however

important to mention that the polishing (*i.e.* de-crusting) method needs to be automatized to obtain fully homogeneous nanostructured surfaces.

The integration of smart polymers and biocatalytic interfaces has a promising future in the development of therapeutic applications. In this sense, a variety of confined geometries can be contrasted in terms of efficiency and stability for sustained release. Consequently, the design of a nanotube brush dimensions will have to be rationalized, as the use of a specific responsive architecture.

Dissemination

Oral Communication

"Brushes of self-assembled nanotubes for responsive bio-catalysis". D.G. Ramírez-Wong, S. Demoustier-Champagne, A.M. Jonas, C. Bonhomme. *Euro Intelligent Materials.* Kiel, Germany. September 25-27, 2013

"Brushes of self-assembled nanotubes for responsive bio-catalysis". D.G. Ramírez-Wong, S. Demoustier-Champagne, A.M. Jonas, C. Bonhomme. *Annual Meeting of the Belgian Polymer Group.* Ghent, Belgium. May 19-20, 2014

"Spectroscopy and simulation: tools of investigation for nanobiomaterials". C. Bonhomme, N. Folliet, T. Azaïs, F. Babonneau, D. Ramírez-Wong, S. Demoustier, A. Jonas. 2001 *MRS Fall Meeting.* Boston, USA. Nov 28 - Dec 02, 2011

Poster

"Self-assembled nanotubes for stimuli-response biocatalysis" D.G. Ramírez-Wong, S. Demoustier-Champagne, A.M. Jonas, C. Bonhomme. *Annual Meeting of the Belgian Polymer Group: Polymers for a Sustainable Society.* Blankenberge, Belgium. May 10-11, 2012

"Brushes of self-assembled nanotubes for temperature or stress responsive bio-catalysis" D.G. Ramírez-Wong, S. Demoustier-Champagne, A.M. Jonas, C. Bonhomme. *2nd NanoWal meeting: Functionalized surfaces at the nanoscale.* Brussels, Belgium. April 3rd, 2012.

Publications

"Effects of geometrical confinement on the layer-by-layer assembly of enzyme-based thin films". D.G. Ramírez-Wong, S. Demoustier-Champagne, A.M. Jonas, C. Bonhomme. *Langmuir.* In preparation.

"PNIPAM thin films on enzymatic compartments". D.G. Ramírez-Wong, S. Demoustier-Champagne, A.M. Jonas, C. Bonhomme, Y. Tran. *Langmuir.* In preparation.

"Layers over Layer-by-Layer Assemblies: Silanization of Polyelectrolyte Multilayers". A. Dirani, A.E. Fernandes, D. Ramírez-Wong, P. Lipnik, C. Poleunis, B. Nysten, K. Glinel, A.M. Jonas. *Langmuir.* Submitted.